DISSERTATION

PROBING FOLDING/UNFOLDING KINETICS, REACTION MECHANISM AND THERMODYNAMIC STABILITY OF NUCLEIC ACID HAIRPINS

Submitted by

Rajesh Kumar Nayak

Department of Chemistry

In partial fulfillment of the requirements

For the Degree of Doctor of Philosophy

Colorado State University

Fort Collins, Colorado

Fall 2013

Doctoral Committee:

Advisor: Alan Van Orden

B. George Barisas
Eugene Chen
Brian McNaughton
AzerYalin

ABSTRACT

PROBING FOLDING/UNFOLDING KINETICS, REACTION MECHANISM AND THERMODYNAMIC STABILITY OF NUCLEIC ACID HAIRPINS

Nucleic acid hairpins play pivotal roles in biological and cellular processes. The functions of the DNA and RNA hairpins depend upon the conformational changes they adopt during the biological process. Therefore, a clear understanding of their conformational dynamics such as folding and unfolding kinetics, reaction mechanism as well as thermodynamic stability is essential to understand their biological functions. This dissertation describes folding kinetics, reaction mechanism and thermodynamic stability of stem-loop nucleic acid hairpins by using rapid-mixing stopped-flow kinetics and other spectroscopic techniques.

Firstly, the folding kinetics and reaction mechanism of a five base-paired stem and twenty one polythymidine loop DNA hairpin as a function of varying mono-valent counter ion concentrations have been discussed. The important observation of this investigation is that the DNA hairpin folding is not simply a two-state process, and based on our experiments and kinetic modeling, we proposed a three-state reaction mechanism, wherein, the intermediate formation occurs on microsecond time scale and the complete hairpin formation occurs on millisecond time scale.

Secondly, the loop length and counter ion dependent thermodynamic stability and folding of DNA hairpins have been described. This investigation provides a detailed understanding of how the stability and folding changes as a function of loop length and counter ion concentrations. The most important conclusion of this part of the investigation is

that the thermodynamic stability of tetraloop hairpins depend upon counter ion concentration regimes and we explained the exceptional stability of atetraloop hairpin in the higher concentration regime, compared to longer loop length hairpins on the basis of base-stacking effect.

Finally, the folding and unfolding kinetics of RNA hairpins with identical four base-paired stem but different nucleotide loop sequence is discussed. Here we observed that the RNA hairpin folding and unfolding can be much more complex than previously thought and also RNA hairpin folding process can be different than DNA hairpin folding process.

ACKNOWLEDGMENTS

First of all, I would like to extend my sincere thanks to my advisor Alan Van Orden for his endless help and inspiration. Alan, your patience and motivation during tough time has been instrumental in this achievement. He is an amazing advisor and mentor to work with. Secondly, I would also like to thank Dr. Olve Peersen of the Department of Biochemistry and Molecular Biology with whom I collaborated and used his research laboratory for my experiments. He has been incredible supportive in allowing me to use his laboratory resources and I also thank him for his kind advice and suggestions. I would also thank our collaborator Dr. Kathleen Hall of Department of Biochemistry and Molecular Biophysics, Washington School of Medicine, St. Louis for her help and allowing me to visit her laboratory to learn about handling RNAs.

I would like to thank my present and former committee members, Eugene Chen, Brian McNaughton, Azer Yalin, George Barisas, Grzegorz Szamel and Thomas Meersman for their help, valuable time and support.

I would like to thank all my colleagues in the Van Orden group- Jeff, Jon, Keir, Rebecca, Kevin, Doug, Duncan, Ming, Jaemeyong and others- for their help and support throughout my time here in Colorado State University. I would like to thank Artem Melnykov of Dr. Hall's lab for his help in RNA training. I thank Peng and Grace in Dr. Peersen's research group for their help and support.

I would like to thank my host family, especially American Grandma Lorraine and Don for their incredible help and support. I would like to extend my special thanks to Don Buchleiter for his selfless help and encouragement during some of my toughest times

(especially during my five eye surgeries). I am indebted you Don! I would like to thank Bruce Webster (Prana Prabhu) for his advice, encouragement and motivation, especially in tough times. I would also thank Mother Nidra for her spiritual advice. I would thank Seth, Nick, Brian, Aditya, Sanatan Priya, Pabitra, Sudeep, Tina Ma, Krishna Chetry and so many other friends for their friendship and support. I would also thank Mohapatro Sir for his motivation and support. I would like to give special thanks to Fran from Academic Computing and Networking Services, Morgan Library, for help and support.

I would like to thank NSF and NIH for the funding support for my research. I would like to thank CSU for its valuable resources.

Finally, I would like to extend my heartfelt thanks to my parents and my family members for their constant encouragement and support. It has been extremely painful experience to lose my father in January. I am sure that without my family's unconditional love, support and encouragement, I could not have made this journey.

DEDICATION

To my beloved late Father

Banshidhar Nayak

TABLE OF CONTENTS

LIST OF TABLES

LIST OF FIGURES

CHAPTER 1: Introduction

1.1 NUCLEIC ACID HAIRPINS

1.1.1 DNA/RNA Hairpin Structures and conformations

Single stranded nucleic acids with complementary base pairs have the potential to form stem-loop hairpin structures. A nucleic acid hairpin is formed when a single strand folds back and forms base pairs with itself.[1]Stem-loop base pairing commonly occurs in single stranded DNA and, even more commonly, in RNA. Basically, the folded hairpin has two structural units: a double stranded stem consisting of primarily Watson-Crick complementary base pairs and a single stranded loop (Figure 1.1). The hairpin is the most common secondary structural feature in RNA.[2] For example, about 70% of the nucleotides in 16S rRNA are hairpin structures.[3] All the base pairs in the stem regions are formed when the hairpin is fully folded. Whereas, the internal loops and bulges are formed due to structural defects or mismatchesin the stems.[1]

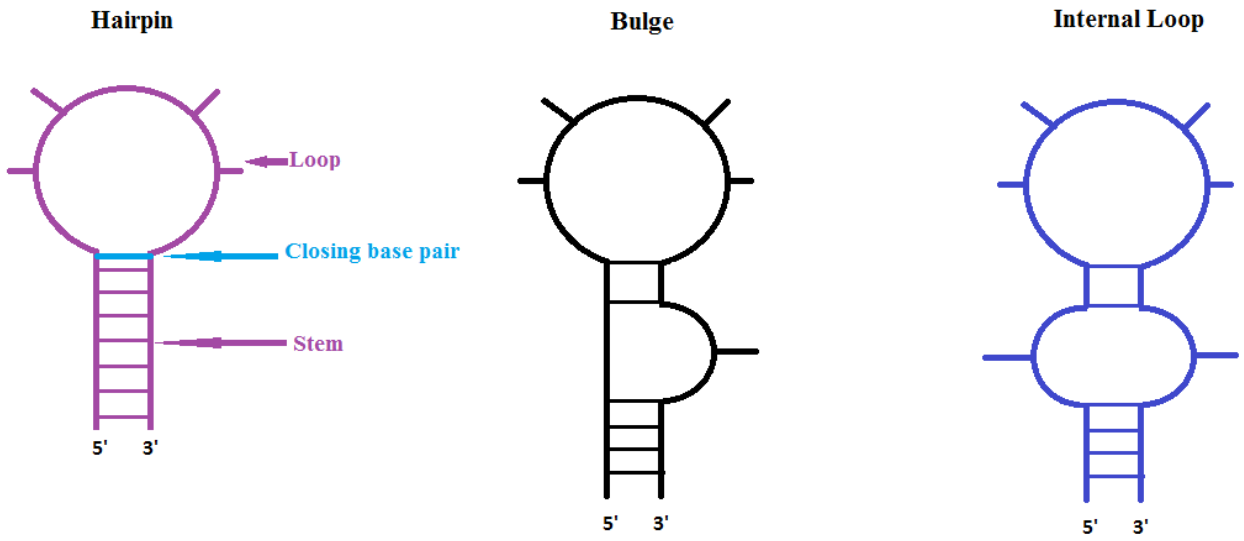

Figure 1.1: The structure of nucleic acid hairpins. The hairpin consists of unpaired nucleotides at the tip of the helical stem. The bulge and the internal loop are characterized by unpaired nucleotides in one strand and both strands, respectively. This figure is adopted from Bevilacquaet al.[1]

Although the stems of DNA and RNA hairpins consist primarily of Watson-Crick base pairs formed by complementary bases, it is possible that there can be some non Watson-Crick base pairing interactions.[4,5] Due to the hydrogen bonding donor and acceptor capabilities of all the bases in RNA, RNA hairpins allow additional non Watson-Crick base pairing between the bases (such as G-U or G-A or G-T).[1,2] These particular types of base pairing interactions, known as wobble base pairing, happen when the overall structure of the hairpin is not stable and can promote non-canonical base pairing interactions. Other interactions, such as phosphate-base and sugar-base interactions, are possible, especially in RNA hairpins.

The thermodynamic stability of nucleic acid hairpins depend on stem size, loop size, stem and loop composition, base stacking, base-pairing, hydrogen bonds on the loop and the closing base-pair of the loop.[6-11] Hairpins comprised of four bases in the loop region, referred to as tetraloops, have been widely studied in the literature.[10,12-36] Due to their exceptional thermal stabilities, DNA and RNA tetraloop hairpins play vital roles in biological functions.[3,32]Because of their key roles in RNA and protein folding, RNA tetraloops have received much attention. The important role of DNA tetraloops in nucleic acid folding and in genome sequences has also been studied.

An important area of current research in biopolymer science is the study of the biological processes by which DNA or RNA molecules form their secondary structures such as hairpins.[37] This research aims to understand the energetics and mechanisms involved, as well as the kinetics of individual steps of the processes.[37]Additionally, the research seeks to understand the dynamics, the stability and factors which affect the stability of such structures.

As hairpins are a common secondary structure for RNA, an understanding of the structural and dynamic aspects of RNA hairpin folding and behavior helps in understanding the folding of larger RNA molecules.[37] The RNA folding process is complex, with a rugged underlying governing energy landscape, especially in the early stages of the RNA folding process.[38,39]

An excellent model system for studying the interactions that stabilize polynucleotide secondary structures is provided by short nucleotides which form hairpin structures in solution.[37] Short DNA and RNA hairpin structures are excellent model systems for research aimed at gaining a better understanding of many aspects of oligonucleotides. Hairpin structures are useful in testing energy-based structure prediction algorithms [40,41]and in evaluating models for the molecular dynamic simulation of nucleic acids.[37,42,43]

1.2 Significance of Nucleic Acid hairpins in Biology

1.2.1 Central Dogma of Molecular Biology

The central dogma, the keystone of molecular biology was first stated by Francis Crick in 1958 and later restated by him in 1970.[44]It states that "The central dogma of molecular biology deals with the detailed residue-by-residue transfer of sequential information. Such information cannot be transferred back from protein to either protein or nucleic acid".[44]The most significant functions of nucleic acids described by the dogma are that the genetic information encoded in DNA is transcribed to RNA, which in turn can be used for protein synthesis, as illustrated in Figure 1.2. Nucleic acid hairpins, which are secondary structures, play pivotal roles in

variousbiological functions such as transcription, replication, translation etc.[1,45] Some of the important biological functions carried out by DNA and RNA hairpins are described below.

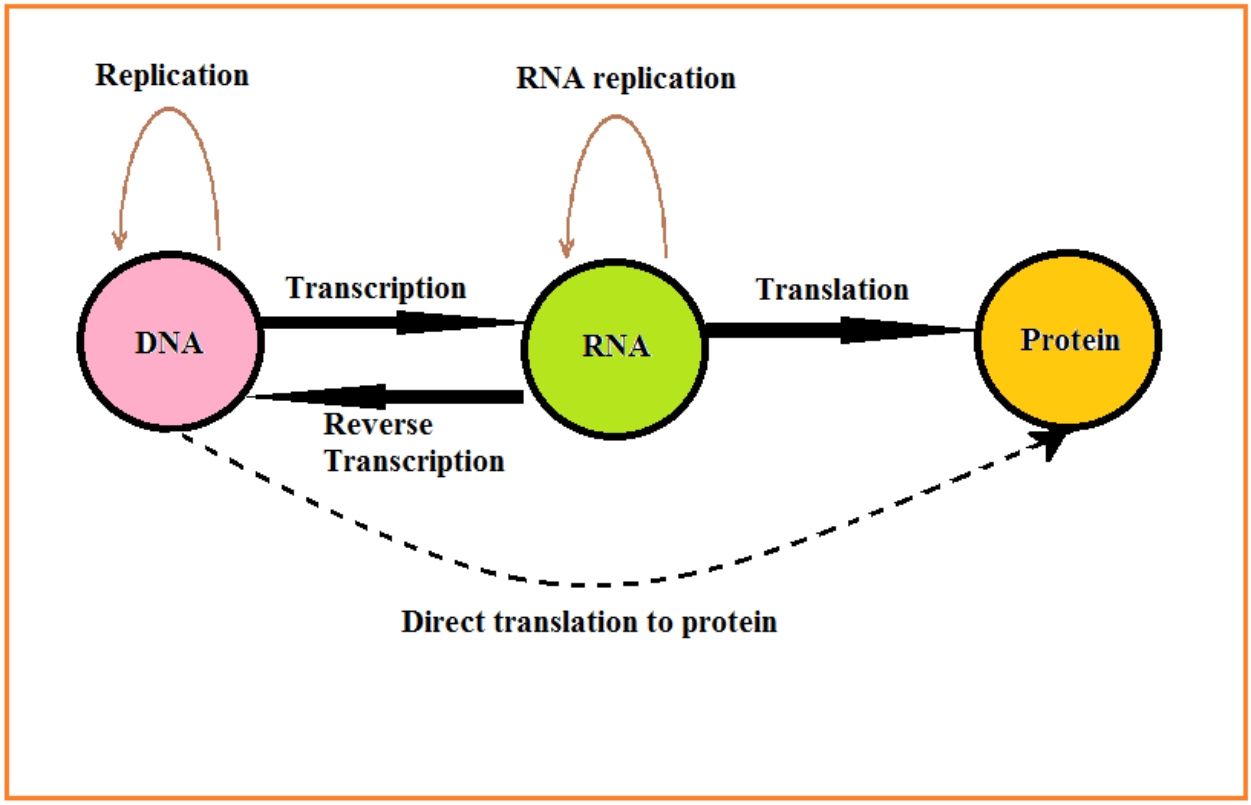

Figure 1.2: Illustration of the central dogma of molecular biology stated by Francis Crick in 1970. Flint, S. J.; Enquist, L. W.; Racaniello, V. R.; Skalka, A. M. The Figure is adopted from *Principles of Virology: Molecular Biology, Pathogenesis, and Control of Animal Viruses* (2nd ed.). Washington, D.C.: ASM Press. p. 217-218. ISBN 1-55581-259-7.

1.2.2 Biological functions of DNA hairpins

DNA hairpins have been shown to have numerous functions in cell biological processes, including: serving as intermediates in genetic recombination,[46-48]serving as protein recognition sites and regulating transcription, *in vivo.*[49,50]In most of the molecular biology phenomena such as transcription, replication, recombination and DNA repair etc., DNA remains partially single stranded.[42] Short ssDNA hairpins are useful drug targets because they differ significantly in geometry and shape from regular double-stranded DNA.

An example of a harmful role of hairpin structures is the formation of DNA hairpins by GC-rich triplet repeats which expand excessively during DNA replication and leads to several genetic diseases.[51]For example, neurological disorders such as Huntington's disease is believed to occur due to triplet repeat expansions.[52] Therefore, the understanding of the kinetics and thermodynamics of hairpin formation is essential to rationalize biological functions.

1.2.2.1 The biological role of DNA hairpin in the replication process

DNA is replicated by a mechanism, known as "rolling circle replication" during E.coli conjugation and the reproduction of certain viruses.[53] Multiple copies of circular molecules of nucleic acids - such as plasmids, the genomes of bacteriophages (phagemids) and the circular RNA genome of viroids- can be rapidly synthesized by the rolling circle replication process.[53]In this mechanism, the initiator protein, or Rep. proteinbinds a hairpin formed by a double-stranded origin (dso). The initiator protein nicks the DNA and covalently remains bound to the 5' phosphate end and the 3' OH is extended by DNA polymerase. The replication proceeds around the circular DNA by using an unnicked strand. The 5' end is replaced and forms a single

stranded DNA. Finally, the RNA polymerase binds with a single stranded origin (sso) hairpin to synthesize a RNA primer for replication.[53]Figure 1.3 shows the illustration of a rolling circle replication mechanism by DNA hairpin and Figure 1.4illustrates the hairpin formation during the replication process.[53]

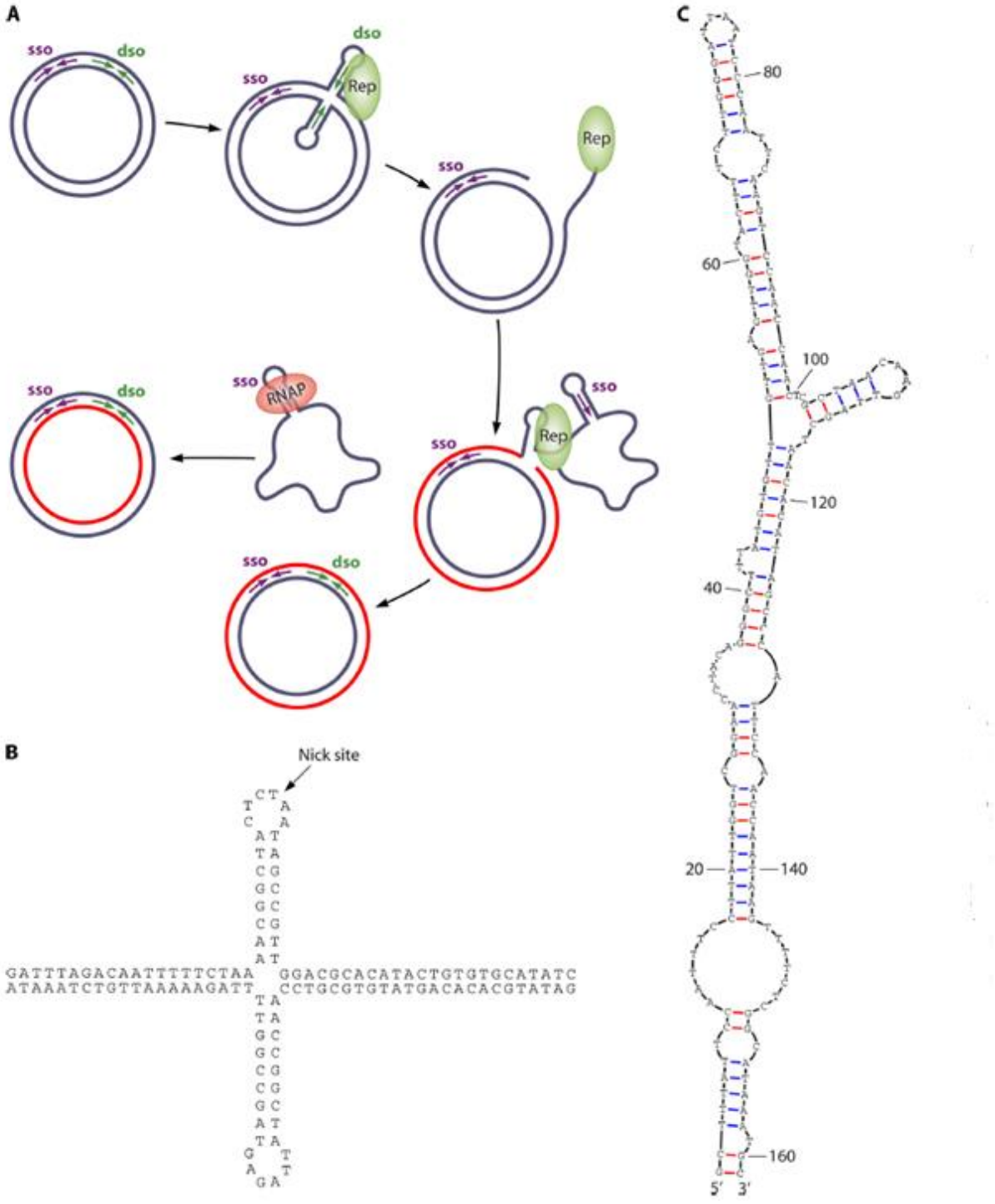

Figure 1.3: (A) Illustration of rolling circle replication by a single stranded DNA hairpin. (B) The plasmid pT 181 dso in cruciform conformation and (C) The pT 181 sso as folded by mfold software. The figure is adopted from Bikard *et al*.[53]

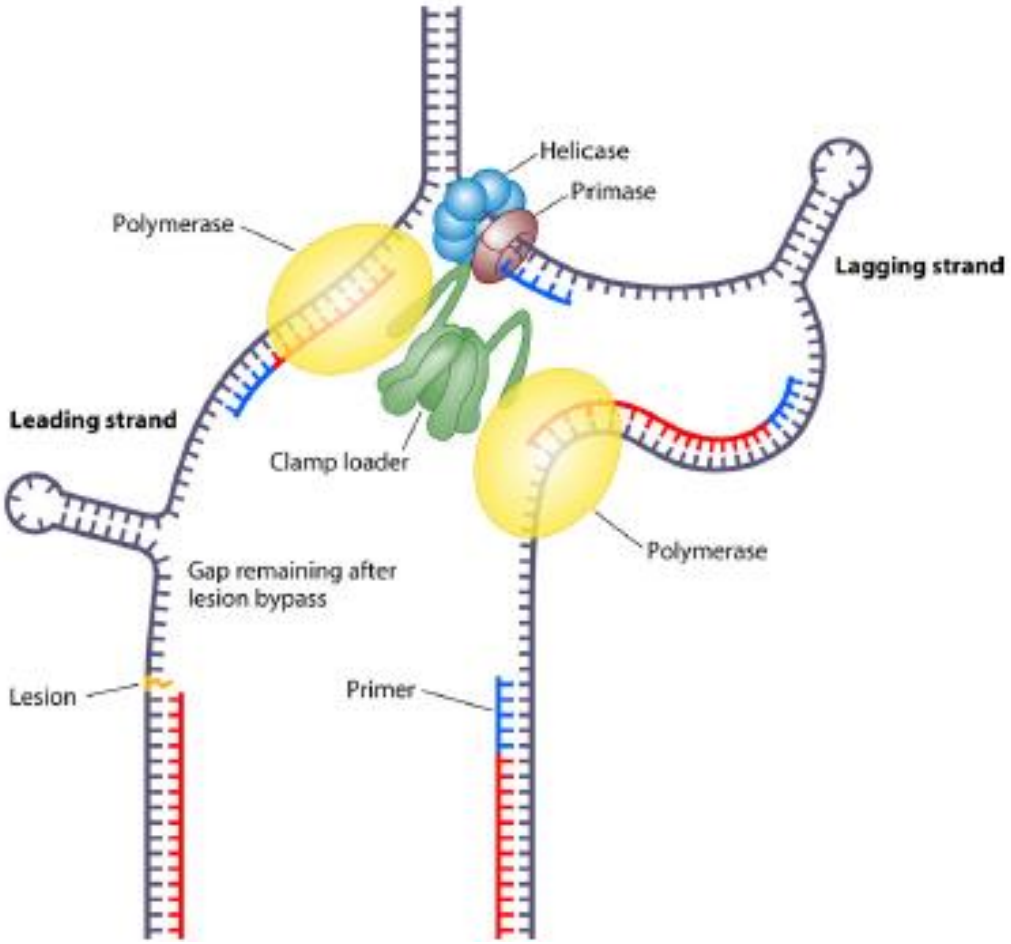

Figure 1.4: Illustration of hairpin formation during the replication process. The figure is adopted from Bikard*et al*.[53]

1.2.3 Biological functions of RNA hairpins

RNA hairpins perform numerous biological functions. They assist in the folding of complex molecules such as the ribozyme, terminate the transcription process, and play an essential role in the final translation.[1]The population of ribozymes and riboswitches can be modulated by RNA hairpin folding and, in this way, hairpins alter gene expression.

RNA hairpins usually have very high thermo stability.[54,55] The roles of RNA hairpins are to keep mRNAs from being degraded[56-58] and also serve as nucleation sites where RNA folding is initiated.[59-60]The RNA secondary structures (hairpins and bulges) interact to form the RNA tertiary structures which regulate numerous activities, including catalysis, ligand binding and RNA-protein recognition.[61,62]

1.2.3.1 Biological function of hairpin ribozyme

The hairpin ribozyme is one of the most important small RNAs and has been very widely studied.[63]Its biological function is to catalyze RNA processing reactions required in replicating the viral satellite RNA molecules of which it is a part and aids in tertiary folding processes.[63] The docking, which is due to the intimate association of loops A and B (shown in Figure 1.5 a),[63] is stabilized by divalent metal ions, such as Mg^{2+}, and helps in catalysis.Figure1.5 b) shows the catalysis process of reversible cleavage of a specific phosphodiester bond of a RNA substrate.[63]The hairpin ribozyme plays a pivotal role in catalyzing the ligation reaction.[63] The hairpin ribozyme is folded into a stable three-dimensional structure and, in the process, favors the ligation reaction.

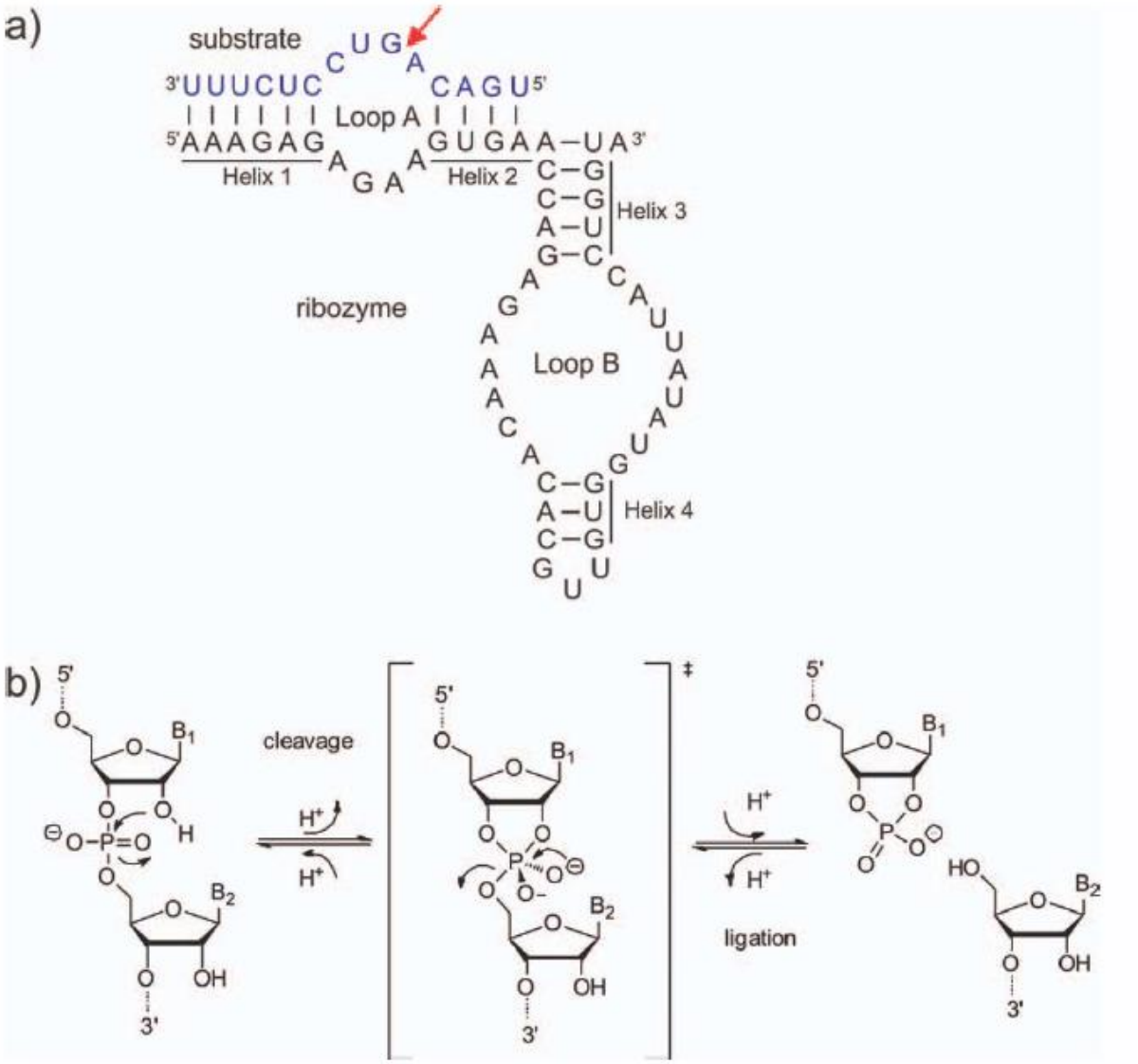

Figure 1.5: a) The hairpin ribozyme secondary structure. **b)** Illustration of reversible phosphodiester cleavage mechanism. These figures have been adopted from Muller *et al*.[63]

1.2.3.2Cellular functions of unstructured RNA

The unstructured RNA molecules control gene expression and perform important biological functions, for example, gene expressions by complementary base pairing with coding and non-coding regions on mRNA.[1,64] Most importantly, the unstructured RNAs form complexes with peptides to affect various cellular functions such as gene regulation and gene recombination etc,[1]

.

1.3 Motivation of Our Experimental Investigations

1.3.1 DNA/RNA Hairpin Folding Problems/puzzles

Biomolecular folding in general, and nucleic acid hairpin folding in particular, have been subjects of extensive theoretical and experimental investigations over the years.[4,5,7,65-81] DNA and RNA hairpins serve as important model systems for studying the dynamic properties of complex biomolecules. Since the majority of the secondary structure motifs consist of nucleic acid hairpins, kinetic and thermodynamic measurements on these hairpins provide greater insights into the conformational dynamics of the nucleic acids and the molecular basis for this biological process of hairpin formation.[1]Over a decade, numerous experimental techniques, such as Fluorescence Correlation Spectroscopy (FCS),[65,66,82] optical trapping,[83,84] temperature-jump spectroscopy[85,86] and various other single molecule techniques,[84,87] have been employed to decipher and measure the kinetics of hairpin formation. Similarly, several theoretical methods such as molecular dynamics simulations[78,88,89] have been used to understand hairpin conformation and dynamics.

The major focus of the above described studies have concentrated on the size and sequences of the stem and loop regions of the hairpins which affect the time scale of folding kinetics and reaction mechanisms. The ultimate goal of these investigations has been to understand and explain the nature of the free energy landscape associated with the folding and unfolding phenomena.[90,91] In the past, the DNA hairpin folding kinetics has been described predominantly as a two-state process with a single-barrier free energy folding landscape.[92-94] The two-state kinetic model, based on a simple energy landscape, hypothesized that the loop formation was the rate limiting step, followed by rapid zippering of the fully base-paired stem. Later, this simple two-state model was challenged by ultra-fast techniques, such as FCS[82,95] and temperature jump,[85,86] as well as some theoretical simulation studies based on more complicated energy landscapes.[96,97] The reviews of these findings briefly described below, with a notion that our understanding of hairpin folding kinetics and thermodynamic studies is still incomplete. Although we have gained tremendous insight into this area of research, many questions are not yet fully answered. In light of these long standing debates on hairpin folding and unfolding, I will describe our motivation for undertaking these dissertation projects seeking to help answer some of the important questions of this bigger folding puzzle.

In 1998, Bonnet et al.[65] studied the folding kinetics of five base-pair (bp) stem and variable polythymidine loops in solution by using FCS. It was hypothesized that the DNA hairpin folding is a two-state process and that the time scale for the hairpin unfolding is on the order of 10 microseconds. Later, in 2005-2006, our research laboratory used FCS[95] to study the folding and unfolding kinetics of DNA hairpins containing a 5-bp stem and 21 nucleotide polythymidine loop. The reaction times observed in those studies were consistent with the previous studies of similar sized hairpins. However, careful analysis of FCS data combined with

Photon Counting Histogram (PCH) analysis showed, although indirectly, that the overall reaction involving fully folded hairpins occurred on a longer time scale than the FCS observable time window. These investigations concluded that the DNA hairpin folding may be more than a two-state process but, due to the time resolution problem of FCS, these experiments could not probe longer time scales.

Ansari and coworkers[7,8,94] conducted laser-induced temperature-jump spectroscopy to investigate the folding kinetics of DNA hairpins having five base-pairs in the stem and variable polythymidine nucleotides (4-12) in the loop regions. The hairpin kinetics was explained by configuration interaction model instead of a previous Markovian two-state model. The configuration interaction model hypothesized that the stable loop formation in the hairpin is hindered by transient trapping into short-lived misfolded states before the hairpin can correctly fold to the native hairpin structure. This model further stated that the unfolded and folded forms of the DNA hairpin represent energy minima and that the transition state ensemble of trapped intermediate states forms a rugged barrier between minima of the DNA energy landscape. Consistent with the previous FCS experiment by Bonnet et al., Ansari's T-jump results reported folding and unfolding time constants on the order of 10 microseconds.

In 2006, Ma etal.[86] explored the energy landscape of a small tetraloop hairpin and proposed four-state mechanism to explain the non-exponential behavior of the RNA folding kinetics. Their proposed four-state reaction mechanism includes an ensemble of reaction intermediates having partially or misfolded stem structures, the fully folded hairpin, an ensemble of fully unfolded state and another intermediate state of misfolded hairpin loop. Significantly, the proposed intermediate states proposed by these authors were stable and long-lived, in contrast to short-lived trapped states proposed by Ansari's configuration interaction model. The notion of

kinetic trapped states containing partially or misfolded states, which can be stable for prolonged period of time, is consistent with the hypothetical free energy landscape proposed by Zewali and coworkers and illustrated in Figure 1.6 below.

Schultz and coworkers[87] investigated the life times of both the unfolded random-coil state and the completely folded state of longer stem DNA hairpins by using an immobilized single-molecule fluorescence resonance energy transfer (smFRET) method. Because of the limitations of the time resolution limitation in their smFRET measurement and also the fact that relatively few events (less than 100 smFRET events for both the hairpins) were monitored, the single molecule experiment could not observe any intermediates.

Similarly, numerous theoretical simulations and calculations have been carried out by various research groups over the years to examine folding and unfolding kinetics of the nucleic acid hairpins. Recently, Pande and coworkers,[78] used replica exchange molecular dynamics (SRMED) simulations to investigate the unfolding and refolding of a small RNA hairpin (5'-GGGCGCAAGCCU-3'). Their findings suggest the existence of intermediate states and competing folding/unfolding pathways. But again due to the time resolution issues, their simulations could not probe the time scale in milliseconds directly. In 2010, Portella et al.[89] studied the folding landscape of small DNA hairpin by using molecular dynamics simulation and proposed multiple routes for hairpin folding. Chen and coworkers[2,67,68] extracted the complete conformational states of small hairpins by using a statistical mechanics approach and proposed several sets of conditions under which an overall reaction could give rise to different exponential relaxation processes.

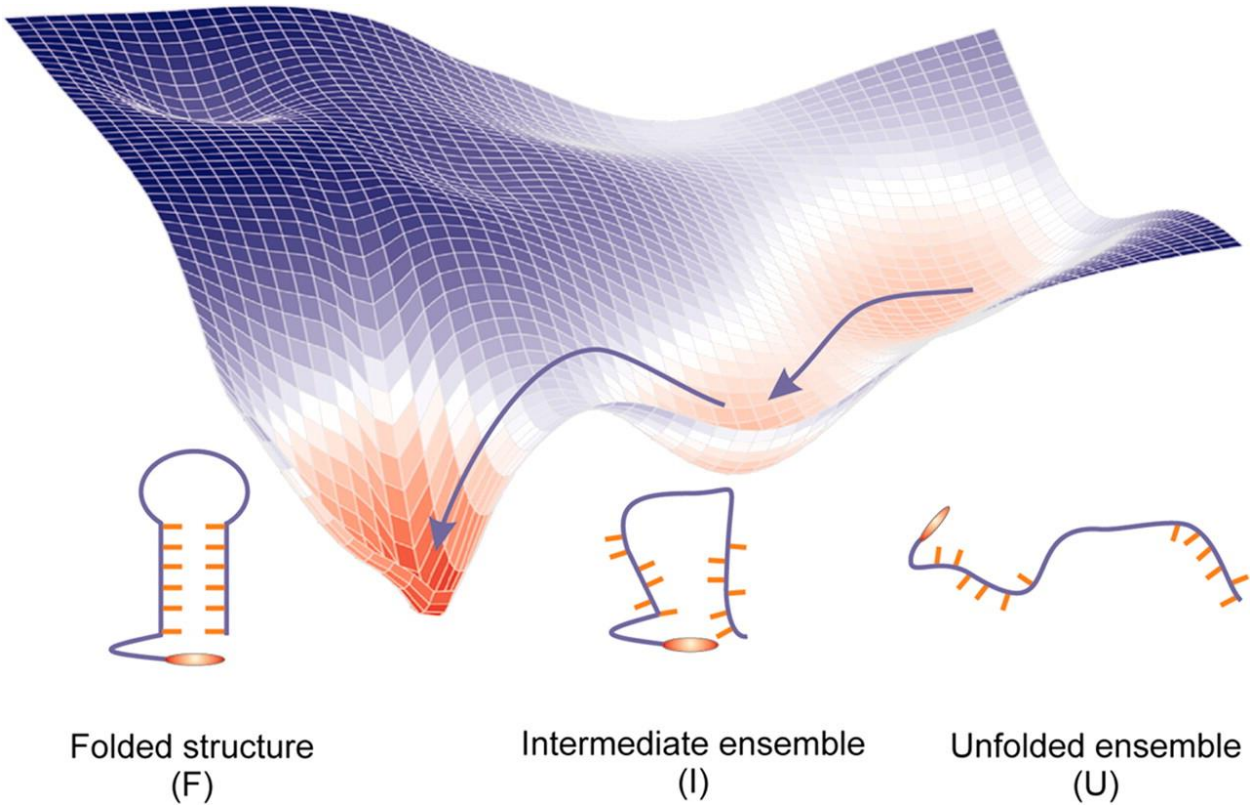

Figure1.6: A hypothetical energy landscape diagram for nucleic acid hairpin folding and melting. The multiple local minima in the free energy surface illustrate folded structure, unfolded structure and intermediate ensemble. The above Figure has been adopted from Ma *et al*.[86]

1.3.2Motivation for Rapid-Mixing Stopped-flow Studies

In the past couple of decades, there have been extensive experimental and theoretical investigations on how nucleic acid hairpins fold and unfold. Yet, several questions remain unanswered or controversial. FCS and T-jump spectroscopy are good techniques for measuring reaction times ranging from tens of nanoseconds to hundreds of microseconds. The time resolution constraints make these two techniques unsuitable for measuring folding and unfolding dynamics of hairpins occurring on a longer time scale of millisecond and beyond. Previous FCS studies in our laboratory indirectly proposed that the DNA hairpin folding is not simply a two-state process but due to the time resolution limitation could not prove it directly. Similarly T-jump studies described above and various theoretical simulation studies on DNA and RNA hairpins suggested complicated energy landscape for nucleic acid folding and unfolding, but failed to probe the formation of the fully folded hairpin which may be occurring on a longer time scale.

These factors motivated us to investigate the folding and unfolding kinetics of nucleic acid hairpins by using rapid-mixing stopped-flow kinetics, a technique for measuring reaction kinetics on a millisecond time scale. The limitation of this technique is that, it cannot measure the reaction kinetics on very fast time scale. However, it can serve as a complementary technique to other ultra-fast techniques, such as T-jump spectroscopy and FCS, so that together, the complete folding trajectory of nucleic acid hairpin formation can be probed over its full time scale.

1.4 Organization of the dissertation

The main objectives of these dissertation projects are to gain insight into the folding kinetics and thermodynamic stability of nucleic acid hairpins. Over the years, there have been numerous debates and discussions concerning DNA/RNA folding kinetics, reaction mechanisms and time scales of folding and unfolding. Yet, there are several unanswered questions and controversies regarding time scales of folding and reaction mechanisms etc. The rapid-mixing stopped-flow kinetics, thermodynamic melting experiments, other spectroscopic techniques along with kinetic modeling as well as some theoretical analysis have been carried out to answer some of the important questions on nucleic acid hairpin folding kinetics and reaction mechanisms.

In **Chapter 2,** the basic principle of rapid-mixing stopped-flow experiments and a brief description of the stopped-flow experimental set-up are presented. This chapter also presents the derivation of two-state and three-state reactions, used for kinetic modeling and analyzing experimental data.

Chapter 3 describes the investigation of the kinetics of DNA hairpin folding as a function of mono-valent counter ion concentration (NaCl) and our proposed three-state reaction mechanism by using rapid-mixing stopped flow techniques, thermodynamic melting experiments and kinetic modeling. The DNA hairpin used for these studies is a five base pair stem and twenty one polythymidine in the loop region and the construct is described as 5'-AACCCTTTTTTTTTTTTTTTTTTTTTGGGTT-3'. The 5' and 3' regions of the hairpin were labeled with fluorescent dye tetra methyl rhodamine (TAMRA) and dabcyl quencher respectively. The most important observation of this investigation is that The DNA hairpin

folding is at least a three-state process and the DNA hairpin formation can occur much more slowly than previously thought. The research presented in this chapter has been published in the Journal of American Chemical Society.

Chapter 4 describes the investigation of the loop length and the counter ion dependent thermodynamics and kinetics of various DNA hairpins. The DNA hairpins examined in these studies consisted of a five base pair stem with the complementary sequences 5'-AACCC and GGGTT-3' and loops containing 4, 8, 12 and 21 polythymidine [poly(dT)] residues. The major findings in these studies are: the stability of all the hairpins increases with increasing counter ion concentrations, and that the stability increases with decreasing loop size. In the case of tetra loop hairpins, the stability pattern depends on the counter ion concentration regime. For counter ion concentrations of 25 mM NaCl and below, the stability of the tetraloop hairpin follows the same trend as that observed for the longer loop length hairpins. However, above 25 mM NaCl, the tetraloop hairpins exhibit exceptional thermodynamic stability above and beyond that observed in longer loop length hairpins. The unusually high stability of tetraloop hairpins in the high counter ion concentration regime is explained by the base- stacking effect in the loop regions due to hydrophobic collapse in the more polar environment. The research presented in this chapter is under minor revision in the Journal of Physical Chemistry B and is likely to be published.

Chapter 5 describes the investigation of RNA hairpin folding kinetics as a function of varying KCl concentrations. The RNA hairpins investigated in these studies consisted of identical four base pair stem with the complementary sequences 5'-CGGU and GCCG-3' and loop regions containing three different sequences of 15 base pair nucleotides. The major finding of these studies is that, for hairpins of comparable loop and stem size, the folding kinetics of RNA hairpins is much more complex than that of DNA hairpins studied in chapters 3 and 4.The

evidence of complex reaction kinetics and mechanisms is understandable, considering that the energy landscape of RNA is much more complex than that of DNA and is similar to protein energy landscapes. The research of this chapter has been prepared as a manuscript for publication.

Chapter 6 concludes by summarizing the dissertation and briefly discusses the future directions of biomolecular folding /unfolding studies and the impact of such studies on molecular biology research in the future.

REFERENCES

(1) Bevilacqua, P. C.; Blose, J. M. *Ann. Rev. Phys. Chem.***2008**, 59, 79.

(2) Chen, S. J. *Ann. Rev.Biophys.***2008**, 37, 197.

(3) Varani, G. *Ann. Rev. Biophys. Biomol. Struct.***1995**, 24, 379.

(4) Ansari, A.; Kuznetsov, S. V.; Shen, Y. *Proc. Natl. Acad.Sci.USA***2001**, 98, 7771.

(5) Kuznetsov, S. V.; Ansari, A. *Biophys. J.***2012**, 102, 101.

(6) Vallone, P. M.; Paner, T. M.; Hilario, J.; Lane, M. J.; Faldasz, B. D.; Benight, A. S. *Biopolymers***1999**, 50, 425.

(7) Shen, Y.; Kuznetsov, S. V.; Ansari, A. *J. Phys. Chem.B***2001**, 105, 12202.

(8) Kuznetsov, S. V.; Shen, Y.; Benight, A. S.; Ansari, A. *Biophys. J.***2001**, 81, 2864.

(9) Ansari, A.; Shen, Y.; Kuznetsov, S. V. *Phys. Rev. Lett.***2002**, 88, 069801.

(10) Moody, E. M.; Bevilacqua, P. C. *J. Am. Chem. Soc.***2003**, 125, 2032.

(11) Moody, E. M.; Bevilacqua, P. C. *J. Am. Chem. Soc.***2003**, 125, 16285.

(12) Abdelkafi, M.; Leulliot, N.; Baumruk, V.; Bednarova, L.; Turpin, P. Y.; Namane, A.; Gouyette, C.; Huynh-Dinh, T.; Ghomi, M. *Biochemistry***1998**, 37, 7878.

(13) Rife, J. P.; Cheng, C. S.; Moore, P. B.; Strobel, S. A. *Nucleic Acids Res.***1998**, 26, 3640.

(14) Leulliot, N.; Ghomi, M.; Jobic, H.; Bouloussa, O.; Baumruk, V.; Coulombeau, C. *J. Phys. Chem.B***1999**, 103, 10934.

(15) Williams, D. J.; Hall, K. B. *Biophys. J.***1999**, 76, 3192.

(16) Shu, Z.; Bevilacqua, P. C. *Biochemistry***1999**, 38, 15369.

(17) Kim, C. H.; Tinoco, I. *Proc. Natl. Acad.Sci.USA***2000**, 97, 9396.

(18) Dale, T.; Smith, R.; Serra, M. J. *RNA***2000**, 6, 608.

(19) Ennifar, E.; Nikulin, A.; Tishchenko, S.; Serganov, A.; Nevskaya, N.; Garber, M.; Ehresmann, B.; Ehresmann, C.; Nikonov, S.; Dumas, P. *J. Mol. Biol.***2000**, 304, 35.

(20) Williams, D. J.; Hall, K. B. *J. Mol. Biol.***2000**, 297, 1045.

(21) Li, W.; Ma, B. Y.; Shapiro, B. A. *J. Biomol. Struct. Dynam.***2001**, 19, 381.

(22) Hannoush, R. N.; Damha, M. J. *J. Am.Chem. Soc.***2001**, 123, 12368.

(23) Zacharias, M. *Biophys. J.***2001**, 80, 2350.

(24) Kawakami, J.; Yoneyama, M.; Miyoshi, D.; Sugimoto, N. *Chem. Lett.***2001**, 258.

(25) Sorin, E. J.; Engelhardt, M. A.; Herschlag, D.; Pande, V. S. *J. Mol. Biol.***2002**, 317, 493.

(26) Young, B. T.; Silverman, S. K. *Biochemistry***2002**, 41, 12271.

(27) Proctor, D. J.; Schaak, J. E.; Bevilacqua, J. M.; Falzone, C. J.; Bevilacqua, P. C. *Biochemistry***2002**, 41, 12062.

(28) Mundoma, C.; Greenbaum, N. L. *J. Am.Chem. Soc.***2002**, 124, 3525.

(29) Nakano, M.; Moody, E. M.; Liang, J.; Bevilacqua, P. C. *Biochemistry***2002**, 41, 14281.

(30) Correll, C. C.; Swinger, K. *RNA***2003**, 9, 355.

(31) Santini, G. P. H.; Pakleza, C.; Cognet, J. A. H. *Nucleic Acids Res.***2003**, 31, 1086.

(32) Hernandez, B.; Baumruk, V.; Gouyette, C.; Ghomi, M. *Biopolymers***2005**, 78, 21.

(33) Sarzynska, J.; Kulinski, T. *J. Biomol. Struct. Dyn.***2005**, 22, 425.

(34) Sarkar, K.; Meister, K.; Sethi, A.; Gruebele, M. *Biophys. J.* **2009**, 97, 1418.

(35) Blose, J. M.; Proctor, D. J.; Veeraraghavan, N.; Misra, V. K.; Bevilacqua, P. C. *J. Am.Chem. Soc.***2009**, 131, 8474.

(36) Sheehy, J. P.; Davis, A. R.; Znosko, B. M. *RNA***2010**, 16, 417.

(37) Stroscio, M. A.; Dutta, M. *Biological nanostructures and applications of nanostructures in biology: electrical, mechanical, and optical properties*; Springer, **2004**; Vol. 2.

(38) Zhuang, X.; Bartley, L. E.; Babcock, H. P.; Russell, R.; Ha, T.; Herschlag, D.; Chu, S. *Science***2000**, 288, 2048.

(39) Thirumalai, D.; Lee, N.; Woodson, S. A.; Klimov, D. *Ann. Rev. Phys. Chem.***2001**, 52, 751.

(40) Mathews, D. H.; Sabina, J.; Zuker, M.; Turner, D. H. *J. Mol. Biol.* **1999**, 288, 911.

(41) Turner, D. H.; Sugimoto, N.; Freier, S. M. *Ann. Rev. Biophys. Biophys. Chem.***1988**, 17, 167.

(42) Sorin, E. J.; Rhee, Y. M.; Nakatani, B. J.; Pande, V. S. *Biophys. J.***2003**, 85, 790.

(43) Srinivasan, J.; Miller, J.; Kollman, P. A.; Case, D. A. *J. Biomol. Struct. Dyn.* **1998**, 16, 671.

(44) Crick, F. *Nature***1970**, 227, 561.

(45) Svoboda, P.; Cara, A. D. *Cellular and Molecular Life Sciences CMLS***2006**, 63, 901.

(46) Lilley, D. M. *Nucleic Acids Res.* **1981**, 9, 1271.

(47) Roemer, R.; Schomburg, U.; Krauss, G.; Maass, G. *Biochemistry***1984**, 23, 6132.

(48) Roth, D. B.; Menetski, J. P.; Nakajima, P. B.; Bosma, M. J.; Gellert, M. *Cell***1992**, 70, 983.

(49) Dai, X.; Greizerstein, M. B.; Nadas-Chinni, K.; Rothman-Denes, L. B. *Proc. Natl. Acad.Sci.USA***1997**, 94, 2174.

(50) Dai, X.; Kloster, M.; Rothman-Denes, L. B. *J. Mol. Biol.***1998**, 283, 43.

(51) Gacy, A. M.; Goellner, G.; Juranic, N.; Macura, S.; McMurray, C. T. *Cell***1995**, 81, 533.

(52) Sinden, R. R.; Potaman, V. N.; Oussatcheva, E. A.; Pearson, C. E.; Lyubchenko, Y. L.; Shlyakhtenko, L. S. *J. Biosci.***2002**, 27, 53.

(53) Bikard, D.; Loot, C.; Baharoglu, Z.; Mazel, D. *Microbiol. Mol. Biol. Rev.***2010**, 74, 570.

(54) Cheong, C.; Varani, G.; Tinoco, I. *Nature***1990**, 346, 680.

(55) Heus, H. A.; Pardi, A. *Science***1991**, 253, 191.

(56) Klausner, R. D.; Rouault, T. A.; Harford, J. B. *Cell***1993**, 72, 19.

(57) Alifano, P.; Bruni, C. B.; Carlomagno, M. S. *Genetica***1994**, 94, 157.

(58) Smolke, C. D.; Carrier, T. A.; Keasling, J. *Appl. Env. Microbiol.***2000**, 66, 5399.

(59) Uhlenbeck, O. C. *Nature***1990**, 346, 613.

(60) Sclavi, B.; Sullivan, M.; Chance, M. R.; Brenowitz, M.; Woodson, S. A. *Science***1998**, 279, 1940.

(61) Rupert, P. B.; Massey, A. P.; Sigurdsson, S. T.; Ferré-D'Amaré, A. R. *Science***2002**, 298, 1421.

(62) Lilley, D. M. *Trends in biochemical sciences***2003**, 28, 495.

(63) Müller, S.; Appel, B.; Krellenberg, T.; Petkovic, S. *IUBMB life***2012**, 64, 36.

(64) Matzke, M. A.; Birchler, J. A. *Nature Reviews Genetics***2005**, 6, 24.

(65) Bonnet, G. G.; Krichevsky, O.; Libchaber, A. *Proc. Natl. Acad.Sci.USA***1998**, 95, 8602.

(66) Jung, J.; Van Orden, A. *J. Phys. Chem. B***2005**, 109, 3648.

(67) Zhang, W.; Chen, S.-J. *Biophys. J.***2006**, 90, 778.

(68) Zhang, W.; Chen, S.-J. *Biophys. J.***2006**, 90, 765.

(69) Garcia, A. E.; Paschek, D. *J. Am.Chem. Soc.***2007**, 130, 815.

(70) Kannan, S.; Zacharias, M. *Biophys. J.* **2007**, 93, 3218.

(71) Nayak, R. K.; Peersen, O. B.; Hall, K. B.; Van Orden, A. *J. Am.Chem. Soc.***2012**, 134, 2453.

(72) Narayanan, R.; Zhu, L.; Velmurugu, Y.; Roca, J.; Kuznetsov, S. V.; Prehna, G.; Lapidus, L. J.; Ansari, A. *J. Am.Chem. Soc.***2012**, 134, 18952.

(73) Pyle, A. M.; Green, J. B. *Current opinion in structural biology***1995**, 5, 303.

(74) Wallace, M. I.; Ying, L.; Balasubramanian, S.; Klenerman, D. *Proc. Natl. Acad. Sci.USA***2001**, 98, 5584.

(75) Zhang, W.; Chen, S. J. *Proc. Natl. Acad.Sci.USA***2002**, 99, 1931.

(76) Kim, J.; Doose, S.; Neuweiler, H.; Sauer, M. *Nucleic Acids Res.***2006**, 34, 2516.

(77) Liphardt, J.; Onoa, B.; Smith, S. B.; Tinoco, I.; Bustamante, C. *Science***2001**, 292, 733.

(78) Bowman, G. R.; Huang, X.; Yao, Y.; Sun, J.; Carlsson, G., Guibas, Leonidas J, Pande, V. S.*J. Am.Chem. Soc.***2008**, 130, 9676.

(79) Lin, M. M.; Meinhold, L.; Shorokhov, D.; Zewail, A. H. *Phys. Chem. Chem. Phys.***2008**, 10, 4227.

(80) Zuo, G.; Li, W.; Zhang, J.; Wang, J.; Wang, W. *J. Phys. Chem.B***2010**, 114, 5835.

(81) Yin, Y. D.; Wang, P.; Yang, X. X.; Li, X.; He, C.; Sheng, X. *Chem. Comm.***2012**, 48, 7413.

(82) Jung, J.; Ihly, R.; Scott, E.; Yu, M.; Van Orden, A.*J. Phys. Chem.B***2008,**112, 127.

(83) Woodside, M. T.; Anthony, P. C.; Behnke-Parks, W. M.; Larizadeh, K.; Herschlag, D.; Block, S. M. *Science***2006**, 314, 1001.

(84) Woodside, M. T.; Behnke-Parks, W. M.; Travers, K.; Larizadeh, K.; Herschlag, D.; Block, S. M. *Proc. Natl. Acad.Sci.USA***2006**, 103, 6190.

(85) Ma, H.; Proctor, D. J.; Kierzek, E.; Kierzek, R.; Bevilacqua, P. C.; Gruebele, M. *J. Am.Chem. Soc.* **2006**, 128, 1523.

(86) Ma, H.; Wan, C.; Wu, A.; Zewail, A. H. *Proc. Natl. Acad. Sci.USA***2007**, 104, 712.

(87) Grunwell, J. R.; Glass, J. L.; Lacoste, T. D.; Deniz, A. A.; Chemla, D. S.; Schultz, P. G. *J. Am.Chem. Soc.***2001**, 123, 4295.

(88) Ding, F.; Sharma, S.; Chalasani, P.; Demidov, V.; Broude, N.; Dokholyan, N. *RNA***2008**, 14(6), 1164.

(89) Portella, G.; Orozco, M. *Angew. Chem.***2010**, 122, 7839.

(90) Chen, S. J.; Dill, K. A. *Proc. Natl. Acad.Sci.USA***2000**, 97, 646.

(91) Gupta, A. N.; Vincent, A.; Neupane, K.; Yu, H.; Wang, F.; Woodside, M. T. *Nat. Phys.***2011**, 7, 631.

(92) Hilbers, C.; Haasnoot, C.; De Bruin, S.; Joordens, J.; Van Der Marel, G.; Van Boom, J. *Biochimie***1985**, 67, 685.

(93) Goddard, N. L.; Bonnet, G.; Krichevsky, O.; Libchaber, A. *Phys. Rev. Lett.***2000**, 85, 2400.

(94) Kuznetsov, S. V.; Ren, C. C.; Woodson, S. A.; Ansari, A. *Nucleic Acids Res.***2008**, 36, 1098.

(95) Jung, J.; Van Orden, A. *J. Am.Chem. Soc.***2006**, 128, 1240.

(96) Ditzler, M. A.; Rueda, D.; Mo, J.; Håkansson, K.; Walter, N. G. *Nucleic Acids Res.* **2008**, 36, 7088.

(97) Woodson, S. A. *Ann. Rev.Biophys.***2010**, 39, 61.

CHAPTER 2: Rapid-Mixing Stopped-Flow Kinetics

2.1 Introduction

Biological processes in general, and bio-molecular folding in particular, are complex processes. Nucleic acid and protein folding and unfolding occur over a broad range of time scales ranging from nanosecond to seconds and beyond.[98,99] To elucidate the structure, function and mechanism[100], information on time dependencies of molecular species over such a broad range of time scales is required[101]. Over the years, various equilibrium and relaxation methods have been employed to study nucleic acid folding and unfolding, such as FCS[102-106], T-Jump[107-112], NMR[113,114] and CD[115], etc. Ultra-fast techniques such as FCS and T-jump usually probe the reaction kinetics over the fast time scale of microseconds. If the folding and unfolding processes involve transient intermediate or meta-stable intermediate species of comparatively longer time scales, rapid-mixing methods are viable methods for studying the kinetics of biomolecular folding[116-119].

In the present studies, we employed rapid-mixing stopped-flow kinetics to study the kinetics of DNA and RNA hairpin folding. This chapter describes the rapid-mixing stopped-flow kinetics method and also describes the instruments and experiments.

2.1.1 Basic Principle of Stopped-flow Spectroscopy

Stopped-flow is a rapid-mixing spectroscopic technique used for studying fast reaction kinetics in solution over time scales ranging from milliseconds up to hundreds of seconds[116,120]. In stopped-flow, two reactant solutions are rapidly mixed together, by action of drive syringes,

and then stopped in an observation cell.[121]The flow in the observation cell is stopped by a stopping syringe. The sample cell is irradiated with monochromatic light and the chemical reaction is observed by monitoring the change in suitable signals such as absorbance and fluorescence as a function of time. The time that is required for the reactants and products to travel to the flow cell or spectrophotometer cell is known as "dead time".[122]The dead time of a stopped-flow instrument is the time between the mixing of the two solutions and the beginning of observation of the kinetics of the reaction. The dead time usually varies from 0.4 ms to 1 ms depending upon the design of the flow cell.[116]

Rapid-mixing stopped-flow fluorescence or absorbance, provides a method to monitor bio-molecular interactions.[123] The analysis of resulting kinetic transients obtained from the stopped-flow instrument can determine reaction rates, the complexity of the reaction mechanism, and information on short-lived reaction intermediates etc.[116] In general, the rapid-mixing stopped flow methods yield rate constants for conformational changes such as folding/unfolding of proteins and nucleic acids, ligand binding and ligand dissociation, etc.[121]

2.1.2 Schematic Description of Stopped-flow set up

The schematic diagram of a typical stopped-flow set up is presented in Figure 2.1.The instrument used in these studies was a commercially-built model SX-20 from Applied Photophysics, London. In stopped-flow experiments, usually a few hundred micro-liters of two reactants are contained in the drive syringes (A and B). For illustration, in the present hairpin folding and unfolding studies, the several nano-molar DNA/RNA solutions were introduced in the channel A and high and low salt buffers were introduced in the channel B (Please see experimental section of Chapter 3, 4 and 5 for details).

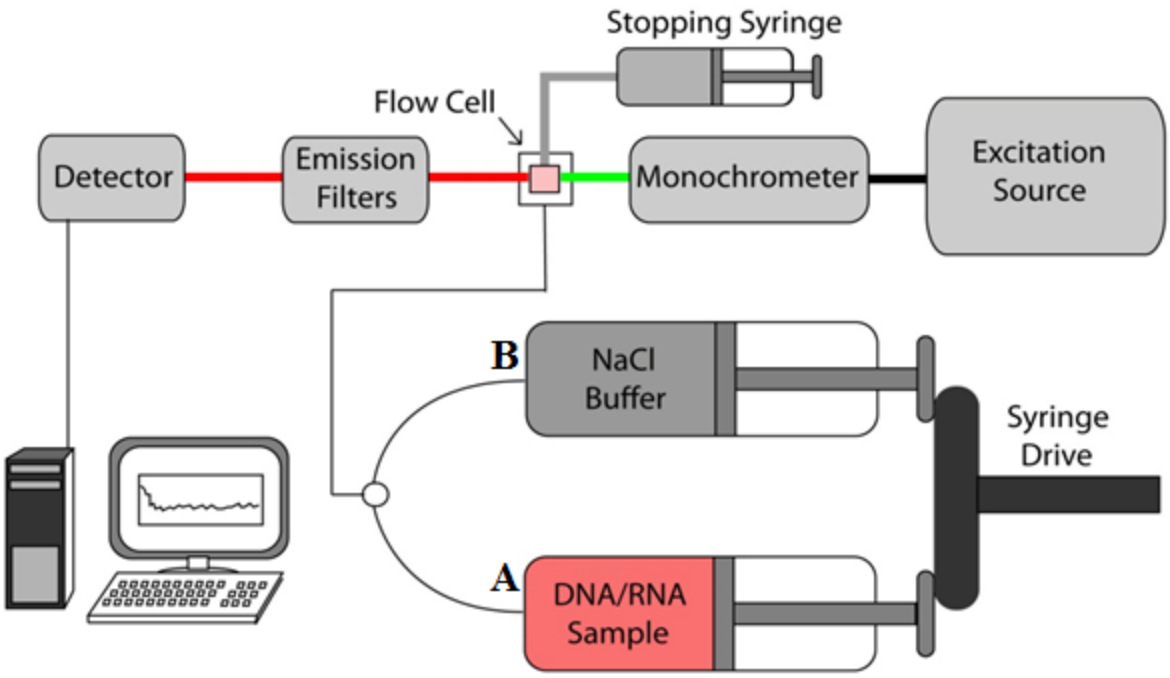

Figure 2.1: Schematic diagram of the rapid-mixing stopped-flow set up.

A syringe driver pushes the syringe pistons such that the reactants are pushed through a mixer and subsequently to the flow cell.[124]The new solution displaces the old solution from the observation cell. The stop-syringe is filled by the flow when the piston hits the trigger-switch. This action simultaneously stops the flow and starts the data acquisition. At this instant the age of the reaction of the newly mixed reactants in the observation cell is about a millisecond. The exact age, or famously called 'dead time', is dependent upon the stopped-flow design and the cell design.[123] Careful calibration of the instrumental dead time is required for the interpretation of rapid-mixing stopped-flow data. In our experimental set up, the dead time of 0.45 ms was achieved.[116]

In our hairpin folding experiments, reaction kinetics were measured by monitoring fluorescence as a function of time in milliseconds. Due to its greater sensitivity, fluorescence monitoring is commonly used in rapid-mixing stopped-flow studies. However, absorbance monitoring is sometimes used. Other biophysical techniques that have been implemented in rapid-mixing stopped-flow studies are FTIR,[125-127] CD,[128,129] NMR[130,131] and calorimetry[132,133]etc.

A typical rapid-mixing stopped-flow experiment involves mixing of equal volumes of two reactant solutions.[27] Therefore, in reporting concentration values, is important to remember that concentrations in the observation cell are half of those concentrations in the syringes.

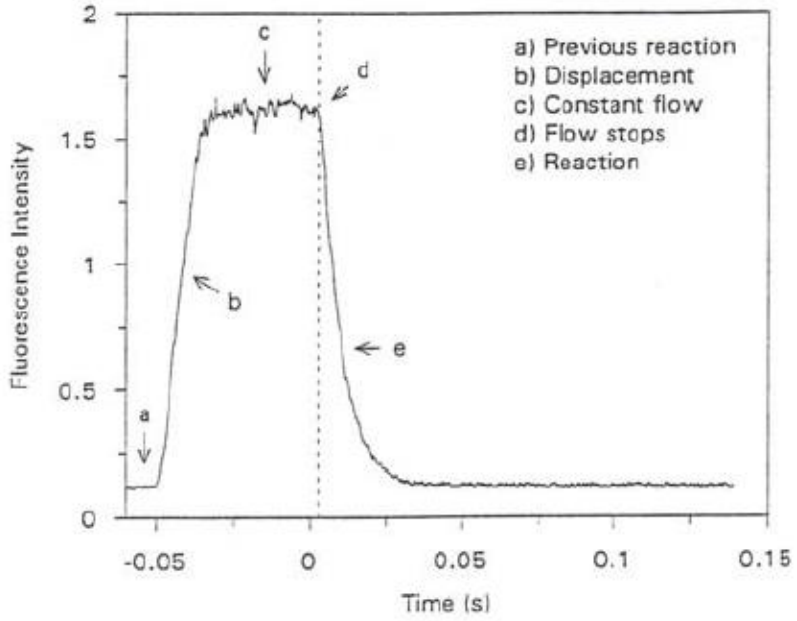

Figure 2.2:A typical stopped-flow trace showing the different phases of the observed signal. In this example, the recording was commenced at 50 ms before flow stopped in order to illustrate all the phases. This figure has been adopted from Eccleston et al.[121]

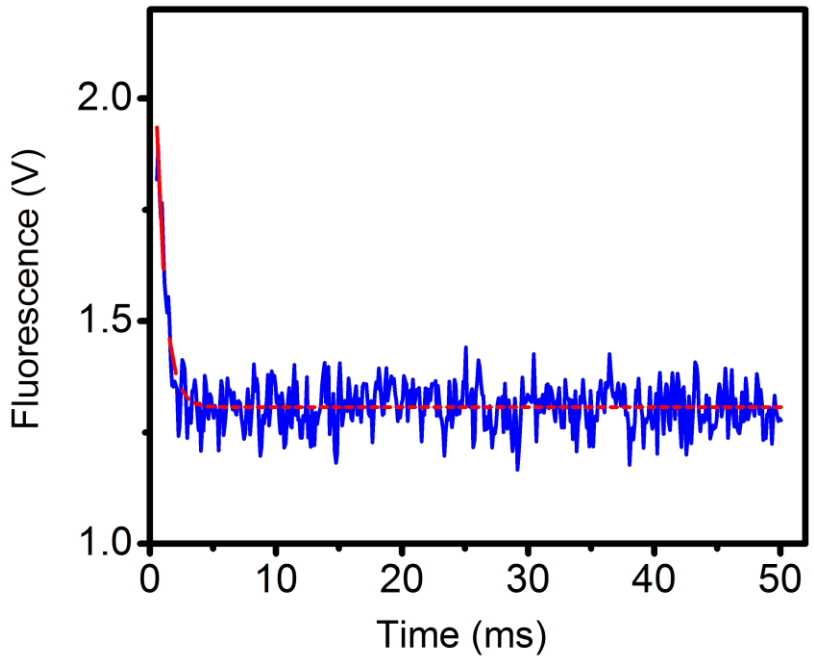

Figure 2.3: A typical stopped-flow trace showing the DNA hairpin folding reaction at 100 mM NaCl buffer. The fluorescence signals, which are the auto PMT voltages of the detector, are plotted as a function of time in milliseconds. This experiment was conducted with our SX20 stopped-flow spectrometer.

2.1.3 Major Parts of the Stopped-Flow Spectrometer

As described in Applied Photophysics technical manual,[134] a Xenon arc lamp is usually used to produce the high intensity light over a wide spectrum (far-UV to NIR region), as needed for fluorescence measurements. For specific applications, alternative light sources are sometimes used. The monochromator is used to select the wavelength of excitation light (directed to the mixed sample solution) used for fluorescence experiments, or the wavelength of interest for absorbance measurements.[37]

Figure 2.4shows a more detailed illustration of the optical cell in the Applied Photophysics SX-20 stopped-flow instrument. The T-mixer is an integral part of the cell in this design. For fluorescence detection, the cell has a dedicated observation window; for absorbance detection, two optical path lengths (1 mm and 5 mm or 2 mm and 10 mm) depending on the cell type, are available.[134]

Other major parts are the sample handling unit, detection system and water circulator.[134]The sample handling unit rapidly mixes the reactant solutions into the observation cell and initiates signal detection simultaneously with stopping of the flow. The detection system monitors and records the optical signal, usually by using one or more photomultiplier detectors. The water circulator regulates the temperature of the observation cell and the reactant solutions, so that experiments are conducted at a uniform temperature.

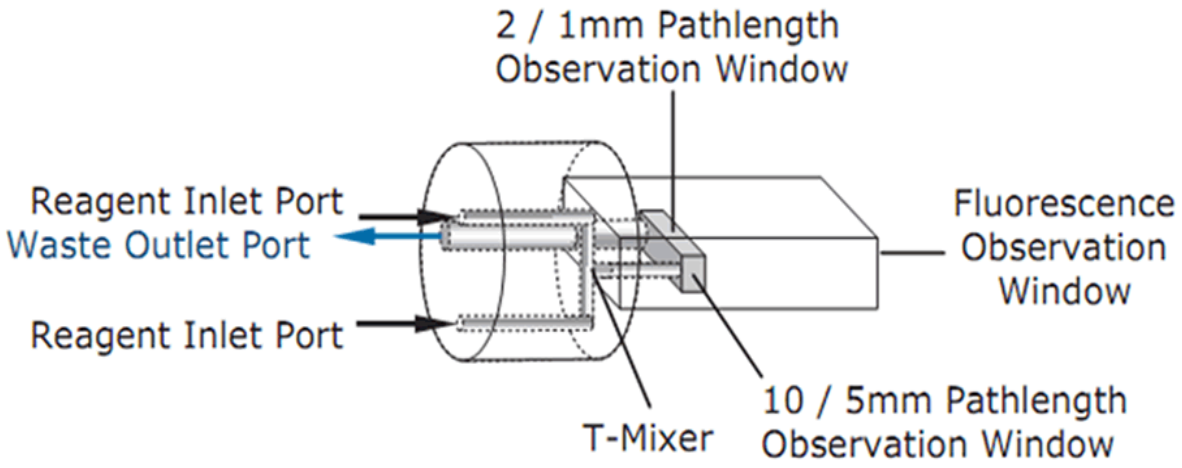

Figure 2.4: Illustration of the optical cell used in Applied Photophysics SX20 stopped-flow instrument. The above Figure has been adopted from Applied Photophysics[134]

2.1.4 Assessing the performance of a stopped-flow instrument

Several aspects of instrument design are key to instrument performance. The mixing chamber is designed to achieve both rapid and complete mixing of the reactant solutions.[121]Various flow geometries have been used in the design of mixing chambers, all with the goal of achieving turbulent flow in a small volume.[124] Turbulence is necessary for achieving mixing efficiency and also for maintaining favorable flow conditions during observation[121,124] and also insures that flow lines are efficiently purged between separate runs.[123,124] Thorough mixing of the reactant solutions needs to occur before the solution reaches the observation point, so that the observed rate of reaction is not limited by the mixing process.[124] Mixing efficiency can be tested by observing a reaction that is instantaneous on the stopped-flow time scale, such as a protonation reaction.[121] Lack of any observed sign of reaction, i.e. a constant signal, shows that complete mixing is occurring during the dead time of the instrument.[121]

The time after mixing in which the reaction cannot be measured is known as the "dead time".[116,122] Complete mixing of the reactants does not occur instantaneously and observation cannot begin precisely when reactants begin mixing.[121] Some finite period of time is required for the flow to travel the distance from the point where reactants begin mixing to the point where the optical signal is observed. Thus, when flow is stopped and measurement begins, the volume being observed in the optical cell has some "reaction age" associated with it.[124]In effect, this reaction age is "time lost", in the sense that the very first part of the reaction could not be observed.[121] Dead-times can be shortened by reducing the volume of the sample cell, but this will also reduce the sensitivity of the observed signal.[121,124,135]

2.1.5 Optimization of the stopped-flow instrument

High intensity light sources such as mercury, xenon, or xenon-mercury arc lamps are generally required as excitation light sources for fluorescence experiments.[121] The emission spectrum for xenon arc lamps is relatively smooth, whereas the emission spectra for mercury and mercury-xenon arc lamps have a series of very intense emission bands, which may be used to advantage, depending on the fluorophore being used.[121,124] Deuterium or quartz halide lamps, which have lower intensity outputs, are generally suitable for absorbance experiments but sometimes may be used for fluorescence excitation in the visible region with some fluorophores. Manufacturer's information on the relationship of light intensity and wavelength is helpful for making lamp selections.[121]

A photomultiplier (also called a photo-detector) is used to detect the emitted light after it has passed through a suitable optical filter, selected to pass only fluorescence emission light and to exclude any of the exciting light scattered by the solution.[124]Sources of scattered light are Rayleigh scattering of the exciting light and Raman scattering from the water. Appropriate band pass and/or cut-off filters should be chosen to maximize the fluorescence emission signal and minimize the scattered light signal.[121]Additionally, in a rapid kinetic experiment, it is important that the signal change should be maximized relative to the background intensity. Since the Tetra methyl rhodamine (TAMRA) was dye labeled for all of our nucleic acid folding and unfolding studies,[116] we used a 570 nm high pass emission filter purchased from Applied Photophysics, London, for the stopped-flow mixing experiments.

Selection of the monochromator slit width, which affects the intensity of the excitation light, is an aspect of the instrument operation that can be adjusted.[121,124] A balance between

spectral purity of the exciting light and the intensity of light transmitted is involved in selecting monochromator slit widths. For fluorophores having a large Stokes shift (the difference between the maximum excitation wavelength and the maximum emission wavelength), the light intensity can be increased by using a larger slit width. However, for fluorophores having a smaller Stokes shift, smaller slit widths are needed to exclude scattered light from the photo-detector.[124] An alternative approach for fluorophores with smaller Stokes shifts is to use shorter wavelengths of excitation light than the maximum wavelength.

If photobleaching of the fluorophore is a potential problem, a smaller slit width can be selected in order to reduce the intensity of the excitation light. For monitoring on time scales of less than one second, photobleaching is not usually a problem.

The time constant of the electronics reduces the electronic noise on the signal.[121]The noise is inversely proportional to the square root of the time constant. For example, if the time constant is increased 25-fold, the noise is reduced five-fold. The time constant value selected should be long enough to reduce noise without affecting the rate of the process being monitored.[121,124] A general guideline is that the time constant selected should be less than 10% of the half time (half life) of the process being observed.[121]

Selection of the volumes of reactants for each run is another operational factor that can be changed.[24]The position of the back-stop of the stopping syringe can be adjusted to change the volume used in each run.[121]Enough solution needs to be mixed such that both a constant flow rate in the flow cell and a short dead-time is achieved, but with minimal waste of often valuable solution/material. Trials with different total pushed volumes of reactant solutions can be made to determine the volume which satisfies both criteria.[121,124]

2.2 Reaction Kinetics probed by Rapid-Mixing Stopped-flow

2.2.1 Derivation for two-state reaction model

$N_1 \square \quad N_2 \qquad \leftrightarrow$

The above two-state kinetic equation can be solved by Laplace transform method,[39]

The rate equations for this reaction can be written as,

$$\frac{-d[N_1]}{dt} = k_1[N_1] - k_{-1}[N_2] \quad \text{.....(2.1)}$$

$$\frac{-d[N_2]}{dt} = k_{-1}[N_2] - k_1[N_1] \quad \text{.....(2.2)}$$

Applying initial conditions, $[N_1] = N_0$ and $[N_2] = 0$ at $t = 0$

We can apply Laplace transform on above two rate equations and the rate equations can be converted in to a set of algebraic equations.

$$(p + k_1)(\mathcal{L}[N_1]) - k_{-1}\mathcal{L}[N_2] = [N_1]_0 \quad \text{.....(2.3)}$$

$$-k_1(\mathcal{L}[N_1] + (p + k_{-1})\mathcal{L}[N_2] = [N_2]_0 \quad \text{.....(2.4)}$$

After using Cramer's rule, we solved for $\mathcal{L}[N_1]$ and $\mathcal{L}[N_2]$.

From the solution of the determinant, we obtain,

$$\mathcal{L}[N_1] = \frac{(p + k_{-1})[N_1]_0}{p(p + (k_1 + k_{-1}))} + \frac{k_{-1}[N_2]_0}{p(p + (k_1 + k_{-1}))} \quad \text{.....(2.5)}$$

and $\mathcal{L}[N_2] = \frac{(p + k_1)[N_2]_0}{p(p + (k_1 + k_{-1}))} + \frac{k_1[N_1]_0}{p(p + (k_1 + k_{-1}))}$ .....(2.6)

We carried out inverse Laplace transformations on equations (2.5) and (2.6) to obtain time-dependent concentrations for N_1 and N_2 .

$$[N_1] = \frac{[N_1]_0}{(k_1 + k_{-1})}(k_{-1} + k_1 e^{-(k_1+k_{-1})t}) + \frac{[N_2]_0 k_{-1}}{(k_1 + k_{-1})}(1 - e^{-(k_1+k_{-1})t}) \quad \text{.....(2.7)}$$

Since $[N_2]_0 = 0$, we obtain,

$$[N_1] = \frac{[N_1]_0}{(k_1 + k_{-1})}(k_{-1} + k_1 e^{-(k_1+k_{-1})t}) \quad \text{.....(2.8)}$$

and $$[N_2] = \frac{k_1[N_1]_0}{(k_1 + k_{-1})}(1 - e^{-(k_1+k_{-1})t}) \quad \text{.....(2.9)}$$

2.2.2 **Derivation for three-state reaction model**

$$N_1 \underset{k_{-1}}{\overset{k_1}{\leftrightarrow}} N_2 \underset{k_{-2}}{\overset{k_2}{\leftrightarrow}} N_3$$

The above equations can be solved by using Laplace transform method as shown below, [39]

(a) At t=0, $[N_1] = [N_2]$
$[N_2] = [N_3]$

We can find $[N_3]$ from: $[N_1] + [N_2] + [N_3] = [N_1]_0$ ……(2.10)

Kinetic equations:

$$\frac{d[N_1]}{dt} = -k_1[N_1] + k_{-1}[N_2]$$
$$\frac{d[N_2]}{dt} = k_1[N_1] - (k_{-1} + k_2)[N_2] + k_2[N_3]$$
$$\frac{d[N_3]}{dt} = k_2[N_2] - k_{-2}[N_3]$$

These can be solved either as a 3 X 3 or a 2 X 2 system using equation (1) to eliminate $[N_3]$.

Laplace transforms, Let $N_1(s) = \mathcal{L}([N_1])$

$$sN_1(s) - [N_1]_0 = -k_1 N_1(s) + k_{-1} N_2(s)$$
$$sN_2(s) = k_1 N_1(s) - (k_{-1} + k_2) N_2(s) + k_{-2} N_3(s)$$
$$sN_3(s) = k_2 N_2(s) - k_{-2} N_3(s)$$

Matrix form

$$\begin{bmatrix} (s+k_1) & -k_1 & 0 \\ -k_1 & (s+k_{-1}+k_2) & -k_{-2} \\ 0 & -k_2 & (s+k_{-2}) \end{bmatrix} \begin{bmatrix} N_1(s) \\ N_2(s) \\ N_3(s) \end{bmatrix} = \begin{bmatrix} [N_1]_0 \\ 0 \\ 0 \end{bmatrix}$$

$$N_1(s) = \frac{\begin{vmatrix} [N_1]_0 & -k_{-1} & 0 \\ 0 & (s+k_1+k_2) & -k_{-2} \\ 0 & -k_2 & (s+k_{-2}) \end{vmatrix}}{\det M} = [N_1]_0 \{(s+k_{-1}+k_2)(s+k_{-2}) - k_{-2}k_2\} \Big/ \det M$$

$$= [N_1]_0 \{s^2 + s(k_{-1}+k_2+k_{-2}) + k_{-1}k_{-2}\} \Big/ \det M$$

$$\det M = \begin{vmatrix} (s+k_1) & -k_{-1} & 0 \\ -k_1 & (s+k_1+k_2) & -k_{-2} \\ 0 & -k_2 & (s+k_{-2}) \end{vmatrix}$$

$$= (s+k_1)[(s+k_{-1}+k_2)(s+k_{-2}) - k_2k_{-2}] - k_{-1}k_1(s+k_{-2})$$

$$= (s+k_1)[s^2 + s(k_{-1}+k_2+k_{-2}) + k_{-1}k_{-2}] - k_{-1}k_1(s+k_{-2})$$

$$= s[s^2 + s(k_{-1}+k_2+k_{-2}) + k_{-1}k_{-2} - k_{-1}k_1] + k_1s^2 + s(k_1k_{-1} + k_1k_2 + k_1k_{-2}) + k_1k_{-1}k_{-2} - k_1k_{-1}k_{-2}$$

$$= s[s^2 + s(k_1+k_{-1}+k_2+k_{-2}) + k_{-1}k_{-2} + k_1k_2 + k_1k_{-2}]$$

$$= s(s+a)(s+b)$$

$$a+b = (k_1+k_{-1}+k_2+k_{-2})$$

$$ab = (k_{-1}k_{-2} + k_1k_2 + k_1k_{-2})$$

$$a,b = \frac{(k_1+k_{-1}+k_2+k_{-2}) \pm \sqrt{(k_1+k_{-1}+k_2+k_{-2})^2 - 4(k_{-1}k_{-2} + k_1k_2 + k_1k_{-2})}}{2}$$

$$N_1(s) = [N_1]_0 \left\{ \frac{s}{(s+a)(s+b)} + \frac{(k_{-1}+k_2+k_{-2})}{(s+a)(s+b)} + \frac{k_{-1}k_{-2}}{s(s+a)(s+b)} \right\}$$

$$N_2(s) = \begin{vmatrix} (s+k_1) & [N_1]_0 & 0 \\ -k_1 & 0 & -k \\ 0 & 0 & (s+k_{-2}) \end{vmatrix} \Big/ \det M$$

$$= \frac{[N_1]_0 (s+k_{-2}) k_1}{s(s+a)(s+b)}$$

$$N_3(s) = \begin{vmatrix} (s+k_1) & -k_{-1} & [N_1]_0 \\ -k_1 & (s+k_{-1}+k_2) & 0 \\ 0 & -k_2 & 0 \end{vmatrix} \Big/ \det M$$

$$= \frac{[N_1]_0 k_1 k_2}{s(s+a)(s+b)}$$

Inverse transform : we use

$$L^{-1}\left[\frac{s}{(s+a)(s+b)}\right]=\frac{1}{a-b}\left(ae^{-at}-be^{-bt}\right)$$

$$L^{-1}\left[\frac{1}{(s+a)(s+b)}\right]=\frac{1}{b-a}\left(e^{-at}-e^{-bt}\right)$$

$$L^{-1}\left[\frac{s}{s(s+a)(s+b)}\right]=\frac{1}{ab}\left(1+\frac{1}{(a-b)}\left(be^{-at}-ae^{-bt}\right)\right)$$

This gives,

$$[N_1]=[N_1]_0\left\{\frac{1}{a-b}\left(ae^{-at}-be^{-bt}\right)+\frac{(k_2+k_{-1}+k_{-2})}{(b-a)}\left(e^{-at}-e^{-bt}\right)+\frac{k_{-1}k_{-2}}{ab}\left[1+\frac{1}{(a-b)}\left(be^{-at}-ae^{-bt}\right)\right]\right\}$$

.....(2.11)

Similarly, we can obtain,

$$[N_2]=[N_1]_0\left\{\frac{k_1}{b-a}\left(e^{-at}-e^{-bt}\right)+\frac{k_{-1}k_{-2}}{ab}\left[1+\frac{1}{(a-b)}\left(be^{-at}-ae^{-bt}\right)\right]\right\}$$ .....(2.12)

$$[N_3]=\frac{k_{-1}k_{-2}[N_1]_0}{ab}\left[1+\frac{1}{(a-b)}\left(be^{-at}-ae^{-bt}\right)\right]$$ ……. (2.13)

REFERENCES

(98) Chen, S. J. *Ann. Rev. Biophys.* **2008**, 37, 197.

(99) Bevilacqua, P. C.; Blose, J. M. *Ann. Rev. Phys. Chem.* **2008**, 59, 79.

(100) Dobson, C. M. *Nature***2003**, 426.

(101) Van Orden, A.; Jung, J. *Biopolymers***2008**, 89, 1.

(102) Bonnet, G. G.; Krichevsky, O.; Libchaber, A. *Proc. Natl. Acad. Sci. USA***1998**, 95, 8602.

(103) Jung, J.; Van Orden, A. *J. Phys. Chem. B***2005**,109, 3648.

(104) Jung, J.; Van Orden, A. *J. Am. Chem. Soc.***2006**, 128, 1240

(105) Kim, J.; Doose, S.; Neuweiler, H.; Sauer, M. *Nucleic Acids Res.* **2006**, 34, 2516.

(106) Jung, J.; Ihly, R.; Scott, E.; Yu, M.; Van Orden, A. *J. Phys. Chem. B***2008**, 112, 127.

(107) Dyer, R. B.; Brauns, E. B. *Methods Enzymol*. **2009**, 469, 353.

(108) Shen, Y.; Kuznetsov, S. V.; Ansari, A. *J. Phys. Chem.B***2001**, 105, 12202.

(109) Ma, H.; Proctor, D. J.; Kierzek, E.; Kierzek, R.; Bevilacqua, P. C.; Gruebele, M. *J. Am. Chem. Soc.***2006**, 128, 1523.

(110) Ma, H.; Wan, C.; Wu, A.; Zewail, A. H. *Proc. Natl. Acad. Sci. USA***2007,**104, 712.

(111) Kuznetsov, S. V.; Ren, C. C.; Woodson, S. A.; Ansari, A. *Nucleic Acids Res.***2008**, 36, 1098.

(112) Kuznetsov, S. V.; Ansari, A. *Biophys. J.***2012**, 102, 101.

(113) Hall, K. B. *Current Opinion in Chemical Biology***2008**, 12, 612.

(114) Ferner, J.; Villa, A.; Duchardt, E.; Widjajakusuma, E.; Wöhnert, J.; Stock, G.; Schwalbe, H. *Nucleic Acids Res.* **2008**, 36, 1928.

(115) Hernandez, B.; Baumruk, V.; Gouyette, C.; Ghomi, M. *Biopolymers***2005**, 78, 21.

(116) Nayak, R. K.; Peersen, O. B.; Hall, K. B.; Van Orden, A.*J. Am. Chem. Soc.***2012**, 134, 2453.

(117) Gray, R. D.; Chaires, J. B. *Nucleic Acids Res.***2008**, 36, 4191.

(118) Tims, H. S.; Widom, J. *Methods***2007**, 41, 296.

(119) Chan, C.-K.; Hu, Y.; Takahashi, S.; Rousseau, D. L.; Eaton, W. A.; Hofrichter, J.*Proc. Natl. Acad. Sci. USA***1997**, 94, 1779.

(120) Gong, P.; Campagnola, G.; Peersen, O. B. *Anal. Biochem.***2009**, 391, 45.

(121) Eccleston, J. F.; Hutchinson, J. P.; White, H. D. *Protein ligand interactions: structure and spectroscopy. A practical approach series***2001**, 201.

(122) Brissette, P.; Ballou, D. P.; Massey, V. *Anal. biochem.* **1989**, 181, 234.

(123) Roder, H.; Maki, K.; Cheng, H.; Ramachandra Shastry, M. *Methods***2004**, 34, 15.

(124) Eccleston, J. F.; Martin, S. R.; Schilstra, M. J. *Methods in cell biology***2008**, 84, 445.

(125) Fabian, H.; Naumann, D. *Methods***2004**, 34, 28.

(126) Zscherp, C.; Barth, A. *Biochemistry***2001**, 40, 1875.

(127) White, A.; Drabble, K.; Wharton, C. *Biochem. J.* **1995**, 306, 843.

(128) Xu, Q.; Keiderling, T. A. *Proteins: Structure, Function, and Bioinformatics***2006**, 63, 571.

(129) Kelly, S. M.; Price, N. C. *Current protein and peptide science***2000**, 1, 349.

(130) Frieden, C. *Biochemistry***2003**, 42, 12439.

(131) Balbach, J.; Forge, V.; van Nuland, N. A.; Winder, S. L.; Hore, P. J.; Dobson, C. M. *Nat. Struct.Mol. Biol.***1995**, *2*, 865.

(132) Howarth, J. V.; Millar, N.; Gutfreund, H. *Biochem. J.* **1987**, *248*, 677.

(133) Kodama, T.; Kometani, K. *Thermochimica Acta***1990**, *163*, 105.

(134) Applied Photophysics. http://www.photophysics.com/tutorials/stopped-flow-spectroscopy/3-important-parameters-for-sf-performance (accessed July 20, 2013).

(135) Talaga, D. S.; Lau, W. L.; Roder, H.; Tang, J.; Jia, Y.; DeGrado, W. F.; Hochstrasser, R. M. *Proc. Natl. Acad. Sci. USA***2000**, *97*, 13021

(136) Steinfeld, J. I.; Francisco, J. S.; Hase, W. L. *Chemical kinetics and dynamics*; Prentice Hall Englewood (New Jersey), **1989**; Vol. 3.

CHAPTER 3: Millisecond Time Scale Folding and Unfolding of DNA Hairpins Using Rapid-Mixing Stopped-Flow Kinetics[A]

This chapter describes the folding kinetics and our proposed three-state reaction mechanism of a DNA hairpin. We report stopped-flow kinetics experiments to study the folding and unfolding of 5 base pair stem and 21 nucleotide polythymidine loop DNA hairpins over various concentrations of NaCl. The reactions occurred on a time scale of milliseconds, considerably longer than the microsecond time scale suggested by previous kinetics studies of similar sized hairpins. In comparison to a recent fluorescence correlation spectroscopy study (J. Am. Chem. Soc. 2006, 128, 1240-1249), we suggest the microsecond time-scale reactions are due to intermediate states and the millisecond timescale reactions reported here are due to the formation of the fully folded DNA hairpin. These results support our view that DNA hairpin folding occurs via a minimum three-state mechanism.

3.1 Introduction

A clear understanding of the biomolecular structures and functions[137] of nucleic acids requires proper insight on how these molecules fold, unfold and sometimes misfold.[138] DNA and RNA hairpins are important model systems for understanding the kinetics and thermodynamics of such processes.[139-141] Consisting of a single-stranded loop and a base-paired stem, these

[A]This chapter has been published as part of: Rajesh K. Nayak,[†]Olve B. Peersen,[‡] Kathleen B. Hall,[§] and Alan Van Orden[†],*_J. Am. Chem. Soc_*2012, *134*, 2453

R. Nayak collected and analyzed the data, A. Van Orden and R. Nayak wrote the manuscript.

molecules can undergo conformational fluctuations[142-144] of the unfolded strand, loop formation, base-stacking,[145-147] and intra molecular Watson-Crick and non-Watson-Crick base-pairing.[148] Hence, a variety of molecular processes in nucleic acids can be investigated by studying these hairpins.

The folding kinetics of DNA and RNA hairpins has been the subject of numerous experimental and theoretical investigations.[145,149-153,159-161] Yet controversy remains concerning many aspects of the folding kinetics, including folding times, mechanisms, rate limiting steps, and their dependence on sequence, loop size, stem size, salt concentration, temperature, etc.[146,154-156] Smaller hairpins, containing up to five base-pairs (bp) in the stem and 4-30 nucleotides in the loop have been examined using laser induced temperature jump[157],[158] and fluorescence correlation spectroscopy (FCS) experiments.[142,159-161] These studies reveal reaction times of ~10-100 μs, depending on loop size and other conditions. Hairpins with longer stems have been studied using single molecule optical trapping techniques,[162,164] revealing much longer folding and unfolding times of milliseconds to hundreds of milliseconds, depending on stem size.

Previously, our laboratory used FCS to study the folding and unfolding kinetics of DNA hairpins containing a 5-bp stem and 21-nt polythymidine loop under various conditions[161]. Reaction times of ~50 μs were observed, consistent with previous studies of similar sized hairpins. However, careful examination of the correlation amplitudes along with photon counting histogram (PCH) analysis revealed the reaction being probed by our FCS experiment was likely due to an intermediate state in a more complex reaction mechanism. We hypothesized that the overall reaction involving the fully folded hairpin occurred on a longer time scale than the FCS observation time and was thus not observed in our experiment. A later study[159] that combined single beam autocorrelation and two-beam cross correlation spectroscopy observed the reactions

of hairpins with 4-bp and 5-bp stem sizes on an extended time scale. This study revealed the reaction time for complete folding of the 4-bp structure was ~400 μs. Only the intermediate reaction of the 5-bp structure was observed, even with the expanded observation time. This implied that complete folding of the 5-bp stem length hairpin may occur on a millisecond time scale or longer.

Here, we report folding kinetics of the 5-bp stem size DNA hairpin on the millisecond time scale using the rapid-mixing stopped-flow technique.[163] Stopped-flow kinetics observes the time evolution of a reaction initiated by the mixing of two or more reagents. A drawback of this method is the finite mixing time, typically 0.5 ms or longer. Reactions that occur faster than the mixing time are not observed. Hence, the ~50-μs reaction observed in our previous FCS experiments is inaccessible using stopped-flow. However, if the overall reaction occurs on a much longer time scale, as suggested previously, we hypothesized that stopped-flow may be an appropriate technique to measure its kinetics.

3.2 Experimental details

3.2.1 Sample Preparation: Fluorescently labeled DNA hairpin samples with HPLC purification were purchased from IBA Gmbh (Gottinigen, Germany). The hairpin consisted of a five base pair stem with the complementary sequences 5'-AACCC and GGGTT-3' and a loop containing 21 deoxythymidine residues. The hairpin is identified as hp-T_{21} and was dual labeled with fluorophore 5-TAMRA at 5'end and a quencher dabcyl at 3' end respectively. A control DNA, poly$(dT)_{40}$ labeled with the dye at 5' end was examined for the comparison. 100 nM DNA samples were prepared in 2.5 mM Tris-HCl buffer and 250 μM EDTA. 1M stock Tris-HCl buffer with RNase, DNase and protease free was purchased from Sigma-Aldrich and molecular

biology grade EDTA with tested RNase, DNase and protease free was purchased from Cal Biochem, New Jersey. Molecular biology grade sodium chloride was also purchased from Cal Biochem, New Jersey. Various concentrations of sodium chloride starting from 0 mM to 1000mM were prepared for stopped flow mixing experiments. All the above mentioned samples were prepared in nuclease free water, purchased from Applied Biosystem, CA. All solutions were filtered through 0.22 micron Nalgene nitrocellulose filter units to remove any contaminating proteins.

3.2.2 Stopped Flow Kinetics Experiments: Folding and unfolding reactions of DNA hairpin[160] hp-T_{21} were carried out in an Applied PhotophysicsSX-20 stopped flow instrument. Folding and unfolding reactions of a control DNA Poly$(dT)_{40}$ were undertaken for comparison. For folding reaction of the hairpins, stopped flow mixing experiments were carried out by mixing 100 nM of DNA hairpin in 0 mM NaCl (low salt buffer) in one channel with varying concentrations of NaCl (0, 10, 20, 50,100, 200, 500 and 1000 mM) in the second channel. In other words we started with completely unfolded structure of DNA hairpin in one channel and mixed this subsequently with varying concentrations of NaCl in the second channel to monitor the folding reaction of the DNA hairpin as a function of sodium chloride concentration. In a stopped flow mixing experiment, two reactants in two different channels are allowed to mix thoroughly in a mixing chamber[163] and then mixed in a flow cell of certain dead time[165](in our stopped flow experiment the dead time of the flow cell is approximately 0.45 millisecond). The kinetics of the reaction is monitored by using spectroscopic signals, such as absorbance, fluorescence, etc. The instrument records the changes in the spectroscopic signal as a function of time. From the trace created by the instrument, the kinetic information about the particular reaction studied can be obtained by fitting to a model of the reaction. Basically the rate constant

which describes the reaction kinetics can be determined by fitting the data in a suitable fitting routine or fitting model. In our stopped flow experiment, the change in spectroscopic signal is the fluorescence voltage (PMT Voltage). The trace shows the fluorescence voltage as a function of time.

In our stopped flow experiment, fluorescence excitation was at 547 nm from a monochromator source with bandwidth set to 2 nm and the emission from the dye was detected using 570 nm high pass filter.

3.2.3 Steady State Fluorescence and UV/Vis Measurements: Steady state fluorescence spectra and temperature dependent fluorescence were obtained using a AVIV ATF-105 fluorometer. Emission spectra were collected using excitation wavelength 547 nm, and excitation spectra were obtained using emission wavelength 580 nm. The bandwidths were set to 1nm on both channels and spectra were background corrected by subtraction of a buffer spectrum. Figure S 1 shows the emission spectra of DNA hairpin hp-T_{21} as a function of various sodium chloride concentrations. These figures show that the fluorescence has been quenched due to the hairpin folding with the subsequent addition of NaCl. Concentration dependent thermal melts were performed by standard methods, using a Varian Cary 50Bio equipped with multi cell holder UV-Vis spectrophotometer and heating/cooling unit. Varying concentrations of DNA samples from 0.3 µM to 43.9 µM were used for the melting experiments. Samples were heated to 90^0 C and were cooled back to 10^0 C to check the reversibility. Absorbance versus temperature curves were monitored at 260, 265 and 295 nm wavelength respectively, using single beam mode and subtracting the absorbance from the cuvette containing buffer. The buffer in the experiments was 100 mM NaCl, 10 mM Na cacodylate and 0.1 mM EDTA. The melting temperatures were

determined for each sample by fitting the absorbance versus temperature at 260 nm by using two state models with linear baselines.

3.2.4 Data Collection and Fitting: In the stopped flow experiment, all our folding and unfolding reactions data for our DNA hairpin and control DNA single strand at various NaCl concentrations were collected and repeated at least three times for the statistical accuracy of our data collections. The error bars were calculated by using propagation of error method to determine the statistical accuracy of our experimental data.

3.3 Results and Discussion

Figure 3.1 shows stopped flow kinetics data obtained for 100-nM DNA hairpins in an aqueous buffer. The DNA hairpins consisted of a 5-bp stem containing the complementary sequences 5'-AACCC and GGGTT-3' connected by a 21-nt polythymidine loop. The DNA hairpin 5'-AACCC$(T)_{21}$ GGGTT-3' was labeled at the 5' end with tetra methyl rhodamine (TAMRA) and at the 3' end with dabcyl quencher. The folding of the DNA hairpin, induced by mixing the DNA with buffer solutions containing varying concentrations of NaCl, was monitored by observing the quenching of the TAMRA fluorophores by dabcyl (Figure 3.1 panel B) after a mixing time of ~450 μs. Unfolding was monitored by observing the recovery of the fluorescence due to mixing DNA solutions containing varying concentrations of NaCl with pure buffer (Figure3.1 panel C). All experiments were carried out at a laboratory temperature of ~22°C. Because DNA is a polyanion, Na^+ counter ions are necessary to stabilize the hairpin in its folded state. Hence, mixing the DNA with NaCl induced the formation of the hairpin; whereas, mixing with pure buffer caused the hairpins to dissociate. The reaction rates increased with increasing NaCl concentration. The same mixing experiments were carried out for a control

DNA sample containing a TAMRA fluorophore in the absence of quencher (Figure3.1, Panel A). These latter experiments demonstrate that NaCl does not affect the intensity of the TAMRA dye fluorescence. Control experiments using zero concentration NaCl (black curves) and blank buffer solutions (red curves) are also shown for comparison. Thermodynamic analysis ruled out the possibility of duplex and/ or quadruplex formation interfering with the stopped-flow kinetics data under our experimental conditions (See 3.5 Supporting Information).

To estimate the reaction times of the DNA hairpin folding and unfolding reactions, we fit the data shown in Figure 3.1 to single exponential functions (solid curves). The reaction times decreased with NaCl concentration, ranging from 6.38 ms for 5-mM NaCl to 0.770 ms for 100-mM NaCl (See Table 3.2). Table 3.2 also shows the apparent equilibrium constant, K_{melt} = [folded]/[unfolded], obtained from analysis of the melting curves assuming a two-state reaction process (See Supporting Information). Within experimental error, the reaction times were identical for folding and unfolding experiments with the same NaCl concentration. For the 500-mM NaCl sample, the folding reaction occurred during the stopped-flow mixing time. Importantly, the reaction times reported here are approximately an order of magnitude longer than those reported in previous kinetics studies on similar sized hairpins.[142,149,154,159-161]

To investigate the relationship between the stopped-flow kinetics experiments reported here and the FCS experiments reported previously, we analyzed our stopped flow data using the three-state mechanism proposed in our previous FCS study (Scheme 3.1).[161]

The Supporting Information section shows the rate equations used to predict the fluorescence decay under initial conditions given by (N_1, N_2,N_3) equal to (N_{total}, 0, 0). The fluorescence decay is assumed to be proportional to the decay of the N_1 concentration over time.

This, in turn, depends on the total DNA concentration and the rate constants, k_1, k_{-1}, k_2, and k_{-2}. The rate constants k_1 and k_{-1} for DNA hairpins in 100 mM NaCl were determined in our previous FCS study.[161]

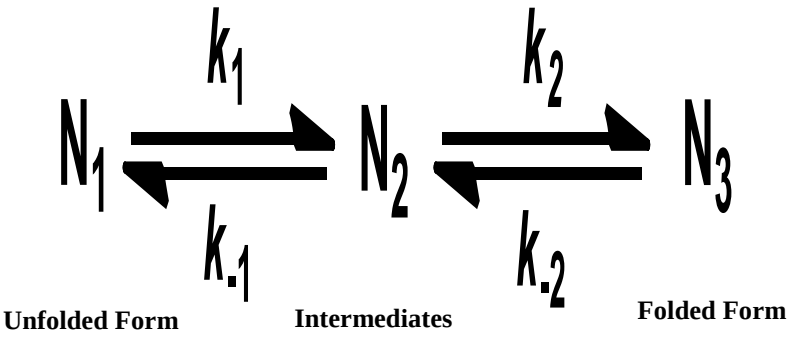

Scheme 3.1. Proposed kinetic mechanism for DNA hairpin folding/unfolding reactions.

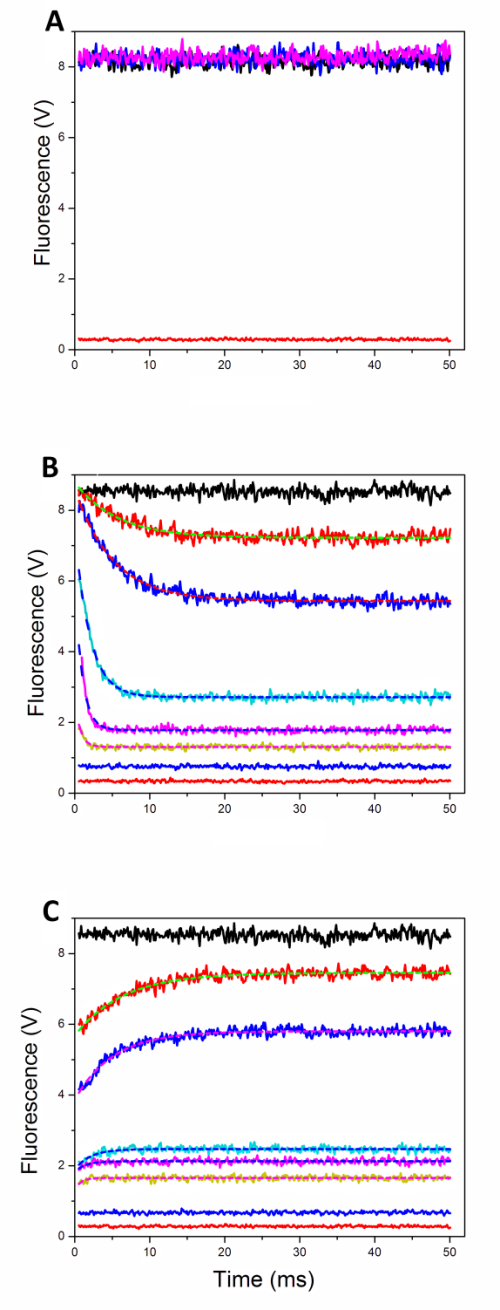

Figure 3.1: Experimental data (solid lines) and corresponding fitting curves (solid dashed lines) from stopped-flow measurements of: A. Folding reaction of control DNA for comparison, B. DNA hairpin hp$(T)_{21}$ folding reaction, C. the DNA hairpin unfolding reaction as a function of varying NaCl concentration (black, 0; red, 5; blue,10; dark cyan,25; magenta,50; dark yellow,100; navy 500 mM NaCl and wine, background buffer).

Figure 3.2 shows the result of fitting our stopped-flow data for the DNA hairpin in 100-mM NaCl to the three-state mechanism. k_1 and k_{-1} were constrained to the values determined by FCS,[25] and the initial fluorescence was constrained to the fluorescence observed from the control sample in the absence of quencher. k_2 and k_{-2}were adjustable parameters in the fit. A fit to a two-state mechanism with the initial fluorescence constrained is also shown for comparison. By plotting the data on a semilog scale, it is easily seen that the bulk of the reaction occurs during the stopped-flow mixing time. In particular, the three-state mechanism predicts a two-phase decay process, with the initial phase going to completion before the mixing is complete. Nevertheless, it is clear from Figure 3.2 and the residual plots below that the stopped-flow data observed after the mixing time fits well to the three-state mechanism but does not fit to the two-state mechanism. Hence, the stopped-flow data reported here are consistent with the three-state mechanism discussed previously for the 100-mM NaCl sample. Note that the single exponential fits displayed in Figure 3.1 fit the data well because the intensities were not constrained.

Table 3.1 shows the parameters of the three-state mechanism based on the present stopped-flow kinetics data and previous FCS data for DNA hairpin folding in 100-mM NaCl. Also shown are the reaction time constants, $1/\tau_{rxn1,2} = k_{1,2} + k_{-1,-2}$, and equilibrium constants $K_1 = k_1/k_{-1}$, $K_2 = k_2/k_{-2}$, and $K_{overall} = K_1 K_2$. The latter constants, K_2 and $K_{overall}$, are in reasonable agreement with those deduced from our previous FCS study[25]. Note that the equilibrium constant $K_{overall}$ should not be compared to the constant K_{melt} shown in Table 2, as this latter constant was obtained from melting curve analysis assuming a two-state reaction mechanism.(See Supporting Information). In our previous FCS study, we showed that the observed melting profile of the DNA hairpins could be reproduced from the proposed three-state mechanism, but the overall equilibrium constant derived from these curves differed depending on the chosen mechanism.

The reaction time constants reported here confirm that the overall DNA hairpin folding reaction occurs on a time scale that is significantly longer than previous kinetics studies suggest. It is concluded that the DNA hairpin folding reaction in 100 mM NaCl is a complex process that occurs over a broad time range and must be examined using complimentary experimental techniques sensitive to disparate time scales. Figure 3.3 illustrates the three-step mechanism of DNA hairpin folding.

.

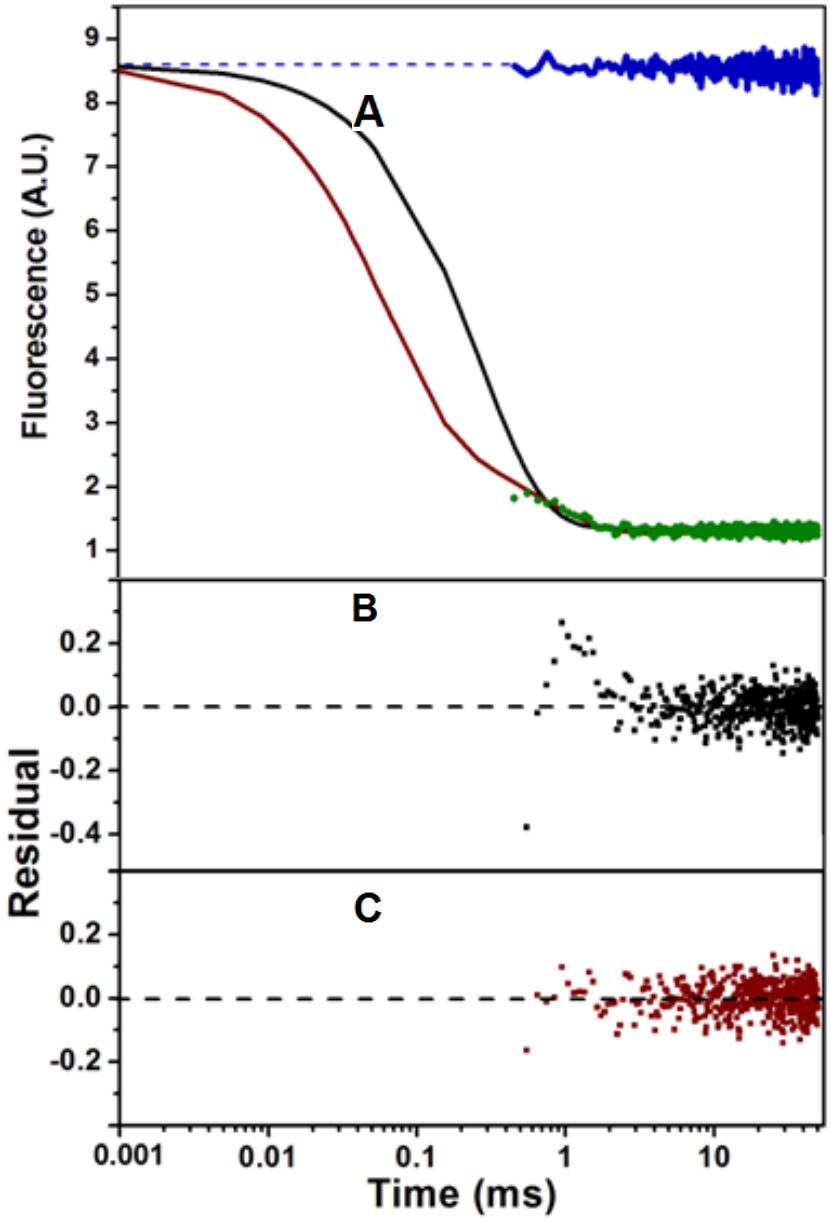

Figure 3.2. (A.) Stopped-flow kinetics data for DNA hairpins in 100 mM NaCl (green dots) and fitting curves to a two-state (black) and three-state (wine) mechanism. The blue curve shows the stopped-flow data of a control DNA hairpin in the absence of quencher. B. Residual plot for the two-state mechanism. C. Residual plot for the three-state mechanism.

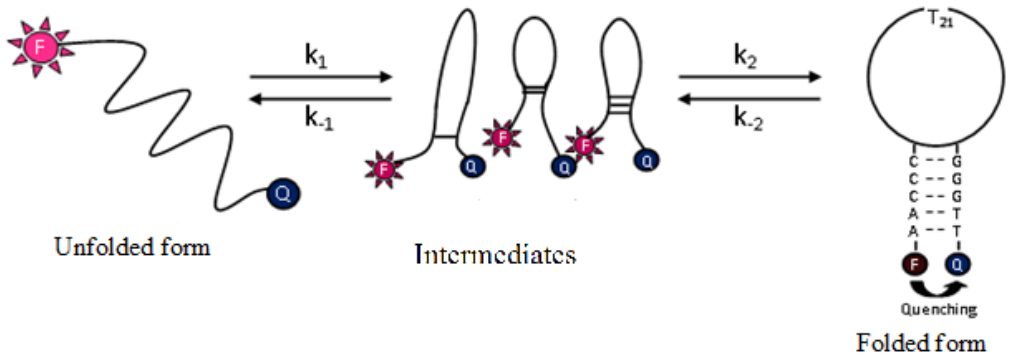

Figure 3.3: Schematic description showing three-state mechanism for the conformational fluctuations of the five base pair stem DNA hairpin hp-$(T)_{21}$ with characteristic rate constants k_1, k_{-1}, k_2 and k_{-2}. Where k_1 and k_{-1} represent forward and reverse unfolding rate constant between unfolded form of the hairpin and intermediates. $k_2$and k_{-2} represent forward and reverse unfolding rate constant between folded form of the hairpin and intermediates

Table 3.1. Kinetic Parameters of DNA Hairpin hp21 at Different NaCl Concentrations (considering two- state model)

[NaCl](mM)	K_{melt}	$\tau_{reaction}$(ms)
5	0.60	6.38 (0.18)
10	1.20	5.05 (0.13)
25	3.94	2.08 (0.19)
50	9.09	1.33 (0.29)
100	21.21	0.77 (0.23)

$\tau_{reaction}$corresponds to the fitting analysis in Figure 1 (B and C) and K_{melt} determined from melting curve analysis (Supporting Information).Numbers in parentheses are uncertainties in the last digits.

The DNA hairpin folding reactions in 25- and 50-mM NaCl can also be explained using a three-state reaction mechanism. However, complete analysis of the stopped-flow data for these samples awaits more careful FCS measurements of the k_1 and k_{-1} rate constants than reported in our previous FCS studies[161]. By contrast, the reactions occurring in 5- and 10-mM NaCl do not appear to fit the three-state mechanism. Rather, the reactions in these samples can be best described as reversible two-state processes with single-exponential decay. These results are similar to our previous FCS study, which found the reactions in NaCl below 25 mM were predominantly two-state reactions. The three-state mechanism was used to explain reactions at higher NaCl concentrations. However, in the previous study, it was assumed the two-state reactions at low NaCl concentration involved the folding and unfolding of the intermediate state. By contrast, the present study suggests a direct folding and unfolding reaction involving the unfolded state and the folded DNA hairpin at low NaCl concentration. Our interpretation of the stopped-flow kinetics data reported here and the FCS data reported previously[161]is as follows. At low NaCl concentration, the DNA hairpin folding reaction occurs as a slow, reversible, two-state process involving direct folding and unfolding of the folded state. As the NaCl concentration increases, the reaction becomes faster, and intermediate forms of the DNA hairpin begin to stabilize. At higher NaCl concentration, the reaction proceeds according to a three-state mechanism involving stable or meta-stable intermediates. Several theoretical studies using statistical mechanics and molecular dynamics models have examined the intermediate forms of RNA and DNA hairpins.[146,150,155,156]

Table 3.2. Kinetic Parameters of DNA Hairpin hp_{21} at 100 mM NaCl Buffer

Kinetic Parameters	Previous work	Present work
$\tau_{reaction1,}$ (μsec)	62.7 (5.1)	–
$k_{1,}$ (s^{-1})	(1.12±0.16)×10^4	–
$k_{-1,}$ (s^{-1})	(4.79 ± .050)×10^3	–
$\tau_{reaction2}$(μsec)	–	–472(±13)
k_2,(s^{-1})	–	(1.39 ±0.26)×10^3
k_{-2},(s^{-1})	–	(0.73 ±0.08)×10^3
K_1	2.33 (0.22)	–
K_2	4.75 (0.33)	1.91(±0.19)
$K_{overall}$	8.35 (1.20)	4.47(±0.85)

Numbers in the parentheses are the uncertainties in the last digits.

Chen and co-workers used statistical mechanics modeling[156] to investigate the role of these intermediates on the reaction rates and mechanism. Several types of intermediate states were identified that involve partial folding of the stem and/or mismatched Watson-Crick and non-Watson-Crick base-pairing in the stem and loop. Formation and disruption of off-path intermediates can serve as the rate limiting step of the reaction; whereas, on-path intermediates can increase the rate compared to a direct two-state mechanism. We suggest the changes in rate and mechanism we observed with NaCl concentration may be due to the role of Na^+counter ions in stabilizing various intermediate forms of the DNA hairpin.

3.4 Conclusion

In summary, we have reported stopped-flow kinetics experiments to investigate the folding and unfolding kinetics of a DNA hairpin molecule. The observed reactions were found to occur on a millisecond time scale, suggesting DNA hairpin formation can occur much more slowly than previously thought. We suggest a three-state reaction mechanism, wherein intermediate formation occurs on tens to hundreds of microsecond time scale, and complete hairpin formation occurs on a millisecond time scale. FCS is useful for probing the intermediate reactions, but cannot observe the complete folding reaction due to the limited observation time of FCS. Likewise, stopped-flow can observe the complete folding reaction, but cannot observe the intermediate reaction due to the finite dead time. When combined with each other, these techniques can monitor the complete folding trajectory of the DNA hairpin.

3.5 Supporting Information

3.5.1 Theory

3.5.1.1 Derivation of the Three-State Model: To investigate the mechanism of DNA hairpin folding, we derived a kinetic model using the three-state mechanism,

$$N_1 \underset{k_{-1}}{\overset{k_1}{\leftrightarrow}} N_2 \underset{k_{-2}}{\overset{k_2}{\leftrightarrow}} N_3$$

Here, N_1, N_2, and N_3 represent the number of molecules in unfolded, intermediate, and folded conformations of the DNA hairpin, respectively. k_1, k_{-1}, k_2, and k_{-2} are the rate constants. This mechanism was proposed in our previous FCS study, in which k_1 and k_{-1} were measured by FCS. k_2 and k_{-2} were considered to be outside the range of our FCS measurement technique.

The above mechanism leads to the following differential equations:

$$\frac{dN_1}{dt} = -k_1 N_1 + k_{-1} N_2 \qquad \text{(S1.1)}$$

$$\frac{dN_2}{dt} = k_1 N_1 - k_{-1} N_2 - k_2 N_2 + k_{-2} N_3 \qquad \text{(S1.2)}$$

$$\frac{dN_3}{dt} = k_2 N_2 - k_{-2} N_3 \quad , \qquad \text{(S1.3)}$$

which can be solved to predict the fluorescence decay observed in our stopped-flow kinetics experiment, assuming the fluorescence is proportional to N_1. Accordingly, the fluorescence decay is given by

$$F(t) = F_0\left[\frac{1}{a-b}\left(ae^{-at} - be^{-bt}\right) + \frac{k_{-1}+k_2+k_{-2}}{b-a}\left(e^{-at} - e^{-bt}\right)\right] + F_\infty\left[1 + \frac{1}{a-b}\left(be^{-at} - ae^{-bt}\right)\right] \qquad \text{(S1.4)}$$

Here, $F(t)$ is the fluorescence as a function of time, t, F_0 is the initial fluorescence, and F_∞ is the equilibrium fluorescence. Also,

$$a,b = \frac{\left(k_1 + k_{-1} + k_2 + k_{-2}\right) \pm \sqrt{\left(k_1 + k_{-1} + k_2 + k_{-2}\right)^2 - 4\left(k_{-1}k_{-2} + k_1k_2 + k_1k_{-2}\right)}}{2} \qquad \text{(S1.5)}$$

Our stopped-flow kinetics data were analyzed by fitting to the above equations, with F_0 constrained to the fluorescence of the control sample and k_1 and k_{-1} constrained to the values reported in our previous FCS experiment. See Figure 2 and Table 1 in the main manuscript for results.

3.5.1.2 Derivation for the Equilibrium Distribution of DNA Hairpin and DNA Duplex

To address whether DNA duplex formation might influence the reported hairpin folding kinetics, we present the following calculation, which predicts the distribution of DNA monomers and DNA duplex in our samples under experimental conditions.

$$2S \underset{\longleftarrow}{\xrightarrow{K_1}} S_2 \qquad \text{(S1.6)}$$

$$S \underset{\longleftarrow}{\xrightarrow{K_2}} H \qquad \text{(S1.7)}$$

where S,H and S_2 refer to single stranded DNA, hairpin DNA and duplex DNA ,respectively.

K_1 and K_2 are equilibrium constants for the above reactions.

$$K_1 = \frac{[S_2]}{[S]^2} \quad \text{(S1.8)}$$

$$[S_2] = K_1[S]^2 \quad \text{(S1.9)}$$

$$K_2 = \frac{[H]}{[S]} \text{ (This constant corresponds to } K_{melt} \text{ in Table 3.1)} \quad \text{(S1.5)}$$

$$[H] = K_2[S] \quad \text{(S1.10)}$$

$$[S]_0 = [S] + [H] + 2[S_2] \text{ (Mass balance equation)} \quad \text{(S1.11)}$$

Here $[S]_0$ is the total DNA concentration. In our experiment, the total DNA concentration was 50 nM.

Combining equations (S1.3), (S1.4), (S1.5), (S1.6) and (S1.7), we obtain

$$2K_1[S]^2 + [1 + K_2][S] - [S]_0 = 0 \quad \text{(S1.12)}$$

Solving the above quadratic equation for [S],

$$[S] = \frac{-(1 + K_2) \pm \sqrt{(1 + K_2)^2 + 8K_1[S]_0}}{4K_1} \quad \text{(S1.13)}$$

For duplex DNA, $\Delta G = -RT \ln K_1$ (S1.14)

$$K_1 = \exp[-\Delta G/RT] \quad \text{(S1.15)}$$

Where K_1 = Equilibrium constant for duplex formation

ΔG = Free energy change for duplex DNA formation

R = Universal gas constant

T = laboratory temperature of 295 K.

Using equation (S1.11), $K_1 = \exp[-(-9.42) *103*4.184 \text{ J mole}^{-1} /(8.314 \text{ JK}^{-1} \text{ mole}^{-1}* 295K)]$ (S1.12)

$$K_1 = 9.54*10^6$$

Where ΔG = -9.42 at 100 mM NaCl (predicted from Oligo Analyzer from IDT)

K_2 = Equlibrium constant for hairpin formation = 21.21 at 100 mM NaCl (from temperature melting, See Table 1 of the manuscript)

Using these above values in equation (S1.9), we obtain $[S] \sim 2.25*10^{-9} = 2.25$ nM

Finally, using (S1.6), we obtain $[H] \sim 47.7*10^{-9} = 47.7$ nM

Thus, the total monomer concentration is predicted to be 49.9 nM out of a total DNA concentration of 50 nM. Using EquationS1.7, we obtain a DNA duplex concentration of 0.05 nM, which is well below 1% of the total DNA present. Hence, we have assumed that the DNA duplex formation is negligible in our samples. This assumption has been confirmed by doing concentration dependent UV/Vis melting experiments reported in the next section.

3.5.2 Thermodynamic Analysis of DNA Hairpins

***3.5.2.1 Temperature Dependent Fluorescence*:** The quality of the sample was verified by performing temperature dependent fluorescence analysis and was confirmed by monitoring the fluorescence intensities at the temperature varying from 5^0C to 80^0C on a steady state fluorometer (MODEL ATF 105,AVIV instrument).The fluorescence of a 50 nM DNA hairpin sample at varying NaCl buffer was collected by exciting the sample at 547 nm. The resulting melting curves at varying NaCl concentration were analyzed using the two state mechanism (see Figure 3.5) to estimate the fraction of molecules in the unfolded state as a function of temperature and NaCl concentration. The fraction of the open state, f(T),can be assessed directly by monitoring the fluorescence intensity I(T): f(T) = (I(T)-I(F))/ (I_{UN}-I_F), where I_{UN} is the fluorescence of the unfolded state and I_F is the fluorescence of the folded state. We evaluated I_{UN} as the fluorescence at 80^0C and I_F at 5^0C. The apparent equilibrium constant $K_{melt}(T)$ = f(T)/(1-f(T)) We define the fitting equations to fit our experimental data to determine melting temperatures and enthalpies (presented below). based on the two-state mechanism.

If we define free energy change of the unfolded state of the DNA hairpin as:

$$\Delta G^0_{uN}(T) = \Delta H^0_{uN,app} - T\Delta S^0_{uN,app} \qquad \text{(S1.16)}$$

The fraction of the unfolded state is

$$f_u(T) = \frac{e^{-\frac{\Delta G^0_{uN}}{RT}}}{1+e^{-\frac{\Delta G^0_{uN}}{RT}}} \qquad \text{(S1.17)}$$

and the resulting fluorescence signal is defined as:

$$F(T) = (1 - f_u(T)) * [F_{N,0} - S_N * T] + f_u(T) * [F_{u,0} - S_u * T] \quad \text{(S1.18)}$$

Where S_N, S_u are defined as the baseline slopes for native conformation and unfolded conformation respectively. F_N, F_u are fluorescence at T=0 for native conformation and unfolded conformation respectively.

If one defines the melting temperature so that

$$0 = \Delta H^0_{uN,app} - T_m * \Delta S^0_{uN,app} \quad \text{(S1.19)}$$

Then, the equation S1.12 becomes

$$\Delta G^0_{uN}(T) = \Delta H^0_{uN,app}(1 - \frac{T}{T_m}) \quad \text{(S1.20)}$$

Our experimental data was fitted to the above equations to determine the melting temperatures and enthalpies at various NaCl concentrations. Results are presented in Tables3.4and 3.5.

3.5.2.2 UV-Vis Melting Curve Analysis: Rule out the Possibility of Duplex and G-Quadruplex Formation

In order to rule out the possibility of duplex formation in our hairpin samples, concentration dependent thermal melts of the DNA samples were performed by UV-Vis melting experiments (procedure described above in the experimental section3.2). The absorbance versus temperature profiles were created at 260 nm for various DNA concentrations and the melting temperatures(T_m s) were calculated by using two state models with linear base lines (see Figure 3.6).Table S4 shows the melting temperatures for various concentrations. It is observed that the

T_m s do not change as a function of DNA concentration, being approximately equal within the statistical error. The fact that the melting temperature does not change with concentration rules out the possibility of duplex formation in our hairpin samples. For the UV-Vis melting experiments, we used micro-molar DNA concentrations and for rapid-mixing stopped flow experiments and FCS experiments, we usednano-molar DNA concentrations. Since there is no chance of duplex formation in micro-molar concentrations of DNA samples, it completely rules out the possibility of duplex in our nano-molar samples. Furthermore, we have presented a theoretical calculation above which shows there is well below 1% of duplex in the hairpin samples.

It is well known that guanine rich oligo deoxinucleotides form a tetrameric structure called G-quadruplex[166,167]. Given the sequence of our DNA hairpin 5'-AACCCTTTTTTTTTTTTTTTTTTTTGGGTT, which has 3 guanines at 3' end , there is a theoretical possibility of G-quadruplex in our samples. Hence, to rule out any possibility of G-quadruplex, the UV-Vis thermals melts at various micro-molar DNA concentrations were performed and were monitored at 295 nm. Figure3.7 shows the melting profiles at both 265nm and 295 nm. The melting monitored at 265 nm (A_{265}) shows a sigmoidal (hyperchromic curve) and the melting monitored at 295 nm (A_{295}) does not show an inverse sigmoidal curve. The fact that the melting curves at 295 nm are not inverse sigmoidal curves[168,169]at various micro-molar DNA concentrations suggest that there is no possibility of G-quadruplexes in our hairpin samples.

Furthermore, we used an algorithm called QuadDB[166]and a program, Quadparser by Simon Rodgers and Julian Huppert in University of Cambridge, United Kingdom. This algorithm is based on a folding rule: A sequence of the form d($G_{3+}N_{1-7}G_{3+}N_{1-7}G_{3+}N_{1-7}G_{3+}$) will fold into a quadruplex under near-physiological conditions'. Here 'N' refers to any base, including guanine,

and the near-physiological conditions are 100 mM KCl and 10 mM Tris-HCl (pH 7.4). We introduced our hairpin sequences into this program in order to check for quadruplex and the program nullified the chances of quadruplex. Therefore, both the melting experiments and the Quadparser program enable us to rule out the possibility of G-quadruplex in our DNA hairpin samples.

3.5.2.3 The Affect of Dye Labels on the Kinetics and Thermodynamics of DNA Hairpin Formation:

To investigate the impact of dye labeling on the DNA hairpin folding kinetics and thermodynamics, we report stopped-flow kinetics data of Rhodamine 6G (R6G) labeled DNA hairpins in Figure3.8. This data can be directly compared to the TAMRA labeled DNA reported in the manuscript. Since R6G is a positively charged dye and TAMRA is neutral we might expect different kinetics for the DNA labeled with the different dyes assuming the dye interferes with DNA hairpin formation. However, as shown in Table 3.3, the reaction times are similar for both samples within experimental error. This suggests the dyes do not interfere with the reaction kinetics.

To investigate the effect of the dyes on thermodynamic stability of the hairpins, we measured the melting temperatures of the DNA of the R6G and TAMRA labeled DNA hairpins, and compared these temperatures with the calculated values for unlabeled hairpins using Oligo Analyzer software from IDT[167]. The results are presented in Table 3.5 below. We found the measured and calculated values were in reasonable agreement, suggesting the dye labels do not significantly alter the thermodynamic stability of the DNA hairpins.

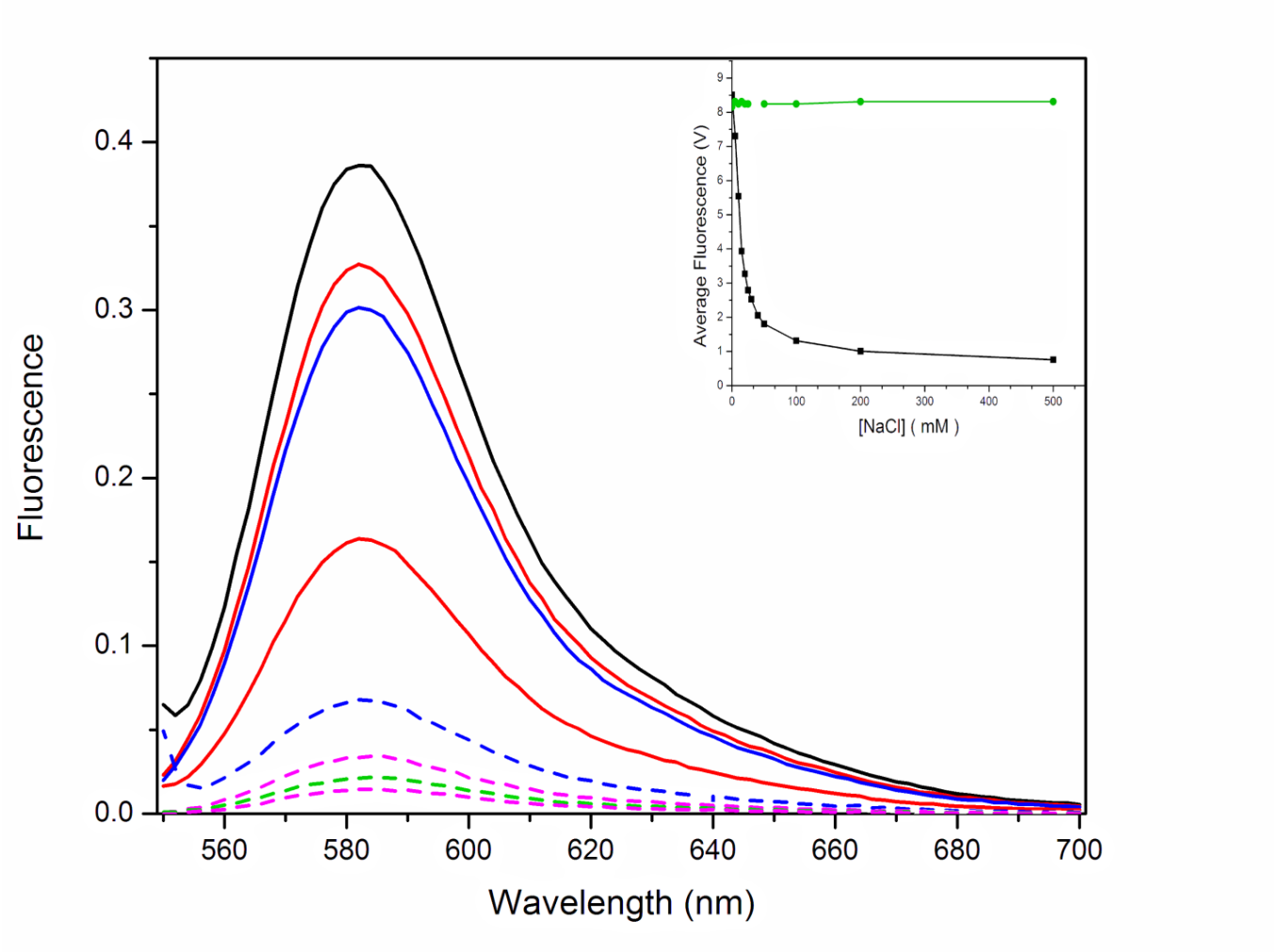

Figure 3.4: The steady state fluorescence spectra of the $hp(T)_{21}$ DNA hairpin at 25^0 C and various NaCl concentrations. The above figure (black, 0; red,5; blue,10; wine,20; dashed navy,50; dashed pink, 100; dashed olive,200; dashed purple,500; mM NaCl) shows the fluorescence has been quenched due to folding at higher NaCl concentrations.

Inset: The average fluorescence voltage as a function of various NaCl concentrations (in mM) for both $hp(T)_{21}$ DNA hairpin (black) as well as control DNA (green) have been plotted. The above figure shows there is no change of fluorescence voltage as a function of NaCl concentration in case of control DNA whereas there is significant change in fluorescence voltage as we go from low to high NaCl concentration in case of $hp(T)_{21}$.

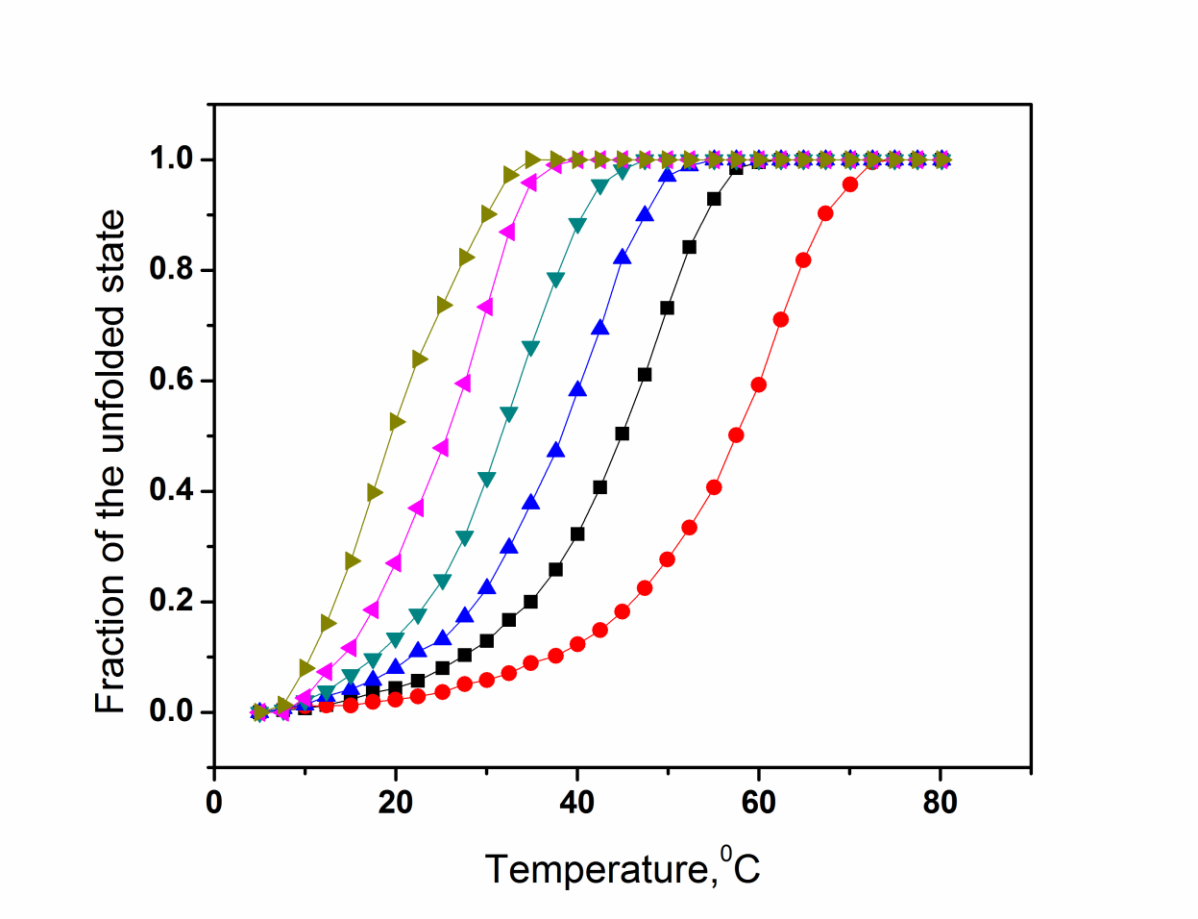

Figure 3.5: The fraction of the unfolded state for the DNA hairpin s as a function of varying NaCl concentration (dark yellow, 5; magenta, 10; dark cyan,25; blue,50; black,100; red,500 mM NaCl respectively).

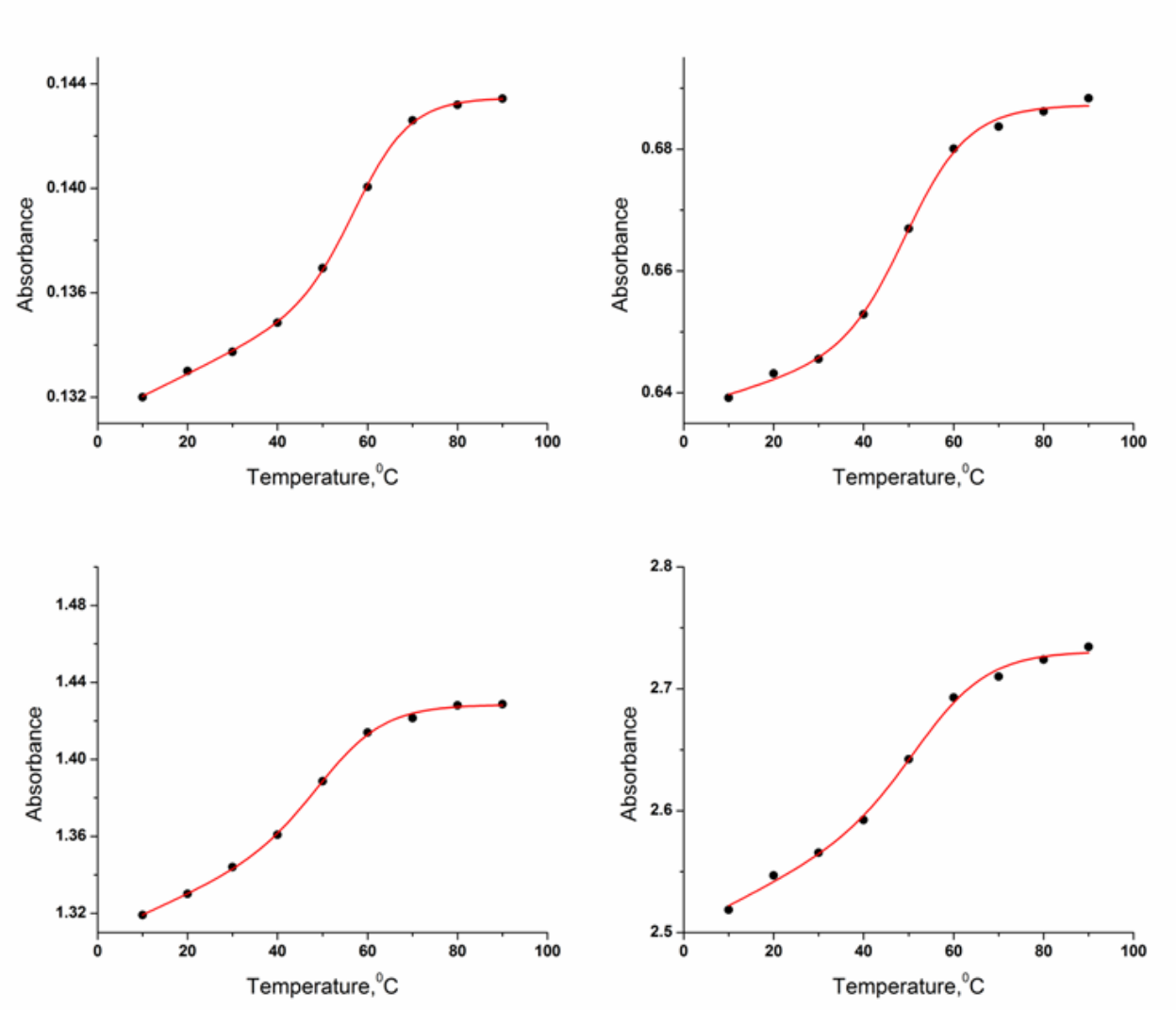

Figure 3.6: The absorbance versus temperature melting profiles for DNA hairpin 5-AACCCTTTTTTTTTTTTTTTTTTTTGGGTT-3.The absorbance at 260 nm has been plotted as a function of temperatures for four different concentrations of DNA hairpin (0.6 µM, top left; 2.8µM,top right; 5.6 µM, bottom left; 10.9 µM, bottom right) in 100 mM NaCl buffer. The T_m has been calculated by fitting the curve by two state models with linear baselines. The value of T_m is shown in the Table 3.3 below.

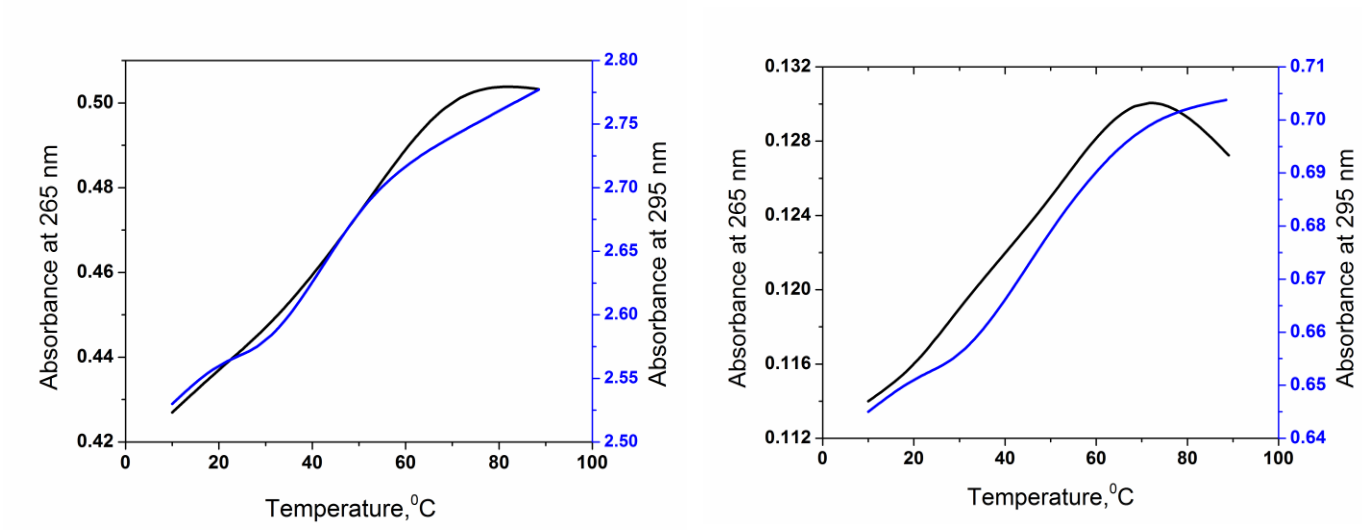

Figure 3.7: Thermal denaturation profiles for DNA hairpin 5-AACCCTTTTTTTTTTTTTTTTTTTTGGGTT-3'in 10 mM sodium cacodylate buffer (pH7.4) and 0.1 mM EDTA containing 100 mM NaCl monitored at 265 nm (black) and 295 nm (blue) respectively. The absorbance profile in the upper panel represents 10.9 µM DNA concentration and the profile in the lower panel represents 2.8 µM DNA concentration.

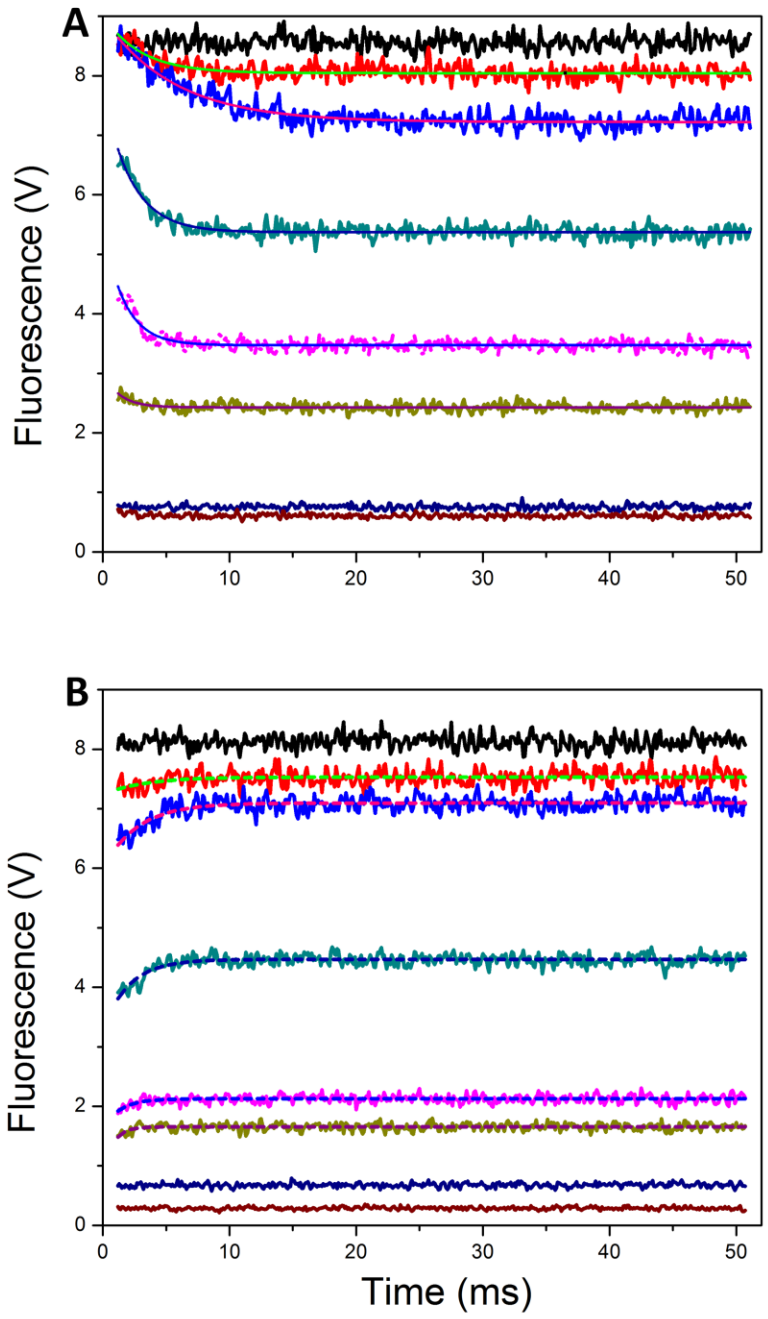

Figure 3.8: Experimental data (solid lines) and corresponding fitting curves (solid dashed lines) from stopped-flow measurements of: A. DNA hairpin $hp(T)_{21}$ folding reaction, B. the DNA hairpin unfolding reaction as a function of varying NaCl concentration (black, 0; red, 5; blue,10; dark cyan,25; magenta,50; dark yellow,100; navy 500 mM NaCl and wine, background buffer).

Table 3.3. Reaction time comparison for different dye labeled DNA hairpins hpT_{21}

[NaCl] (mM)	Reaction time, τ_{rxn}(ms)	
	R6G-DNA hairpin	TAMRA-DNA hairpin
5	5.91 (0.24)	6.38 (0.18)
10	5.28 (0.19)	5.05 (0.13)
25	2.19 (0.15)	2.08 (0.19)
50	1.56 (0.31)	1.33 (0.29)
100	1.02 (0.28)	0.77 (0.23)

The error bar in the parentheses represents the standard deviation from the mean of the three sets of measurements.

Table 3.4. Enthalpy contribution of DNA hairpins hpT_{21} at various [NaCl]

[NaCl] (mM)	Δ H, Kcal/mol
0	-
5	-25.2 (2.1)
10	-31.3 (1.9)
25	-30.9 (2.2)
50	-30.1 (1.5)
100	-29.9 (2.0)
500	-27.6 (1.6)

The error bar in the parentheses represents the standard deviation from the mean of the three sets of measurements.

Table 3.5. Comparison of melting temperature for different labeled hairpins and unlabeled hairpin hpT_{21}

[NaCl] (mM)	Melting Temperature, T_m (° C)		
	R6G-DNA hairpin	TAMRA-DNA hairpin	IDT software (unlabelled DNA hairpin)
0	15	14.6 (2.1)	-
5	-	23.6 (2.7)	31.4
10	-	27.1 (3.1)	34.1
25	28.5	33.7 (2.2)	37.8
50	-	41.1 (2.4)	40.6
100	41.0	44.7 (2.1)	43.4
500	52.5	54.3 (2.9)	50.3

The error bar in the parentheses represents the standard deviation from the mean of the three sets of measurements.

Table 3.6. Concentration dependent melting temperatures, T_ms of DNA hairpin at 100 mM NaCl

[DNA] (μM)	T_m (° C)
	-
0.6	48.8 (1.9)
2.8	49.2 (1.4)
5.6	49.7 (2.2)
10.9	50.1 (1.5)

The error bar in the parentheses represents the standard deviation from the mean of the three sets of measurements

REFERENCES

(137) Hall, K. B. *Curr. Opin.Chem.Biol*.**2008**, 12, 612.

(138) Dobson, C. M. *Nature***2003**, 426, 884.

(139) Bevilacqua, P. C.; Blose, J. M. *Annu. Rev. Phys. Chem*. **2008**, 59, 79.

(140) Chen, S. J. *Ann.Rev. Biophys*.**2008**, 37, 197.

(141) Woodside, M. T.; Anthony, P. C.; Behnke-Parks, W. M.; Larizadeh, K.; Herschlag, D.; Block, S. M. *Science***2006**, 314, 1001.

(142) Bonnet, G.; Krichevsky, O.; Libchaber, A. *Proc. Natl. Acad. Sci. USA***1998**, 95, 8602.

(143) Volker, J.; Makube, N.; Plum, G. E.; Klump, H. H.; Breslauer, K. J. *Proc. Natl. Acad. Sci. USA***2002**, 99, 14700.

(144) Wallace, M. I.; Ying, L.; Balasubramanian, S.; Klenerman, D. *Proc. Natl. Acad. Sci. USA***2001**, 98, 5584.

(145) Grunwell, J. R.; Glass, J. L.; Lacoste, T. D.; Deniz, A. A.; Chemla, D. S.; Schultz, P. G. *J. Am. Chem. Soc*.**2001**, 123, 4295.

(146) Tan, Z. J.; Chen, S. J. *Biophys. J*. **2008**, 95, 738.

(147) Zhang, W.; Chen, S. J. *Proc. Natl. Acad. Sci. USA**2002,*** 99, 1931.

(148) Ansari, A.; Kuznetsov, S. V.; Shen, Y. *Proc. Natl. Acad. Sci. USA***2001**, 98, 7771.

(149) Liphardt, J.; Onoa, B.; Smith, S. B.; Tinoco, I.; Bustamante, C. *Science***2001**, 292, 733.

(150) Portella, G.; Orozco, M. *Angew. Chem*. **2010**, 122, 7839.

(151) Van Orden, A.; Jung, J. *Biopolymers* **2008**, 89, 1.

(152) Werner, J. H.; Joggerst, R.; Dyer, R. B.; Goodwin, P. M. *Proc. Natl. Acad. Sci. USA***2006**, 103, 11130.

(153) Yin, Y.; Zhao, X. S. *Acc. Chem. Res*. **2011**, 19, 12799.

(154) Ansari, A.; Shen, Y.; Kuznetsov, S. V. *Phys. Rev. Lett*. **2002**, 88, 069801.

(155) Sorin, E. J.; Engelhardt, M. A.; Herschlag, D.; Pande, V. S. *J. Mol. Biol.***2002**, 317, 493.

(156) Zhang, W.; Chen, S. J. *Biophysical J.***2006**, 90, 778.

(157) Ma, H.; Proctor, D. J.; Kierzek, E.; Kierzek, R.; Bevilacqua, P. C.; Gruebele, M. *J. Am. Chem. Soc.* **2006**, 128, 1523.

(158) Ma, H.; Wan, C.; Wu, A.; Zewail, A. H. *Proc. Natl. Acad. Sci. USA***2007**, 104, 712.

(159) Jung, J.; Ihly, R.; Scott, E.; Yu, M.; Van Orden, A. *J. Phys. Chem. B*.**2007**, 112, 127.

(160) Jung, J.; Van Orden, A. *J. Phys. Chem. B.***2005**, 109, 3648.

(161) Jung, J.; Van Orden, A. *J. Am. Chem. Soc*.**2006**, 128, 1240.

(162) Gupta, A. N.; Vincent, A.; Neupane, K.; Yu, H.; Wang, F.; Woodside, M. T. *Nat. Phys.*.**2011**, 7, 631.

(163) Gong, P.; Campagnola, G.; Peersen, O. B. *Anal. Biochem*.**2009**, 391, 45.

(164) Woodside, M. T.; Behnke-Parks, W. M.; Larizadeh, K.; Travers, K.; Herschlag, D.; Block, S. M. *Proc. Natl. Acad. Sci.USA***2006**, 103, 6190.

(165) Dickson, P. N.; Margerum, D.W.*Anal.Chem.***1986**, 58, 3153.

(166) Huppert, J. L.; Balasubramanian, S. *Nucleic AcidsRes.* **2005**, 33, 2908.

(167) Owczarzy, R.; Moreira,B. G.; You, Y. ; Behlke, M.A.; Walder, J.A. *Biochem.* **2008**, 47, 5336.

(168) Kaushik, M.; Bansal, A.;Saxena, S.; Kukreti,S. *Biochem.* **2007**, 46, 7119.

(169) Mergny, J. L.; Phan,A. T.; Lacroix, L. *FEBS Lett.***1998**, 435, 74.

CHAPTER 4: Counter-ion and Polythymidine Loop Length Dependent Folding and Thermodynamic Stability of DNA Hairpins Reveal the Unusual Counter-ion Dependent Stability of Tetraloop Hairpins[B]

This chapter describes loop length and mono-valent counter ion dependent thermodynamic stability and folding kinetics of DNA hairpins. Stem-loop DNA hairpins containing 5-base pair (bp) stem and single stranded polythymidine loop were investigated using thermodynamic melting analysis and stopped-flow kinetics. These studies revealed the thermodynamic stability and folding kinetics as a function of loop length and counter ion concentration. Our results show the unusually high thermodynamic stability for tetraloop or 4 poly(dT) loop hairpin as compared to longer loop length hairpins. Furthermore, this exceptional stability is highly counter ion dependent. For example, in the higher counter ion concentration regime of 50 mM NaCl and above, the tetraloop hairpin displays unusually enhanced stability as compared to longer loop length hairpins. However, at lower counter ion concentration of 25 mM NaCl and below, the thermal stability of tetraloop hairpin is consistent with the longer loop hairpins. The enhanced stability of tetraloop hairpins at higher counter ion concentration can be explained on the basis of the combined entropic effect of loop closure as well as unusual base-stacking in the loop regions. The stability of longer loop length hairpins at all counter ion concentrations, as well as tetraloop hairpin at lower counter ion concentration can be explained on the basis of entropic effect of loop closure alone. The thermodynamic parameters at lower and higher counter ion concentrations were determined to quantify the unusual base-stacking effects

---

[B]Rajesh K. Nayak,[†] and Alan Van Orden[†,*]

This paper is under minor revision in the *J. Phys. Chem. B* 2013
R. Nayak collected and analyzed the data, R. Nayak and A. Van Orden wrote the paper.

occurring at higher counter ion concentrations. For example, at 100 mM NaCl, excess Gibbs energy and enthalpy due to base-stacking within the tetraloops were measured to be –1.2±0.14 and –3.28±0.32 kcal/mole respectively, whereas, no excess of Gibbs energy and enthalpy were observed for 0, 5, 10 and 25 mM NaCl. These findings suggest significant base-stacking interactions occurring in the loop region of the tetraloop hairpins at higher counter ion concentration and less significant base-stacking interactions in the lower counter ion concentration regime. We suggest that at higher counter ion concentrations, hydrophobic collapse of the nucleotides in the loop may be enhanced due to the increased polarity of the solvent, thereby enhancing base-stacking interactions which contribute to unusually high stability.

4.1 Introduction

Stem-loop structured hairpins represent major structural elements in DNA and RNA.[170,171] An intra-molecular double helix stabilized by Watson-Crick base pairs defines the hairpin stem capped by a number of unpaired and paired nucleosides called a loop.[172] DNA hairpins play a pivotal role in biological functions such as gene transcription and DNA recombination due to their capacity to act as binding sites for proteins.[173-178] A clear understanding of the role of DNA hairpins requires a thorough investigation of the thermodynamic stability and folding kinetics of hairpin formation.

The structure and stability of a hairpin depends on stem size, loop size, stem and loop composition, base stacking, base-pairing, hydrogen bonds on the loop and closing base-pair of the loop.[179-184] Over the years, there have been numerous theoretical and experimental studies,[182,185-207] to understand the stability and folding of hairpins including optical

spectroscopic techniques such as t-jump spectroscopy,[180,208] fluorescence correlation spectroscopy (FCS),[186,193,203,209] rapid-mixing stopped-flow,[207] NMR,[210,211] UV absorption, and CD studies[172].

Previously, Antao *et al.*[212,213] observed that the thermodynamic stability of the hairpins with identical stem sequence and variable loop length is enhanced by base stacking interaction within the loop region. This excess stability becomes stronger as the loop length decreases such that shorter loop length imparts greater stability to the hairpin structure. Bevilacqua and co-workers[183,184,214-216] have investigated the sequence-dependent stability of small loops in ssDNA and RNA hairpins. Their observations indicate hydrogen bonding network in the loop region as well as interactions between the loop and the closing base pair that contribute significantly to the stability of the studied hairpins. Kuznetsov *et al.*[217]studied loop length dependent stability and kinetics of hairpin formation by using t-jump spectroscopy and melting experiments and hypothesized that small loop hairpins may be stabilized by the interaction of counter cations with the loops. Previously, Hernandez *et al.*[172] studied the formation of tetraloop hairpins by using CD, Raman and Fourier transform (FTIR) and their findings suggested the unusually high thermal stability of tetraloop hairpins in particular.

Stem-loop hairpins consisting of four bases in the loop region, referred to as tetraloops, are abundant in the genome and therefore its structure is widely studied in the literature.[172,183,218-241] DNA and RNA tetraloop hairpins are very important for their exceptional thermodynamic stability and biological functions. For example, GNRA tetraloops are nucleation sites to help the proper folding of larger RNAs.[184,215] Although more attention has been given to RNA tetraloops for their biological roles such as RNA and protein folding, DNA tetraloops also play an important role in nucleic acid folding as well as genome sequences.

Previously our laboratory has investigated the folding kinetics and thermodynamic stability[207] of DNA hairpins containing 5-base pairs (bp) in the stem and 21 polythymidine nucleotides (nt) in the loop. These studies were carried out using a range of NaCl concentrations in the background buffer, ranging from 0 to 500 mM, and revealed an important dependence of hairpin folding and thermodynamic stability on counter ion concentration. In particular, the reaction mechanism changed from three state reactions above 25 mM NaCl to two state reactions below 25 mM NaCl and also the stability increased with the increasing concentration of NaCl. [207]

In this work, we investigate thermodynamic stability of DNA hairpins with identical 5-bp stem size but with varying poly(dT) loop lengths from 4-21 nt, as a function of counter ion concentration. In all of the hairpins, the stability increases with increasing counter ion concentration as expected, and the stability increases with decreasing loop size. In the case of tetra loop hairpins, the stability pattern depends on the counter ion concentration regime. For counter ion concentrations below 25 mM NaCl, the stability of the tetraloop hairpin follows the same trend as that observed for the longer loop length hairpins. However, above 25 mM NaCl, the tetraloop hairpins exhibit exceptional thermodynamic stability above and beyond that observed in longer loop length hairpins. This contrasting stability behavior of tetraloop hairpins at lower and higher counter ion concentrations as compared to longer loop length hairpins may reveal important information regarding DNA tetra loop formation and its biological importance. In particular, we suggest the enhanced stability at higher NaCl concentrations is due to unusual intra-loop base-stacking interactions in the tetraloops and the stem.[242-244] The studies reported here quantify the thermodynamic parameters associated with these unusual base-stacking interactions.

4.2 Experimental Methods

4.2.1 Materials

The DNA hairpins examined in these studies consisted of a five base pair stem with the complementary sequences 5'-AACCC and GGGTT-3' and loops containing 4, 8, 12 and 21 polythymidine [poly(dT)] residues. The hairpins were dual labeled with fluorophore 5-tetramethylrhodamine (5-TAMRA) at 5' end and a quencher 4-(dimethyl amino azo) benzene-4-carboxyllicacid (dabcyl) at 3' end. Control DNA hairpin samples labeled with the dye TAMRA at 5' end but without quencher at 3' end were examined for comparison. Fluorescently labeled poly(dT) loop DNA hairpins were synthesized, HPLC purified, and characterized using mass spectrometry by Integrated DNA Technologies (Coralville, IA). 1M stock tris(hydroxymethyl)aminomethane-hydrochloride (tris-HCl) was purchased from Sigma-Aldrich and sodium cacodylate buffer was purchased from Electron Microscopy Sciences (Hatfield, PA). Molecular biology grade EDTA and sodium chloride (NaCl) were purchased from Cal Biochem (Gibbstown, NJ). All chemical stock solutions were conformed to be RNAs, DNAs and protease free.

4.2.2 Sample preparation

50-100 nM DNA samples were prepared in 2.5 mM Tris-HCl buffer and 250 μM EDTA. Various concentrations of sodium chloride, ranging from 0 mM to 1000 mM, were prepared for stopped-flow mixing experiments as well as thermodynamic melting experiments. Various concentrations of DNA, ranging from 1.4 μM to 10.9 μM, were prepared in 10 mM sodium cacodylate buffer and 0.1 mM EDTA for carrying out UV-Vis melting experiments of tetraloop

hairpins. All the above mentioned samples were prepared in nuclease free water, purchased from Applied Biosystems (Carlsbad, CA).All solutions were filtered through 0.22 micron Nalgene nitrocellulose filter units.

4.2.3 Stopped Flow Mixing Experiments

Stopped-flow mixing experiments were carried out using an Applied Photophysics SX-20 stopped-flow instrument (Surrey, United Kingdom). Buffer solutions containing 100 mM DNA hairpin in 0 mM NaCl were mixed with pure buffer solutions containing varying concentrations of NaCl inside a 5 µl mixing cell. Folding reactions were observed by monitoring the quenching of fluorescence of TAMRA dye after a 450 µs mixing time. To observe the fluorescence, the dye was excited at 547 nm with bandwidth set to 2 nm and the emission from the dye was detected using 570 nm high pass filter. In the stopped flow experiment, all the folding traces for different loop length DNA hairpins and control DNA hairpins without quencher at various NaCl concentrations were collected and repeated at least three times for the statistical accuracy of our data collections.

4.2.4 Fluorescence Melting Experiments

To examine various DNA hairpin samples, we monitored the temperature dependent fluorescence of the dye-quencher labeled DNA from 5ºC to 95ºC on a steady-state fluorometer (AVIV MODEL ATF 105) equipped with a water bath for sample temperature control. The samples analyzed contained 50 nM DNA in Tris/HCl/EDTA buffer and varying concentrations of NaCl, ranging from 0 to 500 mM. The fluorescence of the TAMRA dye was excited at 547

nm, and the emission was monitored at a single wavelength 585 nm (4 nm excitation and emission bandwidths).

4.2.5 UV-Vis Melting Experiments

Temperature dependent UV-Vis absorbance measurements were used to compare the melting profile of a labeled DNA hairpin with an unlabelled DNA hairpin to observe the effect of dye and quencher on the thermodynamic stability of DNA hairpin samples and also to rule out the possibility of duplex and quadruplex formation in the hairpin samples. These measurements were carried out using Varian Cary 50BioUV-Vis spectrophotometer equipped with multi cell holder and heating/cooling unit. Oligo samples of concentrations ranging from 1.4 μM to 10.9 μM, with and without dye and quencher, were used for the melting experiments. Samples were heated to 95^0 C and were cooled back to the starting temperature of the melt to check the reversibility as well as to eliminate the air bubbles in the samples. Absorbance versus temperature melting profiles were monitored at 260, 265 and 295 nm wavelengths respectively, using single beam mode and subtracting the absorbance from the cuvette containing buffer.

4.3 RESULTS

Melting profiles for the DNA hairpin samples were obtained by monitoring the fluorescence intensity of the TAMRA dye label versus the temperature. Figure 4.1panelA shows representative fluorescence intensity versus temperature profiles for 5-bp stem and 4 poly(dT) loop length hairpin at varying NaCl concentrations. Similar melting profiles were also obtained for the 8, 12 and 21 poly(dT) loop length hairpins. We analyze these melting profiles assuming the two-state modelfolded $\rightleftharpoons$ unfolded.[186,193,207] The first step toward determining the

thermodynamic parameters for the folding and unfolding reactions is to estimate the fraction of the DNA hairpins in the unfolded state, as a function of temperature, $f_{UN}(T)$, according to

$$f_{UN}(T) = \frac{I(T) - I_F}{I_{UN} - I_F} \quad (1.1)$$

where $I(T)$ is the fluorescence intensity at temperature T. I_{UN} and I_F are the measured fluorescence intensities at 95^0C and 5^0C respectively.

From the melting curve analysis, we can evaluate the equilibrium constant

$$K(T) = \frac{[unfolded]}{[folded]} = \frac{f_{UN}(T)}{1 - f_{UN}(T)} \quad (1.2)$$

Furthermore, the fraction of the unfolded state, $f_{UN}(T)$ in terms of free energy change, ΔG, is given by

$$f_{UN}(T) = \frac{K(T)}{1 + K(T)} = \frac{\exp(\frac{-\Delta G}{RT})}{1 + \exp(\frac{-\Delta G}{RT})} \quad (1.3)$$

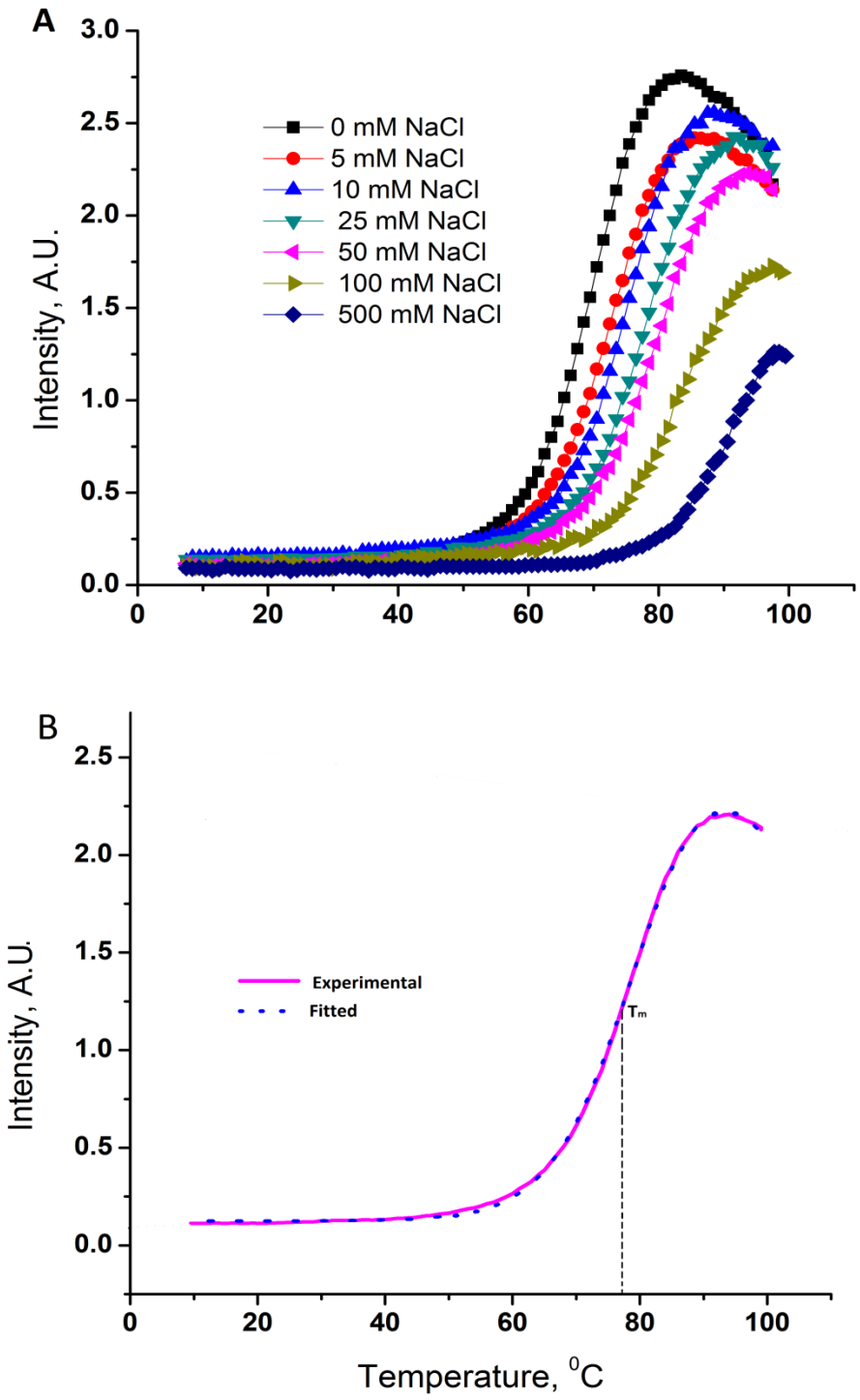

Figure 4.1: Melting profiles for 5-base pair stem and 4 poly(dT) loop length DNA hairpin 5'-AACCC (T)4-GGGTT-3'. Panel A shows the plot of the fluorescence intensity versus varying NaCl concentration (black, 0; red, 5; blue, 10; dark cyan, 25; magenta, 50; dark yellow, 100; navy, 500 mM, respectively) for the tetraloop DNA hairpin. Panel B shows the fitting of temperature melting curve for tetraloop hairpin at 50 mMNaCl. All the above measurements were carried out at ~ 22^0C.

The free energy change of the unfolded state of the hairpin can also be expressed as

$$\Delta G = \Delta H - T\Delta S \quad (1.4)$$

At the melting temperature, equation (1.4) becomes

$$0 = \Delta G = \Delta H - T_m \Delta S \quad (1.5)$$

The change in free energy of the DNA hairpins at the melting temperature can be expressed as

$$\Delta G = \Delta H(1 - \frac{T}{T_m}) \quad (1.6)$$

Introducing the expression for ΔG from equation (1.6) into equation (1.3), the fraction of the unfolded state, $f_{UN}(T)$ in equation (1.3) becomes

$$f_{UN}(T) = \frac{\exp\{\frac{-\Delta H}{R}(\frac{1}{T} - \frac{1}{T_m})\}}{1 + \exp\{\frac{-\Delta H}{R}(\frac{1}{T} - \frac{1}{T_m})\}} \quad (1.7)$$

The melting profile is modeled using the equation (1.7) and the equation below

$$I(T) = [(1 - f_{UN}(T))]*[I_{F,0} - S_F * T] + f_{UN}(T)*[I_{UN,0} - S_{UN} * T] \quad (1.8)$$

where S_F and S_{UN} are defined as the baseline slopes for folded conformation and unfolded conformation respectively. $I_{F,0}$ and $I_{UN,0}$ are fluorescence intensities extrapolated to T=0 for folded and unfolded conformation respectively. The experimental melting data were fitted to equations (1.7) and (1.8) to determine melting temperature and enthalpy of the unfolding reaction. The parameters for this equation are illustrated in Figure 4.1 panel B, which shows the

experimental data and the fit. The melting temperatures (T_ms) evaluated from the fitting at varying NaCl concentrations are shown in *Table 4.1*.

Based on the trends observed in the melting temperatures, we find thatfor each loop length hairpin the melting temperature and thermodynamic stability of the folded state increases with the increase in counter ion concentration. This enhanced stability can be explained on the basis of polyelectrolyte theory. Since DNA is a highly charged polyanion, mono-valent Na^+ is necessary to stabilize its folded state. Furthermore, careful observation of the melting profile of the hairpins and the melting temperatures, T_ms, determined from fitting (see *Table 4.1*) shows that for a given counter ion concentration, the thermodynamic stability of the folded state increases with decreasing loop length, which can be explained by lower entropic cost of loop closure for smaller loop length hairpins.[179,181] In particular, the 4 poly(dT) loop, or tetraloop, hairpin shows exceptional thermodynamic stability at all counter ion concentrations, including 0 mM NaCl. Below, we examine whether this stability is expected based on loop length considerations, or whether other factors enhance the stability above and beyond loop length considerations alone.

To gain a clear understanding about the effect of counter ion concentration on thermodynamic stability of different loop length hairpins, we plotted the melting temperature as a function of varying NaCl concentrations. *Figure 4.2* left Panel (A, B and C) shows the plot of melting temperatures (T_ms) for NaCl concentrations ranging from 50 mM to 500 mM. Similarly, the *Figure 4.2* right Panel (D, E and F) represents the plot of melting temperatures (T_ms) for NaCl concentrations ranging from 0 mM to 25 mM. For higher counter ion concentrations, it was found that the melting temperatures exhibited a nearly linear dependence on loop length for thelonger loop lengths 8, 12 and 21 poly (dT) nucleotide hairpins. Regression analysis of the

temperature melt data for the larger poly (dT) loop length DNA hairpins was performed to obtain the best-fit linear equation expressing T_m as a function of loop length (solid red line). Error analysis was also used to calculate 95% confidence intervals for the regression equation (solid blue and green lines). To investigate the exceptional stability of the tetraloop hairpin as compared to longer loop length hairpins, the T_m values determined from experiment (black squares) and the T_m values predicted by extrapolating the regression equation to a 4 poly(dT) loop (red dots) were compared. For higher counter ion concentration regime (50, 100 and 500 mM NaCl), the determined experimental T_m values for the tetraloop hairpin were higher than the T_m values predicted by the regression equation. Moreover, the experimental $T_m$values for the tetraloop hairpins are well outside (higher than) the confidence level predicted by the regression line. This analysis shows the tetraloop hairpin exhibits exceptionally high thermodynamic stability at higher counter ion concentration regime from 50 mM NaCl and above, as compared to other longer loop length hairpins.

Table 4.1. Thermodynamic parameters for DNA hairpins melting

[NaCl] (mM)	Melting Temperature, T_m (° C)			
	Tetraloophairpin	Poly(dT)$_8$hairpin	Poly(dT)$_{12}$hairpin	Poly(dT)$_{21}$hairpin
0	68.4 (2.4)	45.3 (2.7)	29.1 (2.3)	14.6 (2.1)
5	71.6 (2.3)	50.3 (1.9)	36.5 (2.6)	23.6 (2.7)
10	74.4 (2.3)	53.4 (2.5)	40.5 (2.7)	27.1 (3.1)
25	76.7 (2.0)	56.7 (2.4)	46.4 (2.5)	33.7 (2.2)
50	78.8 (2.2)	60.7 (1.5)	55.3 (2.1)	41.1 (2.4)
100	83.1 (2.1) 80.2±2.4[a] 79.5±2.7[b]	64.5 (1.9)	57.8 (1.7)	44.7 (2.1)
500	91 (2.1)	77.1 (1.8)	72.1 (2.0)	54.3 (2.9)

[a]Melting temperature of labeled tetraloop hairpin carried out by UV absorbance measurements at 100 mM NaCl.
[b]Melting temperature of unlabeled tetraloop hairpin carried out by UV absorbance measurements at 100 mM NaCl.

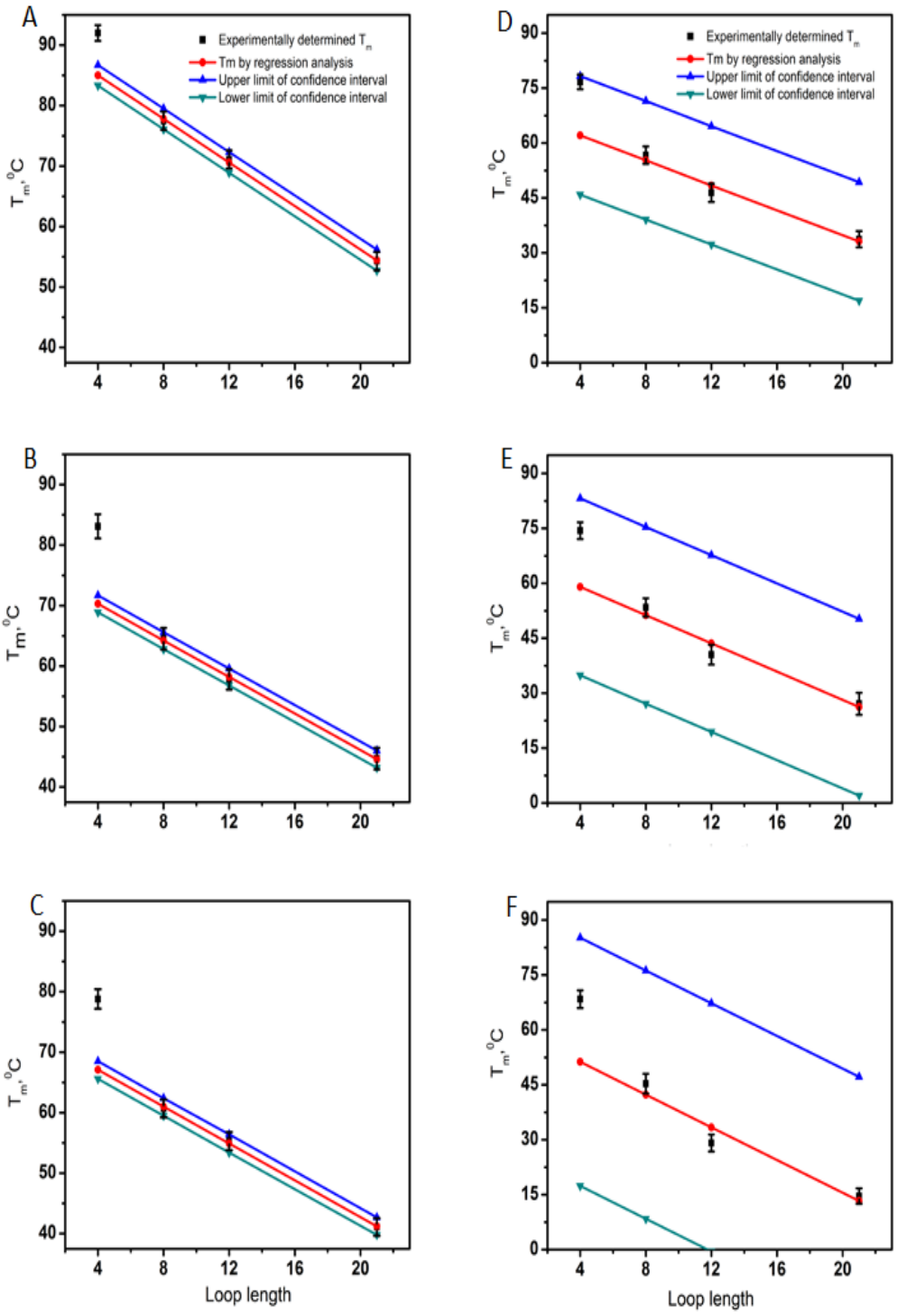
A
B
C
D
E
F
Experimentally determined T_m
Tm by regression analysis
Upper limit of confidence interval
Lower limit of confidence interval
T_m, ^{0}C
Loop length

Figure 4.2: The plot of melting temperature, T_m versus loop length for different poly(dT) loop length hairpins at varying NaCl concentrations. (Left: panel A, 500 mM; panel B, 100 mM; panel C, 50 mM) and (Right: Panel E, 0 mM; panel F, 10 mM; panel G, 25 mM) The black squares represent the experimentally determined T_m values from the fitting algorithm. The red line represents the best-fit linear regression using data for T_8, T_{12} and T_{21} hairpins. The blue and green lines represent the upper and lower limits of the 95% confidence interval based on the regression analysis.

A similar regression and error analysis was carried out for the 8, 12 and 21 poly(dT) loop length hairpins at lower counter ion concentrations (0, 10 and 25 mM NaCl). However, in the lower counter ion concentration regime, the relationship between T_m and the loop length is no longer linear. Therefore, the regression analysis produced larger error bars, such that the melting temperature of the tetraloop hairpin fell within the predicted range. This suggests at lower counter ion concentration, the experimental T_m values for the tetraloop hairpin are consistent with the loop length dependence observed for longer loop length hairpins. In summary, it was found that the tetraloop exhibits unusual thermal stability compared to longer loop length hairpins, but this unusual stability is dependent on counter ion concentrations above 50 mM NaCl, and is less pronounced at lower counter ion concentrations.

To quantify the exceptional counter ion dependent tetraloop stability, we determined the free energy change of different loop length hairpins as a function of varying NaCl concentrations. *Figure 4.3A* shows the change in free energy, ΔG in kcal/mole as a function of varying counter ion concentrations for 4, 8, 12 and 21 poly(dT) loop length hairpins. The change in free energy, ΔG for each loop length hairpin was calculated by using experimental enthalpy change equation (1.6). The free energy change plot clearly shows that the stability increases with the decrease of the loop length and tetraloop hairpin is the most stable hairpin. Remarkably, even at 0 mM NaCl concentration the tetraloop hairpin is highly stable in the wide temperature range from 0^0C to 50^0C in contrast to longer loop length hairpins, as evidenced by the large negative ΔG.

Figure 4.3A also shows ΔG values for the tetraloop hairpin predicted by the equation

$$\Delta G_{predicted} = \Delta H_{predicted}(1 - T/T_{m,predicted}) \quad (1.9)$$

$\Delta G_{predicted}$ are the values that would be obtained assuming the thermodynamic stability of tetraloop hairpin exhibits the same loop-length dependence as the longer loop length hairpins. $T_{m,predicted}$ was obtained using T_m values predicted by regression analysis in T_m vs. [NaCl] plots (Figure 4.2). $\Delta H_{predicted}$ values for the tetraloop hairpin at varying NaCl concentrations were predicted by extrapolation from longer loop length hairpins. Figure 4.3B shows the $\Delta H_{experimental}$ versus loop length plot at various NaCl concentration for 8, 12 and 21 poly(dT) loop length hairpins. The $\Delta H_{predicted}$ values were obtained by extrapolating the line to 4 poly(dT) loop length hairpin. The measured ΔH values for the tetraloop hairpins are also shown for the comparison. The careful observation of experimentally determined $\Delta G_{experimental}$ values (cyano triangles) and predicted $\Delta G_{predicted}$ value shows that in the higher concentration regime of 50 mM NaCl and above, the ΔG values are less negative compared

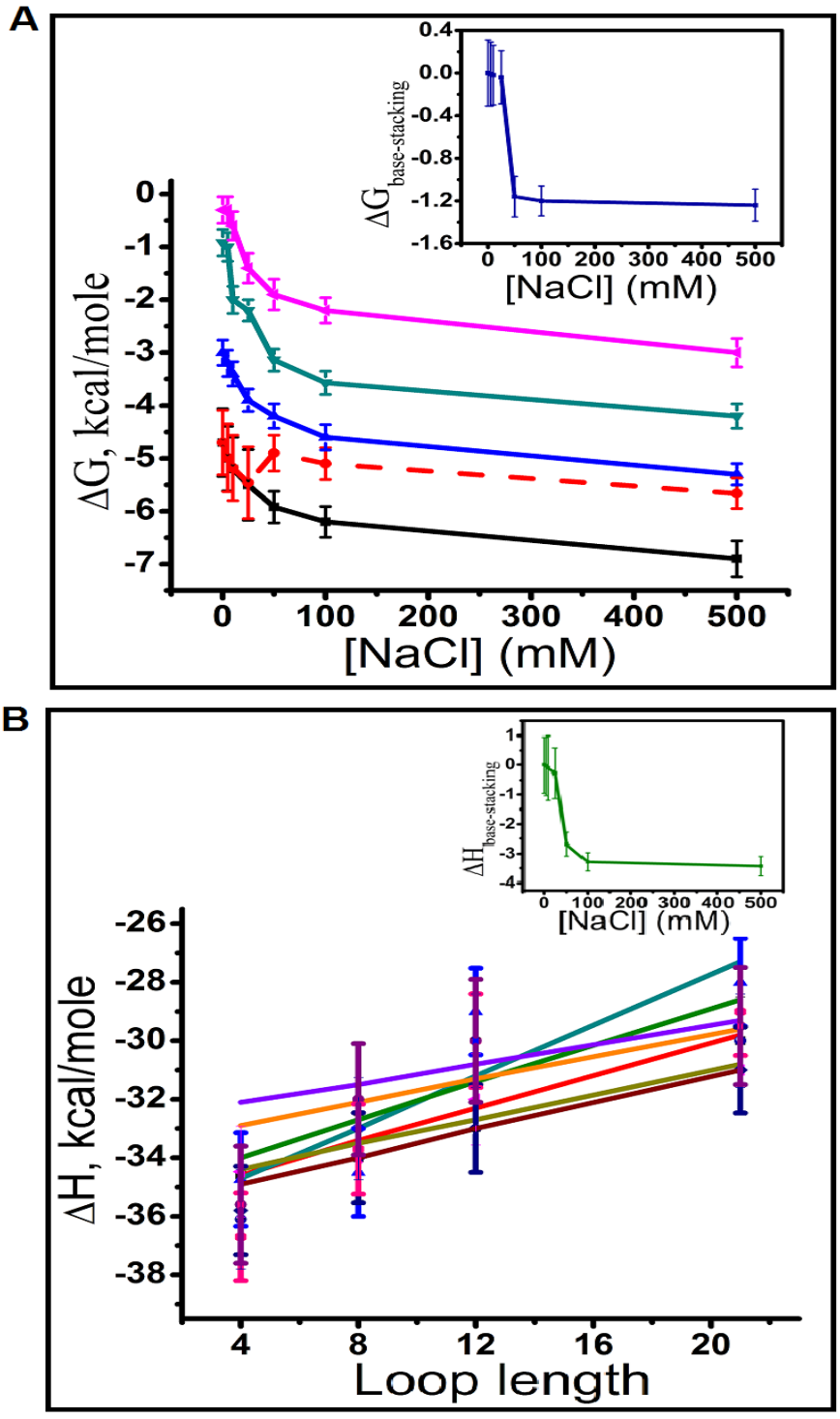
A
ΔG, kcal/mole
[NaCl] (mM)
ΔG base-stacking
[NaCl] (mM)
B
ΔH, kcal/mole
Loop length
ΔH base-stacking
[NaCl] (mM)

Figure 4.3: Panel A presents the plot of experimental ΔG values versus NaCl concentration for different poly(dT) loop length hairpins :T_4 hairpin, black; T_8, royal; T_{12}, dark cyan; T_{21}, magenta. The red circles show the predicted ΔG values for the tetraloop hairpin (T_4) at varying NaCl concentrations. The plot of $\Delta G_{\text{base-stacking}}$ versus NaCl concentration for the tetraloop hairpin is shown in the inset. Panel B shows plots of experimental ΔH values versus loop length at varying NaCl concentrations (0 mM, black square; 5 mM, blue triangle; 10 mM, pink triangle; 25 mM, blue diamond;50 mM, magenta circle; 100 mM, royal circle; 500 mM, purple circle). Regression lines based on ΔH data for 21, 12 and 8 poly(dT) loop length hairpins are shown for different NaCl concentrations (0 mM, red; 5, dark cyan; 10, dark yellow; 25, wine; 50, olive; 100, orange; 500 mM, purple) and are used to predict ΔH for tetraloop hairpins at each NaCl concentration. The inset Figure 4 B shows the plot of $\Delta H_{\text{base-stacking}}$ as a function of varying NaCl concentration for tetraloop hairpin.

to the corresponding ΔG values determined from the experiment. In the lower counter ion concentration regime up to 25 mM NaCl, both predicted and experimentally determined ΔG values nearly overlap with each other. This free energy analysis further supports the unusual counter ion dependent stability of tetraloop hairpin compared to other longer loop length hairpins, as evidenced by our melting temperature versus loop length analysis (Figure 4.2).

Rapid stopped-flow mixing was used to investigate the folding kinetics of the various size DNA hairpins as a function of NaCl concentration. Folding reactions of 4, 8, 12 and 21 poly(dT) loop length hairpins were carried out by mixing 100 nM DNA hairpins in 0 mM NaCl (low salt buffer) in one channel with varying concentrations of NaCl ranging from 0 mm to 1000 mM NaCl in the other channel. Reactions were monitored by observing the quenching of the TAMRA fluorophores by dabcyl after a mixing time of ~450 μs. All experiments were carried out at a laboratory temperature of ~22°C.*Figure 4.4* (panels A, B, C and D) shows stopped flow mixing data obtained for different poly(dT) loop length DNA hairpins in an aqueous buffer. Control experiment data is also shown (on the top of each panel) for comparison.

As we compare the folding reactions of different loop length hairpins (*Figure 4.4*, panels A, B, C and D), we found that the folding reactions of hairpins smaller than 12 poly(dT) loop length cannot be observed on the time scale of our rapid-mixing stopped-flow experiment. For the 12 poly(dT) loop length hairpin, only the reaction at the lower NaCl concentration can be observed. This suggests that the folding reactions generally occur on a faster time scale than the 450 μs mixing time, as the hairpin loops become smaller and as the NaCl concentration increases. The rapid-mixing stopped-flow data also reveals the relative thermodynamic stability of the different sized hairpins after equilibrium is established at the room temperature of the experiment (22^0C). For the larger 8, 12, and 21 poly(dT) hairpins,

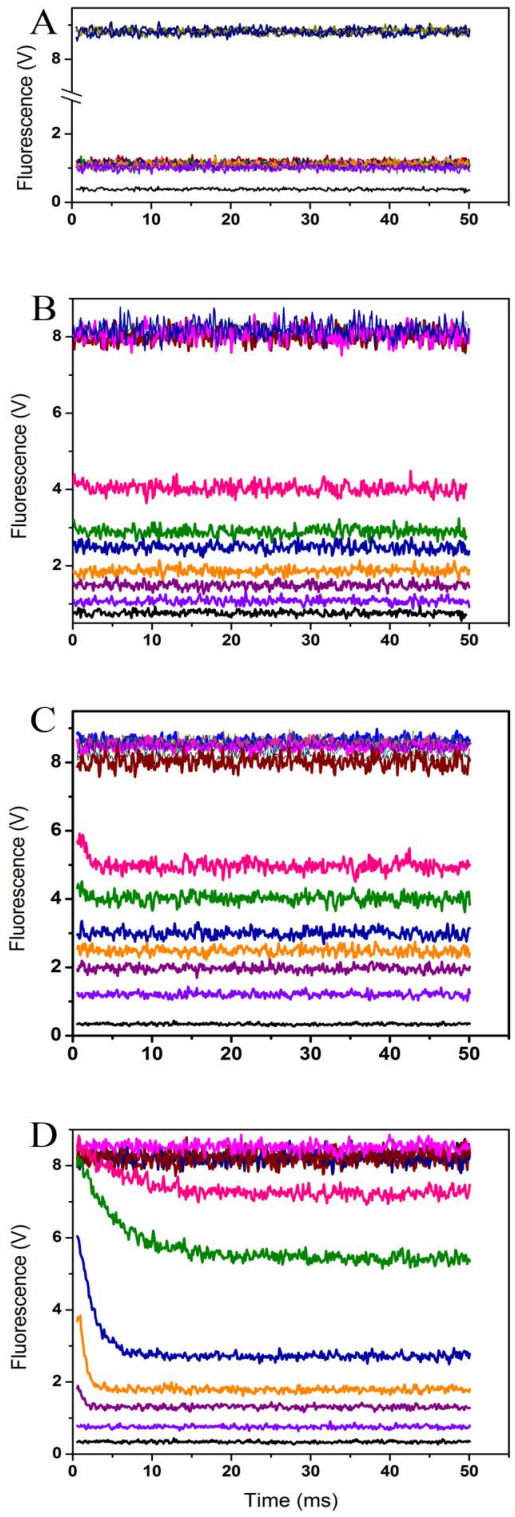
A
B
C
D
Fluorescence (V)
Time (ms)
0
2
4
6
8
10
20
30
40
50

Figure 4.4: Experimental stopped-flow kinetics data for hairpins with a 5-base pair stem and different poly(dT) loop lengths are presented in four panels: Panel A, T4 loop length; Panel B, T8 loop length; Panel C, T12 loop length; Panel D, T21 loop length. In each panel, data is shown for the various NaCl concentrations: (wine,0; pink,5; olive,10; royal,25; orange,50; purple,100; violet,500 mM NaCl; black, background buffer). At the top of each panel, the kinetics data for the respective control DNA hairpins without quencher are shown for comparison. All these measurements were carried out at ~ 22^0C.

the stability of the folded state increases with increasing NaCl concentration, as is evident from the increased quenching of the TAMRA fluorescence. However, the unusual thermodynamic stability of the tetraloop is further revealed by the careful observation of the stopped-flow mixing data shown in Figure 4.4 (panel A). Interestingly, we found that even at 0 mM NaCl (without counter ion concentration) the hairpin has been folded significantly and the extent of quenching does not depend on counter ion concentration.

To further substantiate the above observations, we plotted average fluorescence versus NaCl concentration for different poly(dT) loop length hairpins from rapid-mixing stopped-flow experiments at 22^0C, as shown in *Figure 4.5*. Here we observe that for loop length 8,12 and 21 poly(dT) hairpins, there is significant quenching of TAMRA fluorescence due to folding as we go from 0 mM NaCl (where the hairpins are unfolded) to 500 mM NaCl. Whereas, for 4 poly(dT) loop length hairpin, the quenching is significant even at 0 mM NaCl and the extent of quenching does not depend on NaCl concentration. The folding kinetics of loop length 8 and 12 poly(dT) hairpins follow the same pattern as our previously studied 21 poly(dT) hairpin.[207]

The question might arise whether the dye-quencher interaction may play a role in the thermodynamic stability and folding behavior of the tetraloop hairpin. In order to address this question, we performed UV-Vis melting experiments for both TAMRA dye and dabcyl quencher labeled hairpin and unlabeled tetraloop hairpin at 100 mM NaCl buffer. The melting profiles for labeled and unlabeled tetraloop hairpins are shown in *Figure 4.6*.The melting temperatures, T_ms for both the labeled and unlabeled tetraloop hairpins were determined by fitting the UV-Vis melting data with linear baselines. We found that the melting temperatures, T_ms for labeled and unlabeled hairpins are identical within statistical

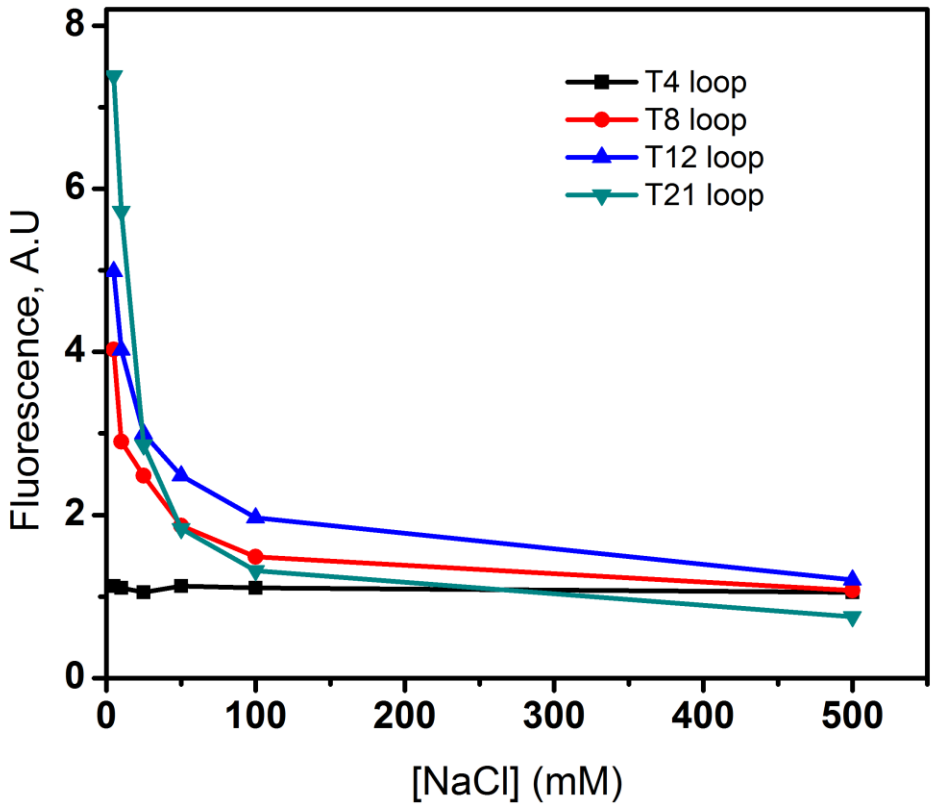

Figure 4.5: The plot of average fluorescence versus NaCl concentration from stopped-flow experiments for different loop length hairpins (black, T4 loop; red, T8 loop; blue, T12 loop; green, T21 loop).

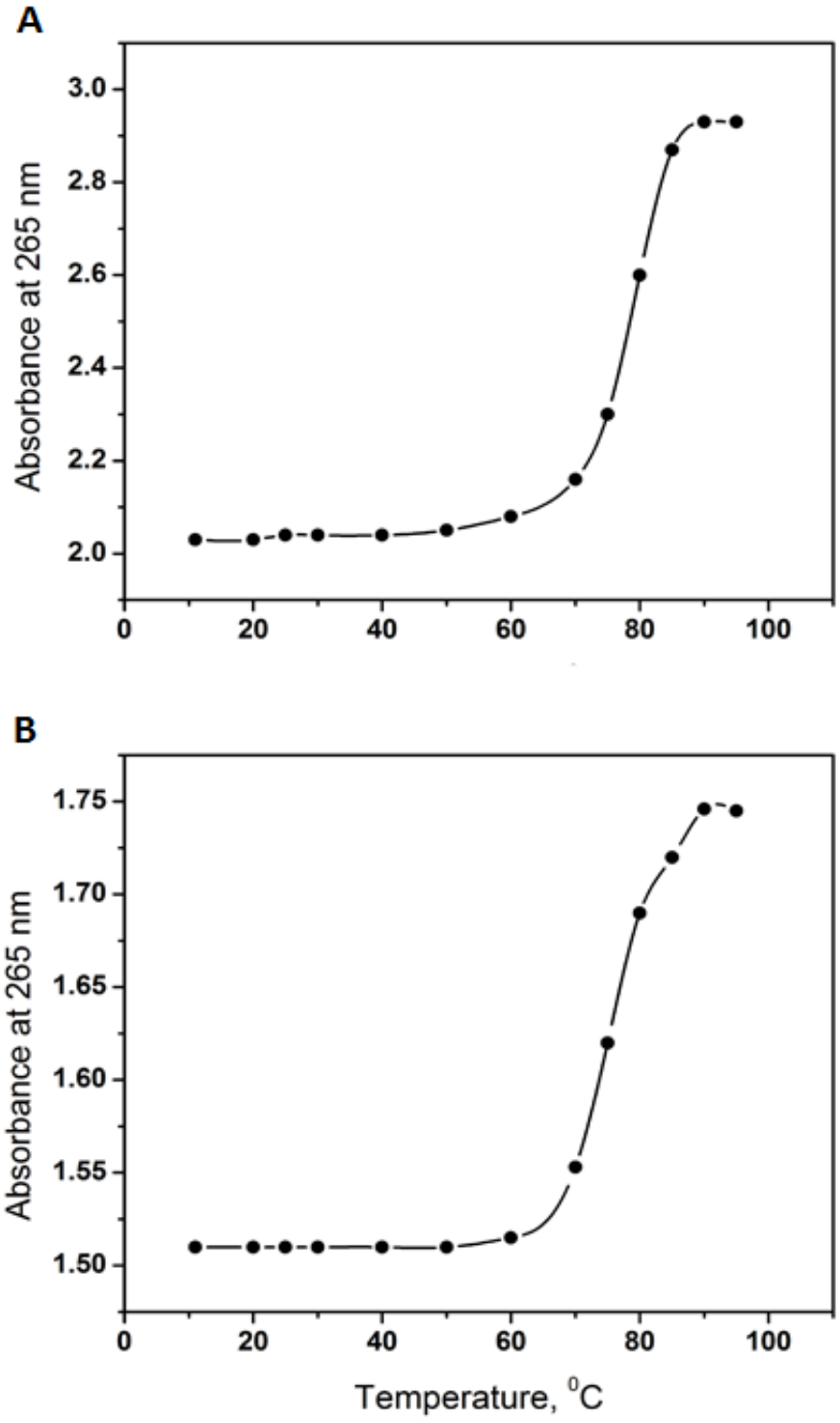
A
Absorbance at 265 nm
3.0
2.8
2.6
2.4
2.2
2.0
0
20
40
60
80
100
B
Absorbance at 265 nm
1.75
1.70
1.65
1.60
1.55
1.50
0
20
40
60
80
100
Temperature, ^{0}C

Figure 4.6: The absorbance versus temperature melting profiles for labeled tetraloop DNA hairpin 5-AACCCTTTTGGGTT-3 (panel A) and the unlabeled tetraloop hairpin (panel B).The absorbance at 265 nm has been plotted as a function of temperature for 10.9 μM oligo concentration (for both labeled and unlabeled hairpins) in 100 mM NaCl buffer. The melting temperatures for both samples are determined to be equal, within statistical error (see Table 4.1)**.**

error *(See Table 4.1)*. The UV-Vis melting experiments suggest that the dye label has no effect on the exceptional thermodynamic stability and unusual folding behavior as compared to other longer loop length hairpins studied in this work. Similar thermodynamic analysis were performed (see supporting information) to rule out the possibility of duplex and/or quadruplex formation interfering with melting and stopped-flow mixing data in the tetraloop hairpin samples.

4.4 DISCUSSION

There have been numerous structural and thermodynamic studies on stem-loop nucleic acid hairpins. The present investigation of counter ion dependent thermodynamic stability and folding kinetics of various loop length DNA hairpins provide important information about the unusual properties of tetraloop hairpins in different counter ion concentration regimes. As expected, the thermodynamic stability of different loop length hairpins increases with the decrease of loop length with smaller loop length hairpins stabilized to a greater extent than longer loop length hairpins. This loop length dependent stability can be explained by entropic cost of loop closure[179,181,245] in which the closure of the longer loop requires more free energy than the closure of the smaller loop. Therefore, from the entropic standpoint, the smaller loop length hairpins are more stable than longer loop length hairpins. Previously it has been suggested that the hydrophobic interactions within the loops, and the exclusion of water from the tight loops, may be important factors in stabilizing smaller loop length hairpins.[246] The most apparent result of our studies is that the tetraloop hairpin exhibits unusually high thermal stability compared to longer loop length hairpins, but this unusual stability is highly dependent on counter ion concentration above 50 mM NaCl and is less pronounced at lower counter ion concentrations. We suggest the exceptional stability of the tetraloop hairpin at higher counter ion

concentration regime can be explained by the combined unusual thymidine-thymidine (T-T) base stacking in the loop regions and the entropic effect of the loop closure. In contrast, the larger polythymidine loop length hairpins are not believed to exhibit significant intra-loop base-stacking, and the base-stacking diminishes with the increase of loop length.[181,245, 247]

Previously, Hare *et al.*[242]performed2D-NMR and distance geometry calculation studies on d(CGCGTTTTCGCG) and observed that the DNA sequence forms hairpins in solution and the bases in the loop region are stacked. Chattopadhyaya*et.al.*[243,245] resolved the crystal structure of a synthetic DNA hexadecanucleotide of sequence C-G-C-G-C-G-T-T-T-T-C-G-C-G-C-G and noticed that it adopts a monomeric hairpin configuration with a Z-DNA hexamer stem. They also observed that in the T4 loop, bases T7, T8 and T9 stack with one another and with the sugar of T7. They also observed that two T10 bases from different molecules stack between the C1-G16 terminal base pairs to simulate a T.T mis-pair. Further, the distances between thymine N and O atom suggest that two thymine bases are hydrogen bonded.[243,245] The tetraloop hairpin in the present studies with the sequence 5'-AACCCTTTTGGGTT-3' probably shows intra loop interaction, whereT6, T7, T8 and T9 thymine bases stack with each other at higher counter ion concentration. Figure 4.7 illustrates the base-stacking effect of tetraloop hairpin at higher counter ion concentration.

However, in the lower counter ion concentration regime up to 25 mM NaCl concentration, the effect of intra loop base stacking is less pronounced and the thermal stability of the hairpin is mainly due to the entropic effect of the loop closure. Therefore, the thermal stability of the tetraloop hairpin is consistent with the trends observed for 8, 12 and 21 poly(dT) loop length hairpins. In summary, the exceptionally stability of the tetraloop hairpins compared to longer loop length hairpins in the higher counter ion concentration regime is due to the

combined effect of unusual base stacking in the loop regions and entropic effect of the loop closure. In the lower counter ion concentration regime, the thermal stability of the tetraloop hairpin is primarily due to entropic effect and the intra loop base stacking effect is less pronounced.

The intra loop base stacking effect which is responsible for the greater stability of tetraloop hairpin in the higher counter ion concentration regime can be quantified in terms of free energy change of base stacking as:

$$\Delta G_{base-stacking} = \Delta G_{observed} - \Delta G_{predicted} \quad (1.10)$$

Where, $\Delta G_{predicted}$ is given by equation (1.9) and represents the free energy change assuming entropic considerations alone. For example, at 100 mM NaCl, we find $\Delta G_{base-stacking}$ = –1.2 ± 0.14 kcal/mole, while at 0 mM NaCl, $\Delta G_{base-stacking}$ = 0.01 ± 0.3 kcal/mole. This represents the enhanced stability provided by the base-stacking interaction in the loop. The plot of $\Delta G_{base-stacking}$ as a function of varying NaCl concentration is shown in the inset *Figure 4.3A* for illustration. Likewise, the intra-loop base-stacking in terms of enthalpy change can be written as:

$$\Delta H_{base-stacking} = \Delta H_{observed} - \Delta H_{predicted} \quad (1.11)$$

For example, at 100 mM NaCl, $\Delta H_{base-stacking}$ = –3.28 ± 0.32 kcal/mole, while at 0 mM NaCl, $\Delta H_{base-stacking}$ = 0.02 ± 0.9 kcal/mole, which shows that at higher counter ion concentration of 50 mM and above, the enthalpic contribution of base-stacking is significant. The plot of

$\Delta H_{base-stacking}$ as a function of varying NaCl concentration is shown in the inset Figure 4.3B for illustration.

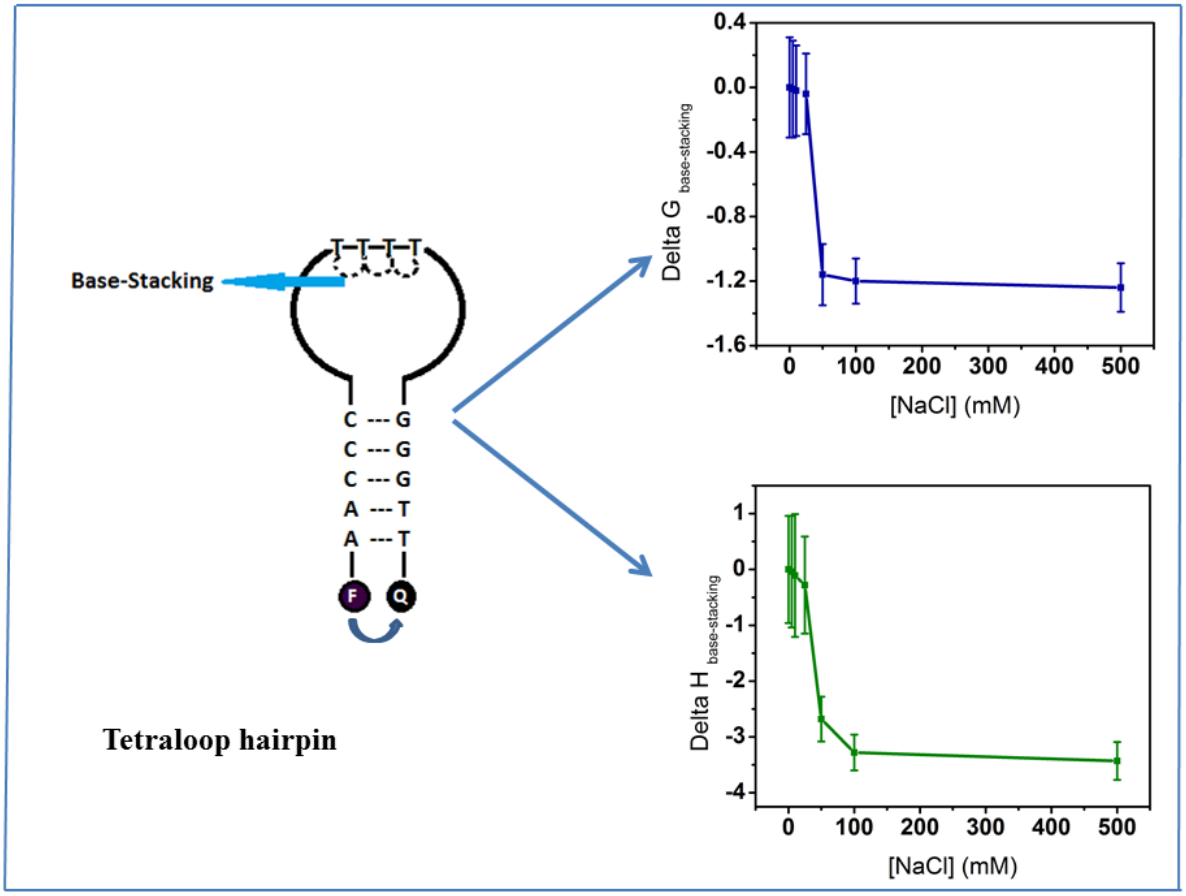

Figure 4.7: Schematic illustration of base-stacking for tetraloop hairpins at higher NaCl concentration.

The enhanced base-stacking interactions at higher counter ion concentration can be further explained by the collapse of the hydrophobic bases in the more polar solvent, famously known as “hydrophobic collapse”. The tetraloop hairpin is structurally rigid and due to the more polar nature of solvents (water) at higher counter ion concentrations, the non-polar hydrophobic bases stack with each other. Once the hydrophobic bases stack, release of water results in an overall entropy gain for water. Whereas, at lower counter ion concentrations, the base-stacking interactions are less pronounced due to the less polar nature of the solvent.

In summary, we found that the free energy change of the base-stacking at higher counter ion concentration regime of 50 mM NaCl and above is significant compared to negligible or almost zero in the lower counter ion concentration regime up to 25 mM NaCl. This suggests that the extra stability of the tetraloop hairpin at higher counter ion concentrations is due to unusual intra-loop base-stacking effect which is less pronounced or negligible at lower counter ion concentrations. Moreover, the base-stacking interactions at higher counter ion concentrations enhance the stability of already more rigid tetraloop hairpins. In other words, the thermal stability of tetraloop hairpin at lower counter ion concentration is more consistent with the longer loop length hairpins where there is no such unusual intra loop base stacking.

4.5 CONCLUSION

In summary, we have reported stopped-flow mixing and thermodynamic melting experiments to investigate the loop length dependent folding and stability of DNA hairpins. We observed that the tetraloop hairpin is exceptionally stable compared to other longer loop hairpins studied and this unusual stability is highly dependent on counter ion concentrations. In the higher counter ion concentration regime of 50 mM NaCl and above, the tetraloop exhibits unusually

high thermal stability as compared to longer loop length hairpins. This unusual high stability of tetraloop hairpin compared to longer loop length hairpins can be explained by combined entropic effect and intra-molecular base stacking. However, in the lower counter ion concentration regime, the thermal stability of tetraloop hairpin is consistent with other longer loop length hairpins due to entropic effects only. Moreover, at higher counter ion concentrations, the hydrophobic collapse of the non-polar bases in more polar solvent enhances the base-stacking interactions, giving extra stability to the already more rigid tetraloop hairpin. Our stopped flow mixing studies reveal that the folding becomes faster with the decrease of the loop length from 21 polythymidine loop to 4 polythymidine loop as a function of counter ion concentration. Remarkably, tetraloop hairpin folds significantly even at 0 mM NaCl and this unusual stability at 0 mM counter ion concentration is due to highly rigid tetraloops and very low entropic cost of loop closure. Since DNA hairpins play important roles in gene transcription, recombination and other important biological processes, these exceptional and unusual counter ion dependent stability studies may help reveal important biological information.

4.6 Supporting Information

We performed concentration dependent melts of the DNA samples using UV-Vis melting experiments (See manuscript for details) to investigate the presence of duplex in our tetraloop hairpin samples. The absorbance versus temperature melting profiles were scanned at 265 nm for various DNA concentrations and the melting temperatures (T_m s) were calculated using two state models with linear base lines (see Figure 4.8). Table 4.2 shows the melting temperatures of the tetraloop hairpin at varying oligo concentrations. We observed that the melting temperatures do not change as a function of DNA concentration and the T_ms at various micro-molar oligo concentrations are approximately equal within the statistical error**.** Since the

melting temperatures do not change with varying DNA concentration, the presence of dimer or duplex formation is ruled out in the hairpin samples. Furthermore,for the UV-Vis melting experiments, micro-molar DNA concentrations were used and for rapid-mixing stopped flow experiments, we used nano-molar DNA concentrations. Since UV-Vis melting experiments rule out the possibility of duplex formation in micro-molar concentrations of DNA samples, the possibility of duplex formation in our nano-molar samples in stopped-flow mixing experiments is also eliminated.

The guanine rich oligodeoxinucleotides can form a tetrameric structure called G-quadruplex[248,249,207] .Giventhe sequence of our DNA hairpin (5'- AACCCTTTTGGGTT) which has 3 guanines at 3' end, there is a theoretical possibility of G-quadruplex formation in our samples. In order to rule out the possibility of G-quadruplex formation, the UV-Vis thermals melts at various micro-molar DNA concentrations were performed and were monitored at 265 and 295 nm. Figure 4.9 shows the melting profiles at both 265 nm and 295 nm for two micro-molar DNA samples. The melting monitored at 265 nm (A_{265}) shows a sigmoidal (hyperchromic) curve and the melting monitored at 295 nm (A_{295}) does not show an inversesigmoidal curve. Since the melting curves at 295 nm are not inverse sigmoidal curves[250,251,207] at various micro-molar DNA concentrations, these results suggest that there is no possibility of G-quadruplex formation in our hairpin samples.

Additionally, we investigated this question of G-quadruplex formation by using an algorithm- called QuadDB[250,207]and a program Quadparser, developed by Simon Rodgers and Julian Huppert at the University of Cambridge, U. K. This algorithm is based on a folding rule: A sequence of the form d($G_{3+}N_{1-7}G_{3+}N_{1-7}G_{3+}N_{1-7}G_{3+}$) will fold into a quadruplex under near-physiological conditions. Here 'N' refers to any base, including guanine, and the near-

physiological conditions are 100 mM KCl and 10 mM Tris-HCl (pH 7.4). Results from this program showed that quadruplex formation would not occur with our tetraloop hairpin sequence hairpin. Therefore, based on both the melting experiments and the Quadparser program, we ruled out the possibility of G-quadruplex formation in our tetraloop DNA hairpin samples.

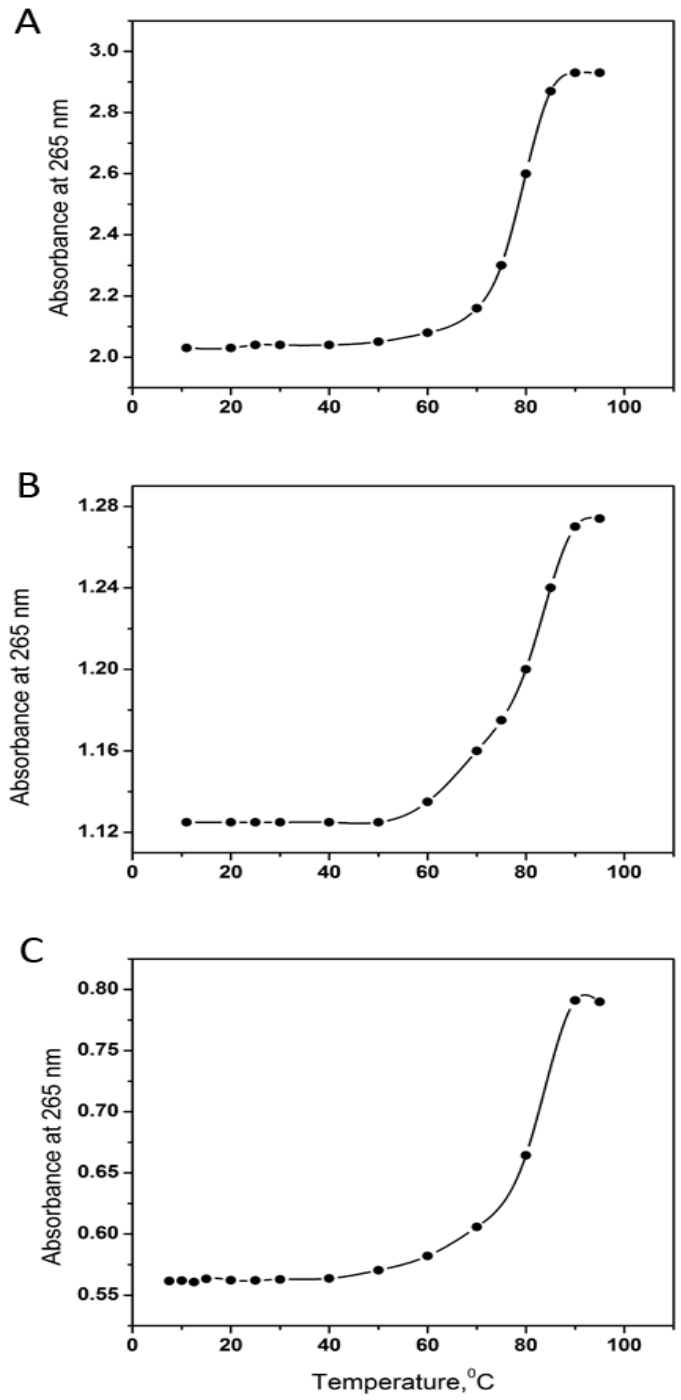

Figure 4.8: The absorbance versus temperature melting profiles for tetraloop DNA hairpin 5-AACCCTTTTGGGTT-3.The absorbance at 265 nm has been plotted as a function of temperatures for three different concentrations of DNA hairpin (2.8 µM, top;5.6µM, middle; 10.9 µM, bottom) in 100 mM NaCl buffer. The melting temperatures have been calculated by fitting the curve using two state models with linear baselines.

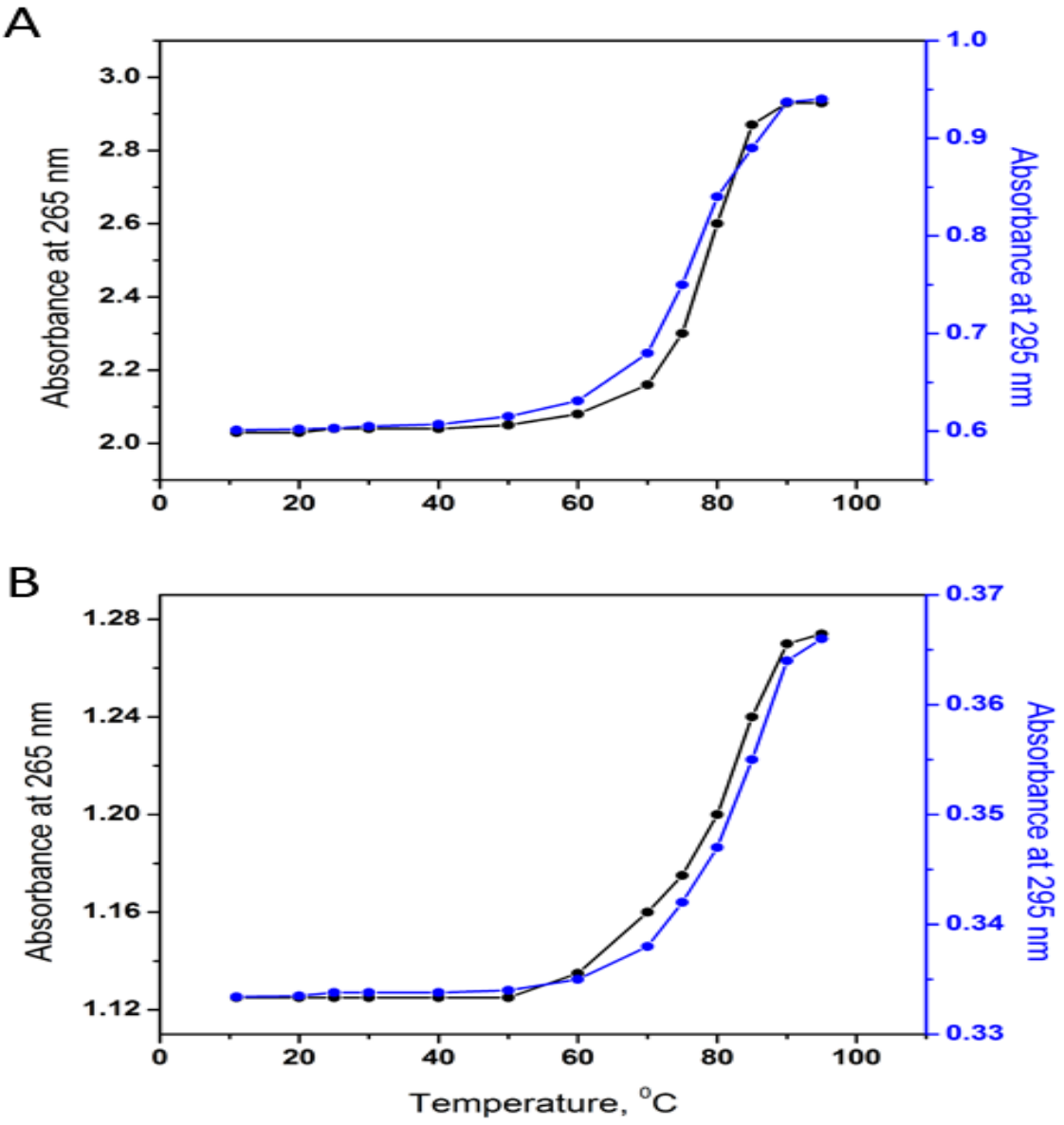

Figure 4.9: Thermal denaturation profiles for tetraloop DNA hairpin in10 mM sodium cacodylate buffer (pH 7.4) and 0.1 mM EDTA containing 100 mM NaCl monitored at 265 nm (black) and 295 nm (blue) respectively. The absorbance profile in the upper panel is for 10.9 µM DNA concentration and the profile in the lower panel is for 5.6 µM DNA concentration.

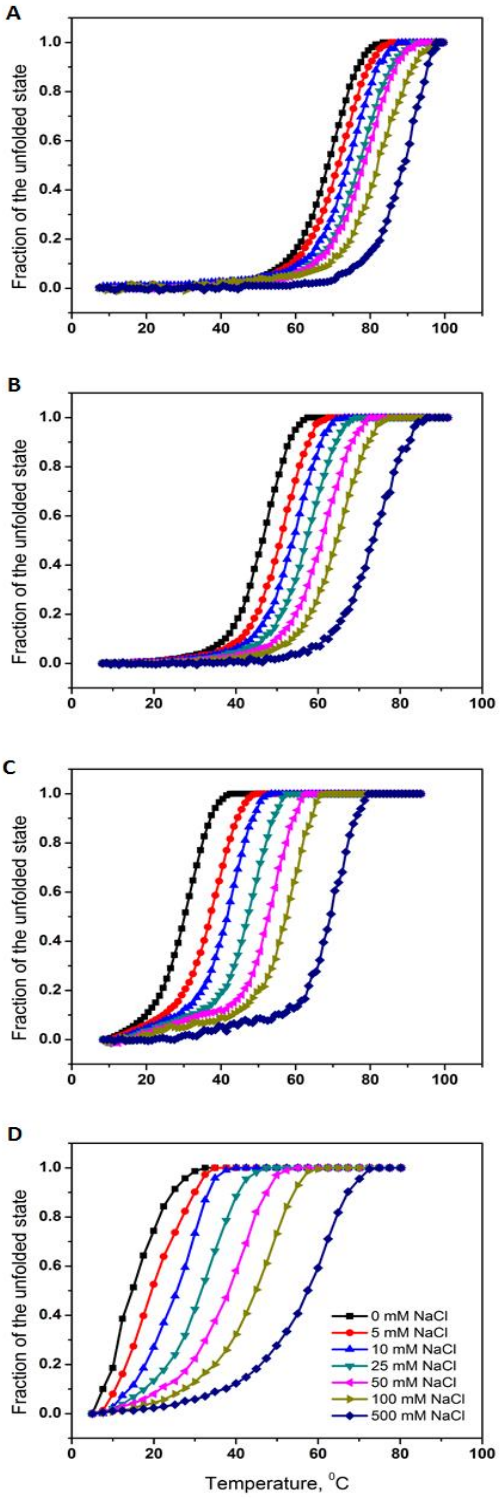
A
B
C
D
Fraction of the unfolded state
1.0
0.8
0.6
0.4
0.2
0.0
0
20
40
60
80
100
0 mM NaCl
5 mM NaCl
10 mM NaCl
25 mM NaCl
50 mM NaCl
100 mM NaCl
500 mM NaCl
Temperature, °C

Figure 4.10: Melting profiles for DNA hairpins with 5-base pair stem and variable poly(dT) loop lengths are shown. (Panel A, T4 loop; Panel B, T8 loop; Panel C, T12 loop; Panel D, T21 loop) In each panel, the fraction of the unfolded state is plotted as a function of temperature for varying NaCl concentrations (black, 0; red, 5; blue, 10; dark cyan, 25; magenta, 50; dark yellow, 100; navy, 500mM).

Table 4.2. Concentration Dependent Melting Temperatures, T_ms of Tetraloop DNA Hairpin at 100 mM NaCl

[DNA] (μM)	T_m (° C)
2.8	80.7 (1.4)
5.6	79.7 (2.2)
10.9	80.2 (2.4)

[a]Numbers in parentheses are the uncertainties in the last digits.

REFERENCES

(170) Uhlenbeck, O. C. *Nature***1990**, *346*, 613.

(171) Varani, G. *Annu. Rev. Biophys. Biomol. Struct.* **1995**, *24*, 379.

(172) Hernandez, B.; Baumruk, V.; Gouyette, C.; Ghomi, M. *Biopolymers***2005**, *78*, 21.

(173) Brázda, V.; Laister, R. C.; Jagelská, E. B.; Arrowsmith, C. *BMC. Mol. Biol.* **2011**, *12*, 33.

(174) Bikard, D.; Loot, C.; Baharoglu, Z.; Mazel, D. *Microbiol. Mol. Biol. Rev.* **2010**, *74*, 570.

(175) Mirkin, S. M. *Nature***2007**, *447*, 932.

(176) Gacy, A. M.; Goellner, G.; Juranic, N.; Macura, S.; McMurray, C. T. *Cell***1995**, *81*, 533.

(177) Wilson, K. S.; Vonhippel, P. H. *Proc. Natl. Acad. Sci. U.S.A* **1995**, *92*, 8793.

(178) Roth, D. B.; Menetski, J. P.; Nakajima, P. B.; Bosma, M. J.; Gellert, M. *Cell***1992**, *70*, 983.

(179) Vallone, P. M.; Paner, T. M.; Hilario, J.; Lane, M. J.; Faldasz, B. D.; Benight, A. S. *Biopolymers***1999**, *50*, 425.

(180) Shen, Y.; Kuznetsov, S. V.; Ansari, A. *J. Phys. Chem. B* **2001**, *105*, 12202.

(181) Kuznetsov, S. V.; Shen, Y.; Benight, A. S.; Ansari, A. *Biophys. J.* **2001**, *81*, 2864.

(182) Ansari, A.; Shen, Y.; Kuznetsov, S. V. *Phys. Rev. Lett.* **2002**, *88*, 069801.

(183) Moody, E. M.; Bevilacqua, P. C. *J. Am. Chem. Soc.* **2003**, *125*, 2032.

(184) Moody, E. M.; Bevilacqua, P. C. *J. Am. Chem. Soc* . **2003**, *125*, 16285.

(185) Heus, H. A.; Pardi, A. *Science***1991**, *253*, 191.

(186) Bonnet, G. g.; Krichevsky, O.; Libchaber, A. *Proc. Natl. Acad. Sci. U.S.A***1998**, *95*, 8602.

(187) Goddard, N. L.; Bonnet, G.; Krichevsky, O.; Libchaber, A. *Phys. Rev. Lett***. 2000**, *85*, 2400.

(188) Lapidus, L. J.; Eaton, W. A.; Hofrichter, J. *Proc. Natl. Acad. Sci. U.S.A***2000**, *97*, 7220.

(189) Grunwell, J. R.; Glass, J. L.; Lacoste, T. D.; Deniz, A. A.; Chemla, D. S.; Schultz, P. G. *J. Am. Chem. Soc.* **2001**, *123*, 4295.

(190) Wallace, M. I.; Ying, L.; Balasubramanian, S.; Klenerman, D. *Proc. Natl. Acad. Sci. U.S.A***2001**, *98*, 5584.

(191) Zhang, W.; Chen, S. J. *Proc. Natl. Acad. Sci. U.S.A***2002**, *99*, 1931.

(192) Jung, J.; Van Orden, A. *J. Phys. Chem. B***2005**, *109*.

(193) Jung, J.; Van Orden, A. *J. Am. Chem. Soc* . **2006**, *128*, 1240.

(194) Woodside, M. T.; Anthony, P. C.; Behnke-Parks, W. M.; Larizadeh, K.; Herschlag, D.; Block, S. M. *Science***2006**, *314*, 1001.

(195) Zhang, W.; Chen, S.-J. *Biophys. J***. 2006**, *90*, 778.

(196) Zhang, W.; Chen, S.-J. *Biophys. J***. 2006**, *90*, 765.

(197) Woodside, M. T.; Behnke-Parks, W. M.; Travers, K.; Larizadeh, K.; Herschlag, D.; Block, S. M. *Proc. Natl. Acad. Sci. U.S.A.* **2006**, *103*, 6190.

(198) Garcia, A. E.; Paschek, D. *J. Am. Chem. Soc.* **2007**, *130*, 815.

(199) Bevilacqua, P. C.; Blose, J. M. *Annu. Rev. Phys. Chem.* **2008**, *59*, 79.

(200) Bowman, G. R.; Huang, X.; Yao, Y.; Sun, J.; Carlsson, G., Guibas, Leonidas J, Pande, Vijay S. *J. Am. Chem. Soc.***2008**, *130*, 9676.

(201) Chen, S. J. *Annu. Rev. Biophys.* **2008**, *37*, 197.

(202) Tan, Z.-J.; Chen, S.-J. *Biophys. J.* **2008**, *95*, 738.

(203) Jung, J.; Ihly, R.; Scott, E.; Yu, M.; Van Orden, A. *J. Phys. Chem. B***2008**, *112*, 127.

(204) Portella, G.; Orozco, M. *Angew.Chem.* **2010**, *122*, 7839.

(205) Yin, Y. D.; Wang, P.; Yang, X. X.; Li, X.; He, C.; Sheng, X. *Chem. Commun.* **2012**, *48*, 7413.

(206) Kuznetsov, S. V.; Ansari, A. *Biophys. J.* **2012**, *102*, 101.

(207) Nayak, R. K.; Peersen, O. B.; Hall, K. B.; Van Orden, A. *J. Am. Chem. Soc.* **2012**, *134*, 2453.

(208) Narayanan, R.; Zhu, L.; Velmurugu, Y.; Roca, J.; Kuznetsov, S. V.; Prehna, G.; Lapidus, L. J.; Ansari, A. *J. Am. Chem. Soc.* **2012**, *134*, 18952.

(209) Van Orden, A.; Jung, J. *Biopolymers***2008**, *89*, 1.

(210) Ferner, J.; Villa, A.; Duchardt, E.; Widjajakusuma, E.; Wöhnert, J.; Stock, G.; Schwalbe, H. *Nucleic Acids Res.* **2008**, *36*, 1928.

(211) Hall, K. B. *Curr. Opin. Chem. Biol.* **2008**, *12*, 612.

(212) Antao, V. P.; Lai, S. Y.; Tinoco, I. *Nucleic Acids Res.* **1991**, *19*, 5901.

(213) Antao, V. P.; Tinoco, I. *Nucleic Acids Res.* **1992**, *20*, 819.

(214) Crews, S.; Ojala, D.; Posakony, J.; Nishiguchi, J.; Attardi, G. *Nature***1979**, *277*, 192.

(215) Moody, E. M.; Feerrar, J. C.; Bevilacqua, P. C. *Biochemistry***2004**, *43*, 7992.

(216) Moody, E. M.; Bevilacqua, P. C. *J. Am. Chem. Soc.* **2004**, *126*, 9570.

(217) Kuznetsov, S. V.; Ren, C. C.; Woodson, S. A.; Ansari, A. *Nucleic Acids Res.* **2008**, *36*, 1098.

(218) Abdelkafi, M.; Leulliot, N.; Baumruk, V.; Bednarova, L.; Turpin, P. Y.; Namane, A.; Gouyette, C.; Huynh-Dinh, T.; Ghomi, M. *Biochemistry***1998**, *37*, 7878.

(219) Rife, J. P.; Cheng, C. S.; Moore, P. B.; Strobel, S. A. *Nucleic Acids Res.***1998**, *26*, 3640.

(220) Leulliot, N.; Ghomi, M.; Jobic, H.; Bouloussa, O.; Baumruk, V.; Coulombeau, C. *J. Phys. Chem. B***1999**, *103*, 10934.

(221) Williams, D. J.; Hall, K. B. *Biophys. J.* **1999**, *76*, 3192.

(222) Shu, Z.; Bevilacqua, P. C. *Biochemistry***1999**, *38*, 15369.

(223) Kim, C. H.; Tinoco, I. *Proc. Natl. Acad. Sci. U.S.A.* **2000**, *97*, 9396.

(224) Dale, T.; Smith, R.; Serra, M. J. *RNA.* **2000**, *6*, 608.

(225) Ennifar, E.; Nikulin, A.; Tishchenko, S.; Serganov, A.; Nevskaya, N.; Garber, M.; Ehresmann, B.; Ehresmann, C.; Nikonov, S.; Dumas, P. *J. Mol. Biol.* **2000**, *304*, 35.

(226) Williams, D. J.; Hall, K. B. *J. Mol. Biol.* **2000**, *297*, 1045.

(227) Li, W.; Ma, B. Y.; Shapiro, B. A. *J. Biomol. Struct. Dyn.* **2001**, *19*, 381.

(228) Hannoush, R. N.; Damha, M. J. *J. Am. Chem. Soc.* **2001**, *123*, 12368.

(229) Zacharias, M. *Biophys. J.* **2001**, *80*, 2350.

(230) Kawakami, J.; Yoneyama, M.; Miyoshi, D.; Sugimoto, N. *Chem. Lett.* **2001**, 258.

(231) Sorin, E. J.; Engelhardt, M. A.; Herschlag, D.; Pande, V. S. *J. Mol. Biol.* **2002**, *317*, 493.

(232) Young, B. T.; Silverman, S. K. *Biochemistry***2002**, *41*, 12271.

(233) Proctor, D. J.; Schaak, J. E.; Bevilacqua, J. M.; Falzone, C. J.; Bevilacqua, P. C. *Biochemistry***2002**, *41*, 12062.

(234) Mundoma, C.; Greenbaum, N. L. *J. Am. Chem. Soc.* **2002**, *124*, 3525.

(235) Nakano, M.; Moody, E. M.; Liang, J.; Bevilacqua, P. C. *Biochemistry***2002**, *41*, 14281.

(236) Correll, C. C.; Swinger, K. *RNA.* **2003**, *9*, 355.

(237) Santini, G. P. H.; Pakleza, C.; Cognet, J. A. H. *Nucleic Acids Res.* **2003**, *31*, 1086.

(238) Sarzynska, J.; Kulinski, T. *J. Biomol. Struct. Dyn.* **2005**, *22*, 425.

(239) Sarkar, K.; Meister, K.; Sethi, A.; Gruebele, M. *Biophys. J.* **2009**, *97*, 1418.

(240) Blose, J. M.; Proctor, D. J.; Veeraraghavan, N.; Misra, V. K.; Bevilacqua, P. C. *J. Am. Chem. Soc.***2009**, *131*, 8474.

(241) Sheehy, J. P.; Davis, A. R.; Znosko, B. M. *RNA.* **2010**, *16*, 417.

(242) Hare, D. R.; Reid, B. R. *Biochemistry***1986**, *25*, 5341.

(243) Chattopadhyaya, R.; Ikuta, S.; Grzeskowiak, K.; Dickerson, R. E. **1988**.

(244) Chattopadhyaya, R.; Grzeskowiak, K.; Dickerson, R. E. *J. Mol. Biol.* **1990**, *211*, 189.

(245) Hilbers, C.; Haasnoot, C.; De Bruin, S.; Joordens, J.; Van Der Marel, G.; Van Boom, J. *Biochimie***1985**, *67*, 685.

(246) Vallone, P. M.; Benight, A. S. *Nucleic Acids Res.***1999**, *27*, 3589.

(247) Haasnoot, C.; De Bruin, S.; Hilbers, C.; Van der Marel, G.; Van Boom, J. *J. Biosci.* **1985**, *8*, 767.

(248) Huppert, J. L.; Balasubramanian, S. *Nucleic AcidsRes.* **2005**, *33*, 2908.

(29) Owczarzy, R.; Moreira,B. G.; You, Y. ; Behlke, M.A.; Walder, J.A. *Biochem.* **2008**, *47*, 5336.

(250) Kaushik, M.; Bansal, A.;Saxena, S. Kukreti,S. *Biochem.* **2007**, *46*, 7119.

(251) Mergny, J. L; Phan,A. T; Lacroix, L. *FEBS Lett.***1998**, *435*, 74

CHAPTER 5: RNA Hairpins Folding/Unfolding and Reaction Mechanism byRapid-Mixing Stopped-Flow Kinetics[C]

This chapter describes the folding and unfolding kinetics of RNA hairpins with identical four base pair stems but different fifteen nucleotide loop sequences as a function of KCl concentration by using rapid-mixing stopped-flow techniques. Our results suggests the reactions occurred on a time scale of milliseconds, considerably longer than the microsecond time scale suggested by previous kinetics studies of similar sized hairpins. Previous Fluorescence Correlation Spectroscopy (FCS) studies of the same loop and stem sequence RNA hairpins suggests intermediate reaction occurs on microsecond time scale but could not probe the reaction kinetics of longer millisecond time scale due to time resolution problems. Importantly, our stopped-flow kinetics results of 4 base pair stem and 15 nucleotide loop hairpin 5'-CGGUUUCCCUCCCUCCUUUGCCG-3' suggests that the forward reaction is very fast as compared to reverse reaction. This finding is contrast to our previous DNA hairpin folding kinetics studies (J. Am. Chem. Soc. 2012, 134, 2453-2456), which suggests the forward and reverse reaction occurs on equal millisecond time scale. Therefore, rapid-mixing studies suggest that the RNA folding kinetics are much more complex than our previously studied DNA hairpins and the folding occurs through more than two states with multiple intermediates. Furthermore, the loop compositions of the RNA hairpins determine the time scales of folding. Finally, the

[C]Rajesh K. Nayak,[†]Artem V. Melnykov, Kathleen B. Hall and Alan Van Orden[†,*]

This chapter has been written as a manuscript. R. Nayak collected and analyzed the data, and wrote the manuscript. ArtemMelnykov of Dr. Kathleen Hall research group designed the RNA hairpin constructs and did the stability experiment.

suitable kinetic model is required to propose the complex reaction mechanism of RNA hairpin folding.

5.1 Introduction

RNA hairpins are one of the most important secondary structures and fundamental building blocks for intricate three-dimensional RNA structures.[252-256] RNA hairpins perform numerous biological functions such as from controlling transcription termination to gene expression and also serve as a nucleation site for RNA folding.[256-261] They facilitate RNA folding by forming tertiary contacts and also influence translational regulation and viral propagation etc.[262] The fact that the RNA hairpins play such a pivotal role in various cellular functions has made it prerogative to determine its structure, function and conformational dynamics.[263] It is therefore a prerequisite to decipher the RNA hairpin folding mechanism in order to understand the complex RNA tertiary structure folding.

The Watson-Crick base-paired stem capped with a loop of unpaired or non-Watson-Crick base paired nucleotides constitute a RNA hairpin.[255] Over the years, there have been numerous experimental and theoretical investigations carried out to understand the structural and dynamic properties concerning RNA hairpin folding.[256,264-306] Yet, there remains controversy whether these hairpins fold in a two-state or multi-state with one or more intermediates. Traditionally, the thermodynamic measurements interpret the two-state model for RNA hairpin folding.[307,308] In the past, kinetics of nucleic acid hairpin folding was interpreted in terms of a two-state process which can be perceived as the initial encounter of RNA strand followed by a rapid zippering to form the stem.[293,309]

Later, ultrafast techniques such as Fluorescence Correlation Spectroscopy (FCS)[59,60] and T-Jump[312,313] experiments hypothesized multi-state folding kinetics. For example, in 2006, Van Orden and co-workers[310] observed the discrepancies between equilibrium distributions from thermodynamic melting experiments and FCS experiment. FCS combined with photon Counting Histogram (PCH) experiment indirectly predicted at least the existence of a three-state mechanism of DNA hairpin folding. But, unfortunately due to the time resolution limitation, the FCS experiments observed the intermediate reaction at micro second time scales but could not directly observe the complete folding trajectory of the hairpin formation which may be happening in millisecond time scales. Then as discussed in Chapter 3 and Chapter 4, we observed a three-state mechanism by using the rapid-mixing stopped-flow kinetics techniques.[314] We suggest a three-state reaction mechanism, wherein intermediate formation occurs on tens to hundreds of micro second time scales, and complete hairpin formation occurs on a millisecond time scale. The stopped-flow technique combined with FCS probed the complete folding trajectory of the hairpin formation.[310,314] Similarly, Ma et al.[312] found the evidence of intermediate formation by using T-jump experiments and these authors proposed that an intermediate state in which the end of the hairpins are in contact but the base-pairing and base-stacking are not yet formed.

Several theoretical studies[285,315-317] have thrown down the gauntlet toward the existence of a two-state model, suggesting that alternative secondary structures can be important as intermediates even in rather small hairpins. For example, Pande and co-workers[292] performed serial replica exchange molecular dynamics simulations of the small GCAA tetraloop hairpin and proposed the existence of several meta-stable intermediates and found that the hairpin folding is simply not a two-state process. However, none of these theoretical models cited base-stacking

interaction in single stranded regions of the RNA hairpins. Although all the experimental observations and theoretical findings of the various research groups are unanimous with the fact that even the folding of the smallest of RNA motifs is quite complex.

Previously (as described in Chapter 3), our laboratory[314] has investigated the folding kinetics and thermodynamic stability of DNA hairpins containing 5-base pairs (bp) in the stem and 21 polythymidine nucleotides (nt) in the loop. These studies were carried out using a range of NaCl concentrations in the background buffer, ranging from 0 to 500 mM, and revealed an important dependence of hairpin folding and thermodynamic stability on counter ion concentrations. In particular, the reaction mechanism changed from three state reactions above 25 mM NaCl to two state reactions below 25 mM NaCl and also the stability increased with the increasing concentration of NaCl. Further, we have also studied the loop length dependent kinetics and thermodynamic stability of DNA hairpins. We observed that the tetraloop hairpin is exceptionally stable compared to other longer loop hairpins studied and further, this unusual stability is highly dependent on counter ion concentrations. In the higher counter ion concentration regime of 50 mM NaCl and above, the tetraloop exhibits unusually high thermal stability as compared to longer loop length hairpins. We also attempted to explain this unusual stability on the base-stacking effect. This unusual base-stacking interaction in tetraloop DNA hairpin motivated us to undertake these present RNA hairpin studies.

Clearly, the folding free energy landscape of RNA hairpins is not fully understood.[297,318-320] Importantly, the role of base-stacking in shaping the energy landscape is poorly understood. Also as described above, although the ultrafast spectroscopic techniques such as FCS and T-jump proposed the three-state mechanism for nucleic acid folding but due to the time resolution problems, we could not prove it directly. In order to probe the folding kinetics of the RNA

hairpins in the longer time scale of milliseconds and above and to address the role of base-stacking interaction in single stranded regions, we investigated the folding kinetics of three RNA hairpins with identical four base-pair stems but different fifteen nucleotide loop sequences . We used rapid-mixing stopped-flow kinetics[314,321] to investigate the reaction kinetics of the above three RNA hairpins as a function of KCl (mono-valent counter ion) concentrations in millisecond time scales.

Our finding suggests that the reaction times as a function of mono-valent counter ion concentration in case of Polypy and PolypyA loop hairpins are closer within the statistical accuracy. Whereas, the reaction times in PolyU loop hairpin is very small as compared to other two hairpins. This observation suggests that the RNA hairpins of different sequences have different base-stacking propensities with PolyU showing no or very negligible base-stacking interactions. Most importantly, the rapid-mixing stopped-flow kinetics studies of Polypy loop hairpin shows that the forward reaction time is much faster than the reverse reaction time in contrast to previously studied DNA hairpins. This finding suggests that the RNA hairpin folding kinetics is much more complex than previously expected and it is not simply a two-state process. These studies further substantiate the notion that RNA hairpin folding is at least a three-state process with multiple intermediates and more complicated than DNA hairpin folding kinetics.

5.2 Experimental Methods

5.2.1 Materials

The RNA hairpins examined in these studies consisted of identical four base pair stem with the complementary sequences 5'-CGGU and GCCG-3' and loop regions containing three different sequences of 15 base pair nucleotides. These hairpins with loop sequences (underlined) along with identical four base pair stems are given below. i) PolyU loop hairpin (hpU) 5'-CGGUUUUUUUUUUUUUUGCCG-3'; ii) polypyrimidine loop hairpin (hpPy) 5'-CGGUUUCCCUCCCUCCUUUGCCG-3'; and iii) polypyrimidine loop with a single adenine (hpPyA) 5'-CGGUUUCCCUCCCACCUUUGCCG-3'.The hairpins were dual labeled with fluorophore 5-tetramethylrhodamine (5-TAMRA) at 5' end and a quencher 4-(dimethyl amino azo) benzene-4-carboxyllicacid (dabcyl) at 3' end. The respective control RNA hairpin sampleslabeled with the dye TAMRA at 5' end but without quencher at 3' end were examined for comparison. Fluorescently labeled identical stem and different loop RNA hairpins were synthesized, HPLC purified, and characterized using mass spectrometry by IBA GmBH, Germany. 0.1M cacodylate buffer was purchased from Electron Microscopy Sciences (Hatfield, PA). Molecular biology grade EDTA and potassium chloride (KCl) were purchased from Cal Biochem (Gibbstown, NJ).Critrion TBE-Urea Gel (15% TBE-UREA) was purchased from Bio-Rad (Los Angeles, CA). All chemical stock solutions were conformed to be RNAs, DNAs and protease free.

5.2.2 Sample preparation

50-100 nMRNA samples were prepared in 2.5 mM sodium-cacodylate buffer (pH7.4)containing 250 µM EDTA. Various concentrations of potassium chloride, ranging from 0 mM to 1000 mM, were prepared for stopped-flow mixing experiments as well as thermodynamic melting experiments. All the above mentioned samples were prepared in nuclease free water, purchased from Applied Biosystems (Carlsbad, CA).All solutions were filtered through 0.22 micron Nalgene nitrocellulose filter units to remove any contaminated proteins.

5.2.3 PolyAcrylamide Gel Electrophoresis (PAGE) of RNA hairpins

The integrity of the hairpin samples were checked by running precast criterion TBE-Urea Gel (15% TBE-UREA).[322] The RNA samples were annealed in buffer solution at 70^0C for 10 min and then the samples were cooled to 4^0C at the rate of -1^0C/min. The running buffer, 1X TBE used for the electrophoresis contained 89 mM Tris, 89 mM boric acid and 2 mM EDTA at pH 8.2., the sample buffer for the electrophoresis experiment was 89 mMTris, 89 mM boric acid and 2 mM EDTA and the loading dye was 0.01 % bromo phenol blue. The comb was inserted into the gel and allowed to polymerize for at least 1 hour. The electrophoresis was filled with 1X TBE buffer and subsequently RNA hairpin samples were loaded on a gel. The electrophoresis was run for about an hour and gel was soaked about 15 to 20 minutes in 1X TBE to remove urea before staining. The gel was stained in 0.5 µgm/ml ethidium bromide in 1X TBE solution for 15 minutes. Finally, the gel images were analyzed by using gel densitometry.

5.2.4 Stopped Flow Mixing Experiments

Stopped-flow mixing experiments were carried out using an Applied Photophysics SX-20 stopped-flow instrument (Surrey, United Kingdom).[314,321] Buffer solutions containing RNA hairpin in 0 mM KCl were mixed with pure buffer solutions containing varying concentrations of KCl inside a 5 µl mixing cell. Folding reactions were observed by monitoring the quenching of fluorescence of TAMRA dye after a 450 µs mixing time. To observe the fluorescence, the dye was excited at 547 nm with bandwidth set to 2 nm and the emission from the dye was detected using a 570 nm high pass filter. In the stopped flow experiment, all the folding traces for different loop length RNA hairpins and control RNA hairpins without quencher, at various KCl concentrations, were collected and repeated at least three times for the statistical accuracy of our data collections.

5.2.5 Fluorescence Melting Experiments

To examine various RNA hairpin samples, we monitored the temperature dependent fluorescence of the dye-quencher labeled RNA from 5ºC to 85ºC on a steady-state fluorometer (AVIV MODEL ATF 105) equipped with a water bath for sample temperature control. The samples analyzed contained 50 nM RNA in sodium-cacodylate buffer and varying concentrations of KCl, ranging from 0 to 500 mM. The fluorescence of the TAMRA dye was excited at 547 nm, and the emission was monitored at a single wavelength 585 nm (4 nm excitation and emission bandwidths).

5.3 Results

5.3.1 PolyAcrylamide Gel Electrophoresis (PAGE) to check degradation.

Prior to investigating the folding and unfolding kinetics of the RNA hairpins, the quality of the samples were checked by running the criterion TBE-Urea Gel (15% TBE-UREA).[322,323] Figure 5.1 shows the image of the RNA hairpins after the electrophoresis experiment. The extreme left (row 1) band in the Figure 5.1 is the image of three base pair stem and fifteen polyU loop hairpin. The second, third and fourth rows represents the bands of four base pair stem and fifteen loop hpU, hpPy and hpPyA RNA hairpins. It can be carefully observed that no smearing occurred at all on those bands, which shows that the RNA hairpin samples are not degraded and most of the samples are intact.

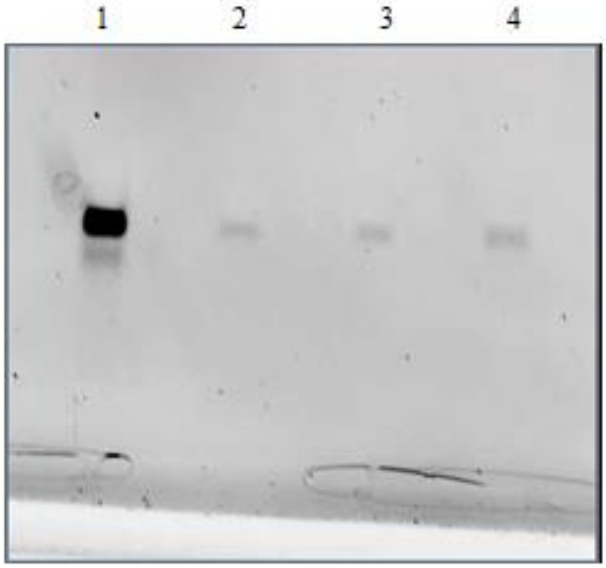

Figure 5.1: 15% TBE-UREA criterion gel electrophoresis of the RNA hairpins. Lanes 1-4: 3-base pair stem RNA hairpin (5'-CGG UUUUUUUUUUUUUU CCG-3'); 4-base pair stem PolyU loop hairpin, hpU (5'-CGGUUUUUUUUUUUUUUGCCG-3'); 4-base pair stem Poly pyrimidine loop hairpin, hPpy (5'-CGGUUUCCCUCCCUCCUUUGCCG-3'); and 4-base pair stem Poly pyrimidine loop with single adenine hairpin hPpyA (5'-CGGUUUCCCUCCCACCUUUGCCG-3').

5.3.2 Thermodynamic Melting Experiment of RNA hairpins.

Melting profiles for different loop RNA hairpin samples were obtained by monitoring the fluorescence intensity of the TAMRA dye label versus the temperature. Figure 5.2 shows the plot of the fraction of the unfolded state versus temperature profiles for 4-bp stem and PolyU loop hairpin (hpU) at varying NaCl concentrations for illustration. The fraction of the RNA hairpins in the unfolded state, as a function of temperature, $f_{UN}(T)$, according to

$$f_{UN}(T) = \frac{I(T) - I_F}{I_{UN} - I_F}$$

where $I(T)$ is the fluorescence intensity at temperature T. I_{UN} and I_F are the measured fluorescence intensities at 85^0C and 5^0C respectively. The temperature dependent melting curve analysis suggests that the melting temperature increases with the increase of KCl concentrations. Furthermore, KCl stabilizes the folded state of the hairpin in accordance with the polyelectrolyte theory.[324,325]

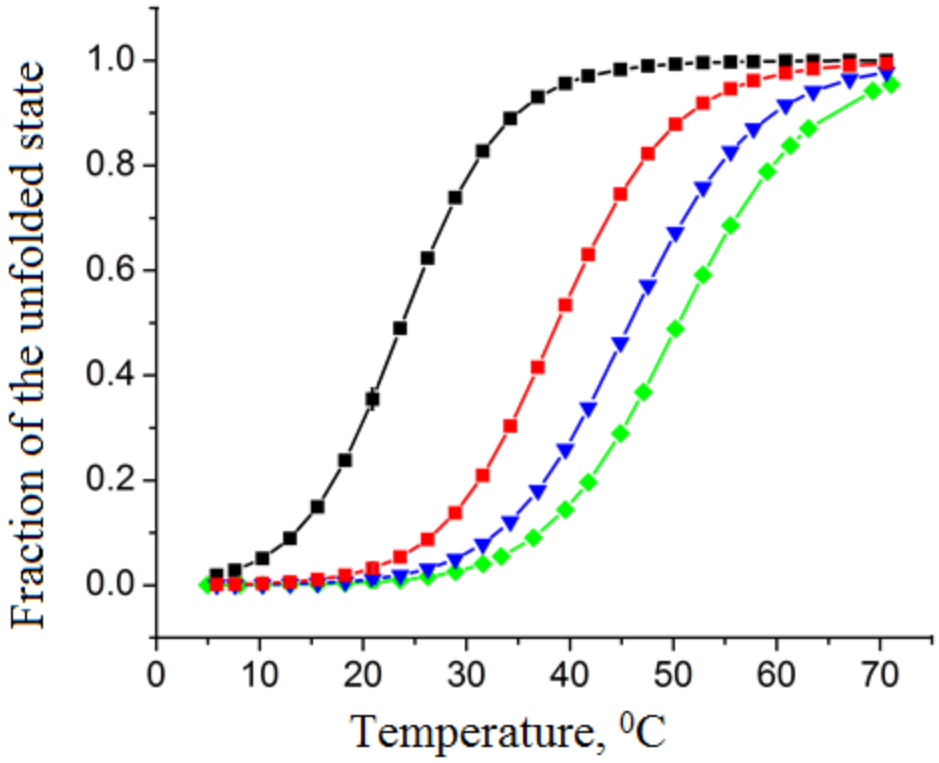

Figure 5.2: Melting profiles for 4-base pair stem and PolyU loop length RNA hairpin 5'-CGGUUUUUUUUUUUUUUGCCG-3'. The fraction of the unfolded state of the hairpins plotted as a function of temperature for varying KCl concentrations (black, 0; red, 20; blue, 50; green, 100 mM).

5.3.3 RNA hairpin kinetics as a function of KCl concentration for different loop sequence.

To gain clear insight on the effect of the loop composition on RNA folding, rapid-mixing stopped-flow kinetics was performed to investigate the folding kinetics of identical four base-pair stem but different fifteen loop sequence hairpins as a function of KCl concentration. The hairpins are identified as hpU, hpPy and hpPyA hairpins respectively for simplicity. Folding reactions of above three different loop hairpins were carried out separately by mixing RNA hairpin in 0 mM KCl (low salt buffer in one channel with varying concentrations of KCl ranging from 0 mM to 1000 mM KCl in the other channel. Folding reactions of these hairpins were monitored by observing the quenching of TAMRA fluorophores by dabcyl quencher after a mixing time of ~450 μs. Figures 5.3, 5.4 and 5.5 show the stopped-flow mixing (folding) reactions of hpU, hpPy and hpPyA hairpins respectively for illustration.

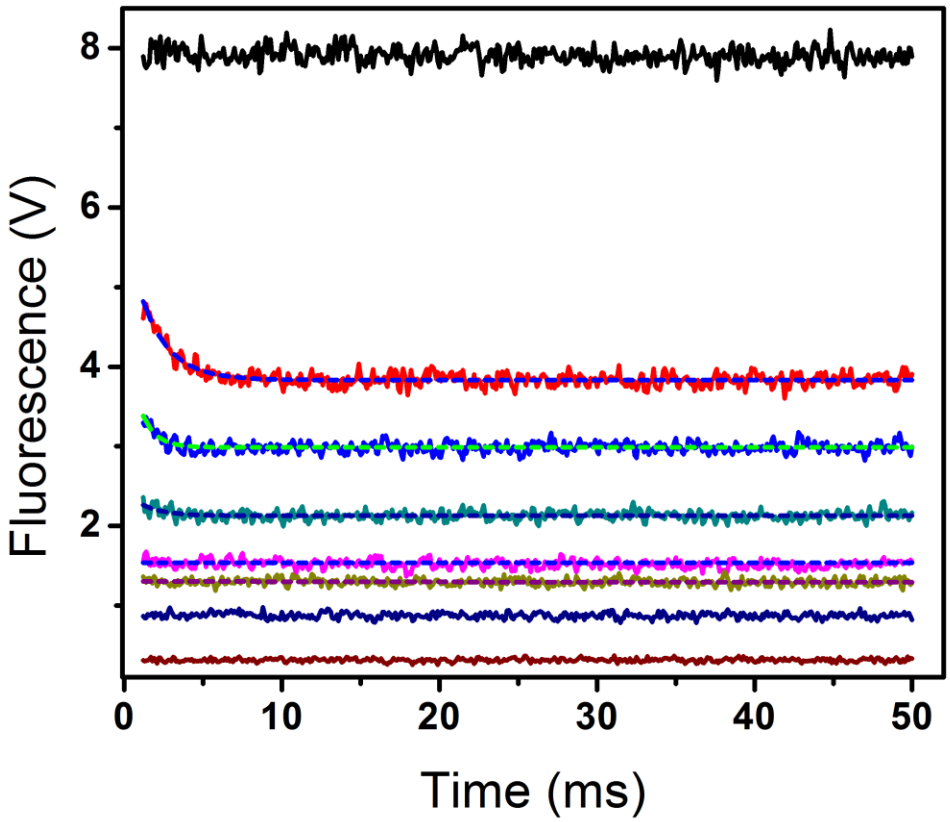

Figure 5.3: Experimental data (solid lines) and corresponding fitting curves (solid dashed lines) from stopped-flow measurements of the folding reaction of 4-base pair stem and hpU RNA hairpin as a function of varying KCl concentrations (black, 0; red, 5; blue,10; dark cyan,25; magenta,50; dark yellow,100; navy 500 mM KCl and wine, background buffer). The fluorescence at various concentrations has been quenched due to folding at millisecond reaction times. All the experiments were carried out at ~ 22^0C.

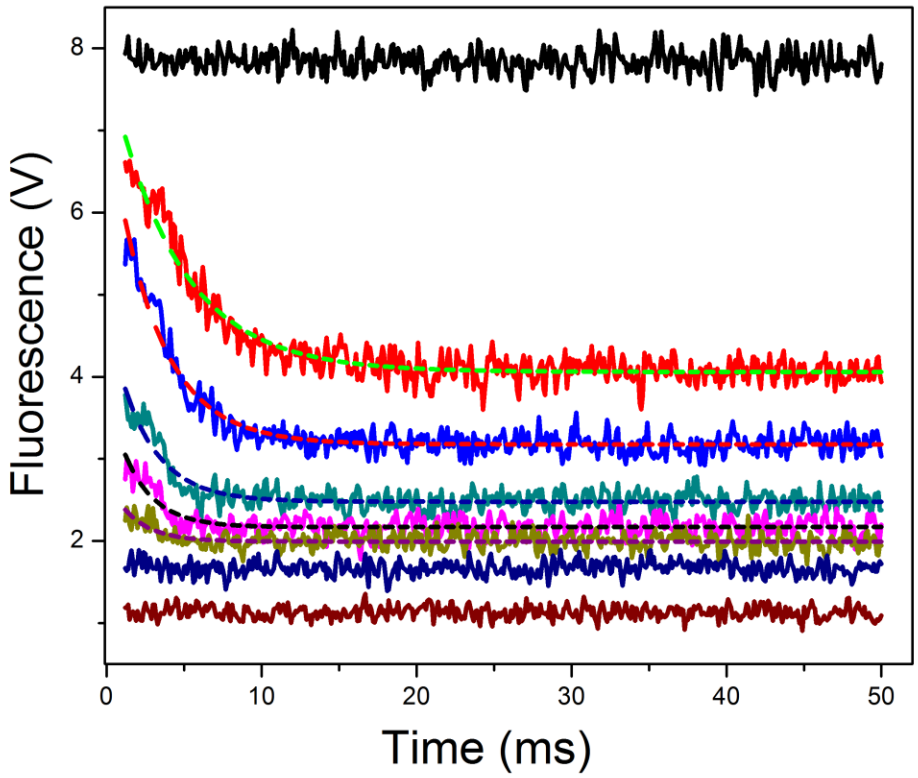

Figure 5.4: Experimental data (solid lines) and corresponding fitting curves (solid dashed lines) from stopped-flow measurements of the folding reaction of 4-base pair stem and hpPy RNA hairpin as a function of varying KCl concentrations (black, 0; red, 5; blue,10; dark cyan,25; magenta,50; dark yellow,100; navy 500mMKCl and wine, background buffer). The fluorescence at various KCl concentrations is quenched due to folding at millisecond reaction times. All the experiments were carried out at ~ 22^0C.

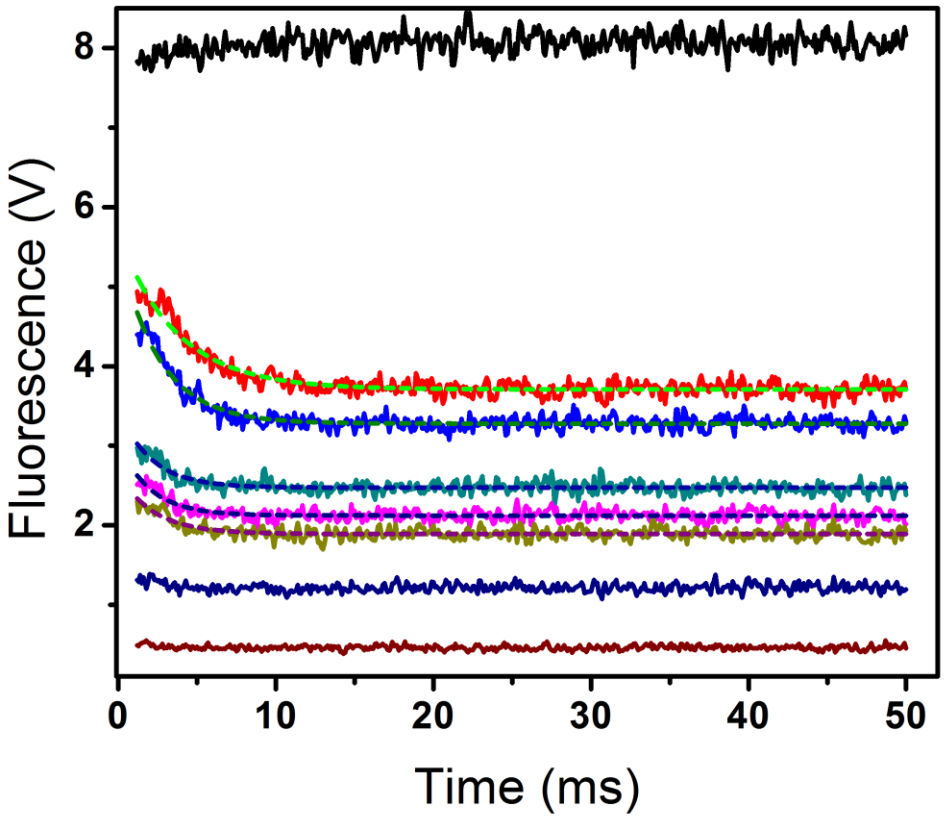

Figure 5.5: Experimental data (solid lines) and corresponding fitting curves (solid dashed lines) from stopped-flow measurements of the folding reaction of 4-base pair stem and hpPyA RNA hairpin as a function of varying KCl concentrations (black, 0; red, 5; blue,10; dark cyan,25; magenta,50; dark yellow,100; navy 500 mM KCl and wine, background buffer). The fluorescence at various KCl concentrations is quenched due to folding at millisecond reaction times. All the experiments were carried out at ~ 22^0C.

Similarly, the reverse reaction (unfolding) reactions for above hairpins were performed by reversing the mixing conditions. For example, the mixing was started with 100 mM RNA hairpin in 0 mM KCl (low salt buffer) and subsequently increasing the KCl concentration up to 1000 mM but keeping 0 mM KCl (low salt buffer) in the other channel each time it was mixed. Figure 5.6 shows the reverse (unfolding) reactions of polpy hairpin for illustration. The folding reaction of the hpPy hairpin without quencher is shown in Figure 5.7 for comparison and also the average fluorescence of polypy hairpin as a function of varying concentration of KCl is shown to probe the extent of folding with the increase of salt concentrations.

The careful observation of the stopped-flow mixing data of several RNA hairpins as a function of varying KCl concentration reveals the loop composition effect on hairpin folding. As we compare the folding reactions of three different hairpins (Figures 5.3, 5.4 and 5.5), we found that the TAMRA fluorescence has been quenched significantly with the increase of KCl concentration. The experimental data for above three hairpins were fitted using single exponential decay equations to obtain reaction time information. The experimental data along with fitting has been shown in Figures 5.3, 5.4, 5.5. From the fitting, it can be observed that the folding reaction of all the hairpins occurred in millisecond time scales.

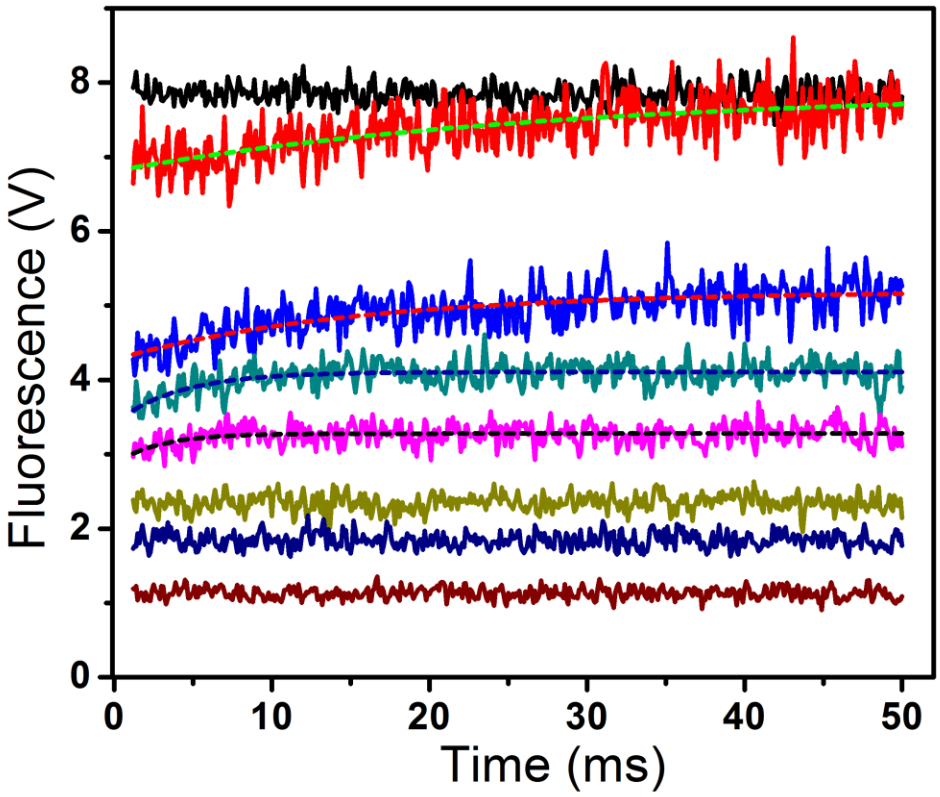

Figure 5.6. Experimental data (solid lines) and corresponding fitting curves (solid dashed lines) from stopped-flow measurements of the un-folding reaction of 4-base pair stem and hpPy RNA hairpin as a function of varying KCl concentrations (black, 0; red, 5; blue,10; dark cyan,25; magenta,50; dark yellow,100; navy 500 mM NaCl and wine, background buffer). The fluorescence at various concentrations are un-quenched due to un-folding at millisecond reaction times. All the experiments were carried out at ~ 22^0C.

(A)

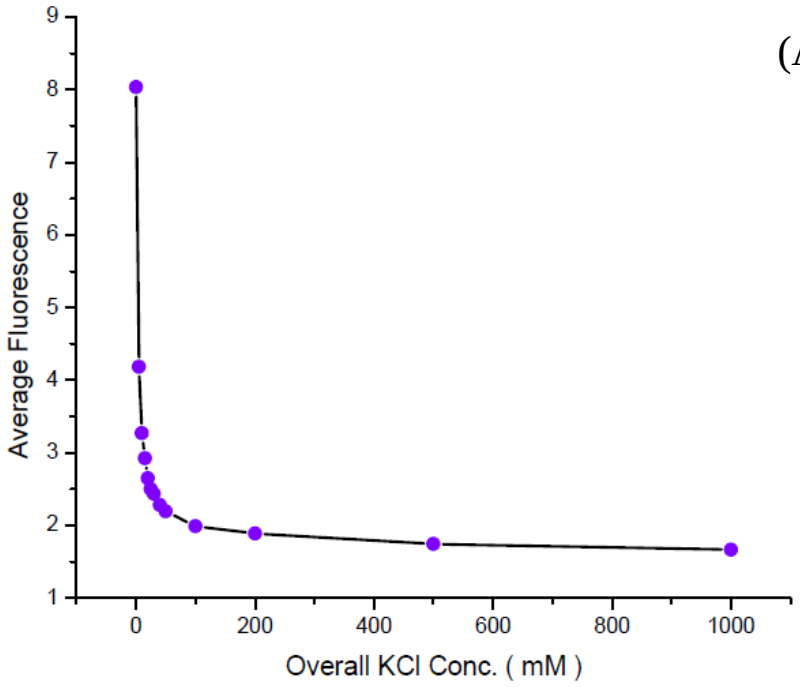
Average Fluorescence
Overall KCl Conc. (mM)
9
8
7
6
5
4
3
2
1
0
200
400
600
800
1000

(B)

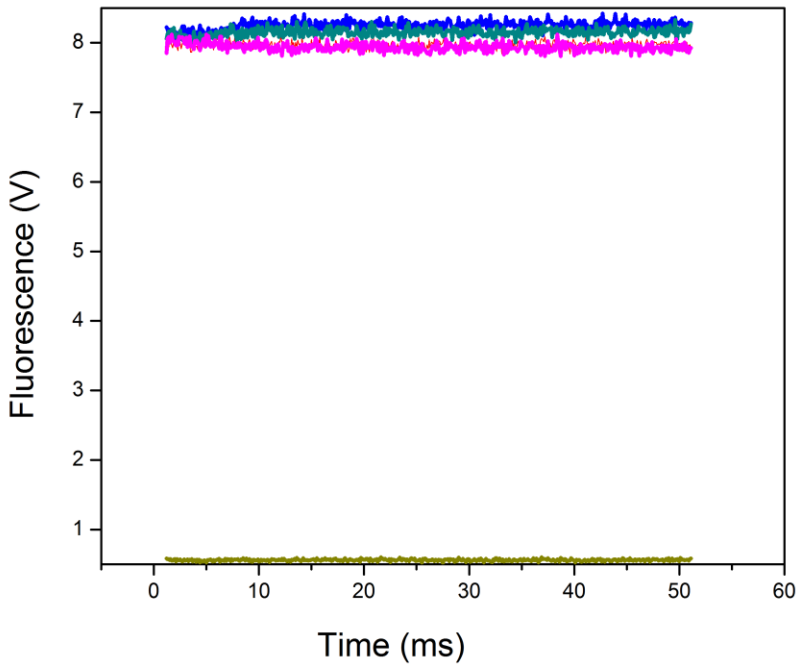
Fluorescence (V)
Time (ms)
8
7
6
5
4
3
2
1
0
10
20
30
40
50
60

Figure 5.7:**(A)** The plot of average fluorescence vs. varying concentration of KCl for polypy loop hairpins; (**B**) Experimental data (solid lines) from stopped-flow measurements of the folding reaction of 4-base pair stem and hpPy control hairpin as a function of varying KCl concentrations (black, 0; red, 5; blue,10; dark cyan,25; magenta,50; dark yellow,100; navy 500 mM KCl and dark cyano, background buffer).

To quantify the effect of the loop composition on hairpin folding, we plotted reaction times as a function of KCl concentration for different hairpins. Figure 5.8 shows the plot of reaction times for PolyU, Polypy and PolypyA loop hairpins as a function of varying KCl concentrations. Here we observed that the reaction times for polypy and polypyA loop hairpins at corresponding KCl concentrations are similar within the statistical accuracy. Whereas, the reaction times of PolyU loop hairpin is the smallest among all the hairpins studied. This finding suggests the notion that base-stacking, not the base pairing, stabilizes the folded state of the short stem hairpins.

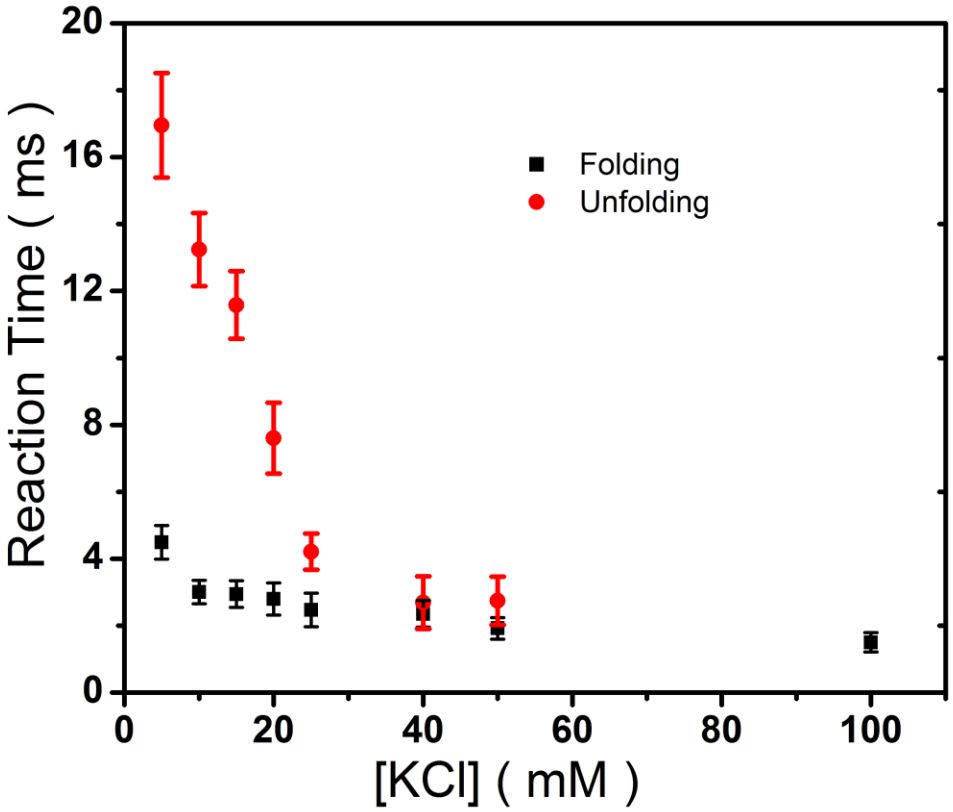

Figure 5.8: The forward and the reverse reaction times as a function of varying KCl concentrations have been plotted for hpPy RNA hairpin. The forward reaction is faster compared to reverse reaction. At higher counter ion concentration, the reaction times of forward and reverse reactions become closer.

As we compared the forward and reverse reaction times of as a function of KCl concentration, we found that the forward reaction is very fast as compared to reverse reaction times at lower KCl concentrations. Figure 5.9 shows the forward and reverse reaction times of hpPy hairpin for illustration. The forward and reverse reaction times for hpPy hairpin at different KCl concentration have been shown in Table 5.1 for illustration. But at higher counter ion concentration, the forward and reverse reaction time becomes closer within the statistical error. This observation of fast and slow reactions in the case of RNA hairpins is very different as compared to the reaction time observed for DNA hairpins at comparable loop and stem sequence. This interesting observation in RNA hairpins suggests that RNA hairpin folding is much more complex than DNA hairpin folding. Our observation suggests that RNA hairpin folding is not a two-state process and at least the folding is a three-step process with more than one intermediate.

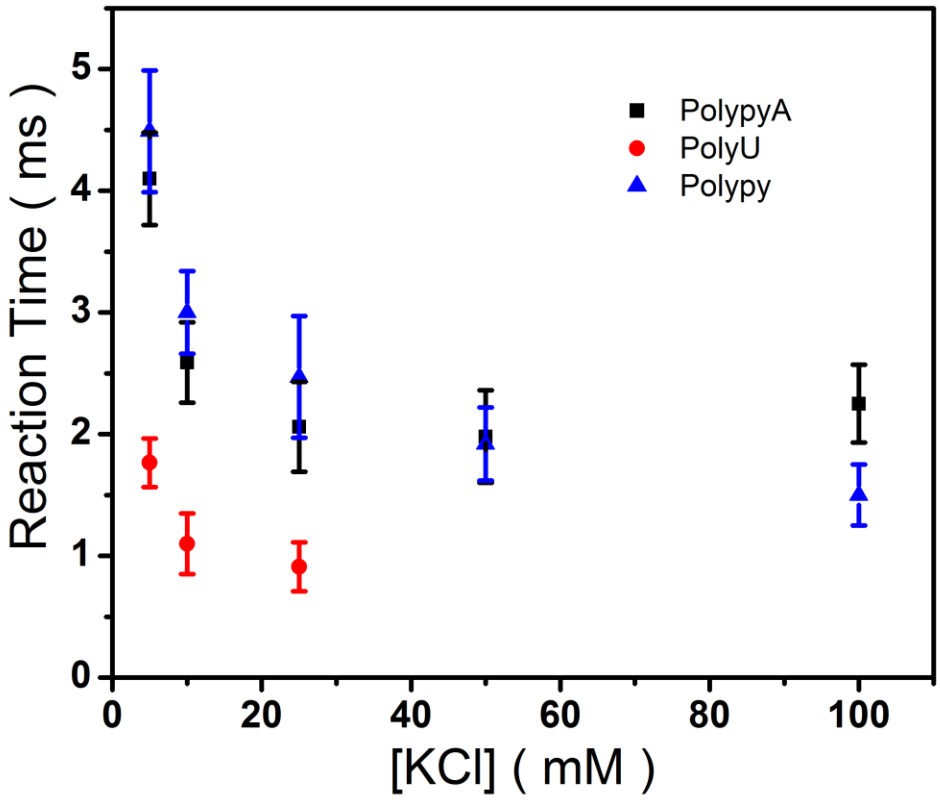

Figure 5.9: The reaction times as a function of KCl concentration for three different RNA hairpins have been plotted. The reaction times for hpPy and hpPyA hairpins are closer within the statistical accuracy. hpU hairpin has the smallest reaction times among all the hairpins studied.

Table 5.1. Thermodynamic parameters for hpPy RNA Hairpin Melting

Net KCl conc. after mixing (mM)	Reaction time(ms)	
	Folding	Unfolding
5	4.49	16.95
10	3.0	13.24
15	2.94	11.58
20	2.8	7.6
25	2.47	4.21
30	2.32	-
40	2.35	2.69
50	1.92	2.73
100	1.72	-

5.4 DISCUSSION

The investigation of mono-valent counter ion dependent folding kinetics studies of three RNA hairpins suggest that the RNA folding is much more complex than DNA hairpin folding. The most important finding in our present rapid-mixing stopped-flow kinetics results, seen in the perspective of previous FCS studies[310] and theoretical studies,[265,285,292] is that the RNA folding is not simply a two-state process. Previous FCS studies on DNA hairpins[310] and similar RNA hairpins[61] propose at least a three-state mechanism indirectly which cannot access the slow phase due to the constraints of time resolution. The stopped-flow studies support the evidence of a multi-step mechanism by directly probing the kinetics on millisecond time scales.[314]

In the past, there have been numerous theoretical and experimental investigations carried out on RNA hairpins to understand folding kinetics but still there remains controversy regarding the reaction mechanisms. Prior to recent ultra-fast studies such as FCS[314,315]and T-jump,[312] it was believed that hairpin folding is predominantly a two-state reaction within a simpler free energy landscape.[309] The two-state model was first challenged by our research group by combining FCS and Photon Counting Histogram (PCH) analysis on DNA hairpin folding studies. Later, Pande's group investigated the refolding and unfolding of a small RNA hairpin (5'-GGGCGCAAGCCU-3') by using molecular dynamics simulation.[292] They hypothesized the existence of competing folding and unfolding pathways with intermediates with partially zipped and partially compacted states. Similarly, Ma et al. used T-jump spectroscopy[312] and proposed multi step reactions for RNA hairpin folding through complex free energy landscapes.

Although, the above ultra-fast studies and molecular dynamics simulation proposed more than a two-state reaction but due to the time resolution limitation, these studies could not

measure the reaction kinetics on millisecond time scales and beyond. The present Stopped-flow studies probe the reaction kinetics of three RNA hairpins on millisecond time scales and suggest the energy landscape of RNA may be much more complex than previously thought. Particularly, the stopped-flow studies on our 4 base pair stem and polypyrimidine loop hairpin (hpPy) shows very interesting results. The careful analysis of stopped-flow kinetics results show that the forward reaction is very fast compared to reverse reaction on millisecond timescales. The different timescales of forward and reverse reactions of RNA hairpins is different than our previously studied DNA hairpin experiments with comparable stem and loop size as described in Chapter 2. These results suggest that the RNA hairpins display a broader range of relaxation times and the hairpin folding is not a two-state process.

Another important observation of our rapid-mixing studies shows that the reaction time difference among three hairpins with the same stem and different loop can be explained by base-stacking effects. The reaction times at varying KCl concentration for hPpy and hPpyA hairpins are approximately equal within statistical error but the reaction times for PolyU loop hairpin (hpU) is smaller compared to the other two hairpins. Our recent findings on loop length dependent thermodynamic stability studies on DNA hairpins suggest that tetraloop DNA hairpins exhibits enhanced stability as compared to longer loop length hairpins with the same stem due to the base-stacking interaction in the loop regions. Generally, the base-stacking effect in the RNA hairpins is poorly understood or not fully understood. Therefore our results suggest that loop composition may affect RNA hairpin folding kinetics due to base-stacking interaction in the loop region of hairpins.

The realization of the fact that the folding in RNA hairpins is not a two-state process requires a broad range of experimental techniques and theoretical models to probe folding kinetics. For example, previous FCS[59] and T-jump[293] studies probe the reaction kinetics on microsecond timescales, the present rapid-mixing studies probe the kinetics on millisecond timescales.[314] The energy landscape of RNA hairpins can be very complex, for example proteins, and therefore there is a possibility that each experimental procedure is probing a very small part of a broader landscape. Therefore, combinations of various experimental and theoretical calculations are necessary to clearly predict the complex RNA hairpin folding structure, kinetics and stability.

5.5 CONCLUSION

In summary, we presented the rapid-mixing stopped-flow kinetics of loop-stem RNA hairpins as a function of counter ion concentration. Our results suggest that the RNA hairpin folding is not just simply a two-state process and much more complex than previously thought. The careful observation of present studies and previous experimental and theoretical prediction shows that the RNA folding process can be multi-step with several intermediates. The hairpin energy landscape can be very complex, like proteins, with several global minima for which combinations of various experimental and theoretical studies are needed to explore. Furthermore, the present studies on three different RNA hairpins of the same stem and different loop suggest that loop composition can be an important factor to determine the reaction times. The difference in reaction times in RNA hairpins can be explained by base-stacking interactions in the loop regions.

REFERENCES

(252) Pyle, A. M.; Green, J. B. *Current opinion in structural biology* **1995**, 5, 303.

(253) Thirumalai, D.; Woodson, S. *Acc. Chem. Res.* **1996**, 29, 433.

(254) Zhang, W.; Chen, S. J. *Proc. Natl. Acad. Sci.USA* **2002**, 99, 1931.

(255) Bevilacqua, P. C.; Blose, J. M. *Annu. Rev. Phys. Chem.* **2008**, 59, 79.

(256) Woodson, S. A. *Annu. Rev. Biophys.* **2010**, 39, 61.

(257) Roth, D. B.; Menetski, J. P.; Nakajima, P. B.; Bosma, M. J.; Gellert, M. *Cell***1992**, 70, 983.

(258) GlucksmannKuis, M. A.; Dai, X.; Markiewicz, P.; Rothman-Denes, L. B. *Cell***1996**, 84, 147.

(259) Dai, X.; Kloster, M.; Rothman-Denes, L. B. *J. Mol. Biol.* **1998**, 283, 43.

(260) Narayanan, R.; Zhu, L.; Velmurugu, Y.; Roca, J.; Kuznetsov, S. V.; Prehna, G.; Lapidus, L. J.; Ansari, A. *J. Am. Chem. Soc.* **2012**, 134, 18952.

(261) Wei, H.; Zhou, B.; Zhang, F.; Tu, Y.; Hu, Y.; Zhang, B.; Zhai, Q. *PloS one***2013**, 8, 56842.

(262) Thirumalai, D.; Hyeon, C. In *Non-Protein Coding RNAs*; Springer: **2009**, p 27.

(263) Chen, S.J. *Annu. Rev. Biophys.* **2008**, 37, 197.

(264) Tinoco Jr, I.; Bustamante, C. *J. Mol. Biol.* **1999**, 293, 271.

(265) Chen, S. J.; Dill, K. A.*Proc. Natl. Acad. Sci.USA***2000**, 97, 646.

(266) Kim, C. H.; Tinoco, I. *Proc. Natl. Acad. Sci.USA***2000**, 97, 9396.

(267) Dale, T.; Smith, R.; Serra, M. J. *RNA.***2000**, 6, 608.

(268) Williams, D. J.; Hall, K. B. *J. Mol. Biol.* **2000**, 297, 1045.

(269) Smolke, C. D.; Carrier, T. A.; Keasling, J. *Appl. Environ. Microbiol.* **2000**, 66, 5399.

(270) Zhuang, X.; Bartley, L. E.; Babcock, H. P.; Russell, R.; Ha, T.; Herschlag, D.; Chu, S. *Science***2000**, 288, 2048.

(271) Li, W.; Ma, B. Y.; Shapiro, B. A. *J. Biomol. Struct. Dyn.* **2001**, 19, 381.

(272) Hannoush, R. N.; Damha, M. J. *J. Am. Chem. Soc.***2001**, 123, 12368.

(273) Thirumalai, D.; Lee, N.; Woodson, S. A.; Klimov, D. *Annu. Rev. Phys. Chem.* **2001**, 52, 751

(274) Sorin, E. J.; Engelhardt, M. A.; Herschlag, D.; Pande, V. S. *J. Mol. Biol.***2002**, 317, 493.

(275) Young, B. T.; Silverman, S. K. *Biochemistry***2002**, 41, 12271.

(276) Mundoma, C.; Greenbaum, N. L. *J. Am. Chem. Soc.***2002**, 124, 3525

(277) Rupert, P. B.; Massey, A. P.; Sigurdsson, S. T.; Ferré-D'Amaré, A. R. *Science***2002**, 298, 1421.

(278) Zhang, W.; Chen, S.J. *Proc. Natl. Acad. Sci.USA***2002**, 99, 1931.

(279) Correll, C. C.; Swinger, K. *Rna-a Publication of the Rna Society***2003**, 9, 355.

(280) Lilley, D. M. *Trends Biochem. Sci.* **2003**, 28, 495.

(281) Sorin, E. J.; Rhee, Y. M.; Nakatani, B. J.; Pande, V. S. *Biophys. J.* **2003**, 85, 790.

(282) Moody, E. M.; Feerrar, J. C.; Bevilacqua, P. C. *Biochemistry***2004**, 43, 7992.

(283) Nivon, L. G.; Shakhnovich, E. I. *J. Mol. Biol.***2004**, 344, 29.

(284) Hyeon, C.; Thirumalai, D. *Proc. Natl. Acad. Sci.USA***2005**, 102, 6789.

(285) Zhang, W.; Chen, S.-J. *Biophys. J.* **2006**, 90, 778.

(286) Zhang, W.; Chen, S.-J. *Biophys. J.***2006**, 90, 765.

(287) Cao, S.; Chen, S.-J. *Nucleic Acids Res.* **2006**, 34, 2634.

(288) Nagel, J.; Flamm, C.; Hofacker, I.; Franke, K.; de Smit, M.; Schuster, P.; Pleij, C. *Nucleic Acids Res.***2006**, 34, 3568.

(289) Li, P. T.; Collin, D.; Smith, S. B.; Bustamante, C.; Tinoco I. J. *Biophys. J.* **2006**, 90, 250.

(290) Garcia, A. E.; Paschek, D. *J. Am. Chem. Soc.***2007**, 130, 815.

(291) Cao, S.; Chen, S.J. *J. Mol. Biol.***2007**, 367, 909.

(292) Bowman, G. R.; Huang, X.; Yao, Y.; Sun, J.; Carlsson, G., Guibas, Leonidas J, Pande, Vijay S.*J. Am. Chem. Soc.***2008**, 130, 9676.

(293) Kuznetsov, S. V.; Ren, C. C.; Woodson, S. A.; Ansari, A. *Nucleic Acids Res.***2008**, 36, 1098.

(294) Van Orden, A.; Jung, J. *Biopolymers***2008**, 89, 1.

(295) Tan, Z. J.; Chen, S. J. *Biophys. J.* **2008**, 95, 738.

(296) Villa, A.; Widjajakusuma, E.; Stock, G. *J. Phys. Chem. B***2008**, 112, 134.

(297) Sarkar, K.; Meister, K.; Sethi, A.; Gruebele, M. *Biophys. J.***2009**, 97, 1418.

(298) Ditzler, M. A. *Folding and Conformational Dynamics of the Hairpin Ribozyme and the Spliceosome: Combining Computational and Experimental Analyses*; ProQuest, 2009.

(299) Sheehy, J. P.; Davis, A. R.; Znosko, B. M. *Rna-a Publication of the Rna Society***2010**, 16, 417.

(300) Deng, N. J.; Cieplak, P. *Biophys. J.* **2010**, 98, 627.

(301) Sarkar, K.; Nguyen, D. A.; Gruebele, M. *RNA***2010**, 16, 2427.

(302) Huang, X.; Yao, Y.; Bowman, G. R.; Sun, J.; Guibas, L. J.; Carlsson, G. E.; Pande, V. S. In *Pacific Symposium on Biocomputing*; World Scientific: 2010; Vol. 15, p 228.

(303) Zuo, G.; Li, W.; Zhang, J.; Wang, J.; Wang, W. *J. Phys. Chem. B* **2010**, 114, 5835.

(304) Horwitz, T. S.; Vanegas, P.; Znosko, B. M. *Abstracts. Papers. Am. Chem. Soc.***2011**, 241.

(305) Narayanan, R.; Velmurugu, Y.; Kuznetsov, S. V.; Ansari, A. *J. Am. Chem. Soc.***2011**, 133, 18767.

(306) Varani, G. *Annu. Rev. Biophys. Biomol. Struct.* **1995**, 24, 379.

(307) Xia, T.; SantaLucia, J.; Burkard, M. E.; Kierzek, R.; Schroeder, S. J.; Jiao, X.; Cox, C.; Turner, D. H. *Biochemistry***1998**, 37, 14719.

(308) Mathews, D. H.; Sabina, J.; Zuker, M.; Turner, D. H. *J. Mol. Biol.***1999**, 288, 911.

(309) Bonnet, G. g.; Krichevsky, O.; Libchaber, A. *Proc. Natl. Acad. Sci.USA***1998**, 95, 8602.

(310) Jung, J.; Van Orden, A. *J. Am. Chem. Soc.***2006**, 128, 1240.

(311) Jung, J.; Ihly, R.; Scott, E.; Yu, M.; Van Orden, A. *J. Phys. Chem. B***2008**, 112, 127.

(312) Ma, H.; Proctor, D. J.; Kierzek, E.; Kierzek, R.; Bevilacqua, P. C.; Gruebele, M. *J. Am. Chem. Soc.***2006**, 128, 1523.

(313) Ma, H.; Wan, C.; Wu, A.; Zewail, A. H. *Proc. Natl. Acad. Sci.USA***2007**, 104, 712.

(314) Nayak, R. K.; Peersen, O. B.; Hall, K. B.; Van Orden, A. *J. Am. Chem. Soc.***2012**, 134, 2453.

(315) Flamm, C.; Fontana, W.; Hofacker, I. L.; Schuster, P. *RNA***2000**, 6, 325.

(316) Lin, M. M.; Meinhold, L.; Shorokhov, D.; Zewail, A. H. *Phys. Chem. Chem. Phys.***2008**, 10, 4227.

(317) Portella, G.; Orozco, M. *Angew. Chem.***2010**, 122, 7839.

(318) Stancik, A. L.; Brauns, E. B. *Biochemistry***2008**, 47, 10834.

(319) Hyeon, C.; Thirumalai, D. *J. Am. Chem. Soc.***2008**, 130, 1538.

(320) Riccardi, L.; Nguyen, P. H.; Stock, G. *J. Phys. Chem. B* **2009**, 113, 16660.

(321) Gong, P.; Campagnola, G.; Peersen, O. B. *Anal. Biochem.* **2009**, 391, 45.

(322) Rio, D. C.; Ares, M.; Hannon, G. J.; Nilsen, T. W. *Cold Spring Harbor Protocols* **2010**, *2010*, pdb. prot5444.

(323) Kaushik, M.; Bansal, A.; Saxena, S.; Kukreti, S. *Biochemistry* **2007**, 46, 7119.

(324) Anthony, P. C.; Sim, A. Y.; Chu, V. B.; Doniach, S.; Block, S. M.; Herschlag, D. *J. Am. Chem. Soc.***2012**, 134, 4607.

(325) Manning, G. S. *Acc. Chem. Res.* **1979**, 12, 443.

CHAPTER 6: Summary and Future Directions

The major objective of this thesis was to describe our efforts to address the folding and unfolding kinetics as well as thermodynamic stability of nucleic acid hairpins by using rapid-mixing stopped-flow kinetics and other spectroscopic techniques. In our venture to understand the intricate folding puzzle of nucleic acid hairpins, we learned various things concerning kinetics and thermodynamic stability of nucleic acid hairpin formation. As a result, we were able to contribute some important and relevant information regarding hairpin folding problems and the reaction mechanisms. The hairpin folding process is a complex phenomena with multiple pathways that occurs much more slowly than previously thought. Secondly, various experimental and theoretical techniques used to probe the kinetics of hairpin formation might be measuring different events of a very broad and complex energy landscape.

As described in Chapter 3, our rapid-mixing stopped-flow kinetics studies on DNA hairpin folding kinetics studies shows that the DNA hairpin folding is not simply a two-state process.[326] The hairpin folding reaction involves at least a three-state process with intermediates. One important aspect of our stopped-flow findings is that the observed reactions occurred on a timescale of milliseconds, suggesting DNA hairpin formation can occur much more slowly than previously thought. We proposed a three-state reaction mechanism of hairpin folding, wherein intermediate formation occurs on tens to hundreds of microsecond time scales, and complete hairpin formation happens on a millisecond time scale. Ultrafast techniques like T-jump[327] and FCS are useful for probing the intermediate reactions,[328] but cannot detect the complete folding reactions due to the time resolution problem of the instrument. Similarly, rapid-mixing stopped-flow can observe the complete folding reaction but cannot detect the intermediate reactions due

to the “dead time” constraint. The advantage of the stopped-flow method is that it can measure the reaction kinetics on the longer time scales from millisecond to second and minute. The disadvantage of this technique is its reliance on the dead time of the instrument. When stopped-flow technique combined with FCS or T-jump can be able to probe the complete folding trajectory of the DNA hairpins.

Since the thermodynamic stability stem-loop DNA hairpin formation depends upon various factors such as stem size, loop size, stem and loop composition, base stacking, base-pairing, hydrogen bonds on the loop and the closing base-pair of the loop,[329-331] we investigated the loop length and counter ion dependent stability of various DNA hairpins. As described in Chapter 4, we found very interesting observations regarding tetraloop DNA hairpins in comparison to longer loop length DNA hairpins. As published in various literatures, the DNA and RNA tetraloop hairpins are exceptionally stable but to the best of our knowledge, the thermal stability in the different counter ion regimes were not studied in detail. Our observation showed that the tetraloop hairpin exhibits unusually high stability compared to other longer loop length hairpins and this exceptional stability is counter ion concentration dependent.

We observed that the DNA tetraloop hairpin exhibits exceptional high stability in the higher counter ion concentration regimes of 50 mM NaCl and above. Whereas, in the lower counter ion concentration regimes of 25 mM NaCl and below, the stability of tetraloop hairpins are consistent with the longer loop length hairpins of the same stem length but variable 8,12,16 and 21 polythymidine loops that were studied. We explained this counter ion concentration regime dependent stability of tetraloop hairpins on the basis of the base stacking effect and hydrophobic collapse. We suggested, at higher counter ion concentrations, hydrophobic collapse of the nucleotides may have been increased due to the more polar solvent, which facilitates base

stacking in the loop regions of the hairpins. These factors resulted in the stability enhancement of the tetraloop hairpin in the higher counter ion concentration regimes. Due to the extremely important biological role of tetraloop hairpins, for example in genome sequence, gene expressions etc, our findings may shed light on other biological functions.

The kinetics and reaction mechanism of RNA hairpin folding is usually analyzed on the basis of a two-state model. The folding is usually described by a two-state, single barrier free energy landscape, in which the loop formation in the strand is the rate limiting step, followed by rapid zippering of the stem. The folding, free energy landscape of the RNA hairpin has been clearly misunderstood over the years. The free energy landscape of RNA is very complex,[332-334] is similar to proteins and is represented by numerous mountains and ridges. The folding landscape of simple stem-loop hairpins is rugged, as evidenced from the small stability gap between the native state and the mis-folded conformation state.[335]There have been numerous investigations by biophysicists, physical chemists, biochemists and molecular biologists over the years to understand the energy landscape of the folded and unfolded hairpins. Similarly, there have been extensive studies on RNA hairpins to unravel the kinetics of folding and thermodynamic stability.

With this motivation, we investigated RNA hairpin folding kinetics by using rapid-mixing stopped-flow kinetics experiments and observed that the folding kinetics of RNA hairpins of comparable loop and stem size are very complicated. As described in Chapter 5, our findings suggest that the folding and unfolding pathways of RNA hairpin folding can be very different and more complex than DNA hairpins and require careful analysis of experimental data along with suitable kinetic modeling to propose the reaction mechanism. From our rapid-mixing stopped flow data of different RNA hairpins, we can clearly predict that the RNA hairpin folding

is not a two-state process and the folding is at least a three-state or multi state with meta-stable or partially stable intermediates. Furthermore, base-stacking instead of base pairing plays an important role in case of RNA hairpin folding and unfolding.

The research work described in this dissertation and the various research work presented in the literatures show that we have come a long way as far as nucleic acid hairpin folding and unfolding processes are concerned. Our observations regarding nucleic acid hairpin folding, in this dissertation work, further makes it clear that hairpin folding reactions are much more complex than previously thought or realized. FCS and T-jump experiments are good techniques to measure the relaxation kinetics on microsecond time scales. In other words, these techniques presented a very small fraction of the very complex and broader energy landscape. Initially, it was believed that the hairpin folding is simply a two-state process, later this two-state process was challenged by FCS and T-jump studies. The FCS studies on DNA hairpins, in our laboratory, for the very first time proposed a three-state reaction mechanism but due to the time resolution problems, these studies could not probe the complete formation of the folded hairpin on millisecond time scales.[3]Our present work in this dissertation used rapid-mixing stopped-flow kinetics to resolve the folding reaction on millisecond time scales and by this we suggested a clear three-state reaction mechanism for DNA hairpin folding reactions. In the process, our present rapid-mixing stopped-flow work revealed another part of the broader energy landscape puzzle.

Now, one thing is very clear in the perspective of hairpin folding and unfolding is that a single experimental or theoretical technique is not sufficient to explain the much broader free

energy landscapes. A combination of experimental techniques, as well as theoretical calculation/modeling, is necessary to probe the complex biomolecular folding. For example, microfluidic mixing is a good candidate in this regard. If we could build a micro-fluidic mixer that enables us to have very short mixing times of several nanoseconds or even a few microseconds and combined this technique with FCS or T-jump, we would be able to measure the kinetics on a broad range of time scales simultaneously.

Finally, since the biological molecules are very complex and our endeavor to understand the mechanistic details and dynamics of the biochemical and biophysical processes are necessary to unravel the mystery of various deadly diseases. I think that science has come a very long way, as far as understanding the various biophysical and biochemical processes are concerned. I have no doubt that the emergence of biophysical chemistry and various innovative experimental methods and theoretical calculations will make a significant contribution toward furthering our understanding of biological phenomena for many years to come. I hope that the contributions in this dissertation will help us in our understanding of much more complex cellular processes.

REFERENCES

(326) Nayak, R. K.; Peersen, O. B.; Hall, K. B.; Van Orden, A. *J. Am. Chem. Soc.***2012**, 134, 2453.

(327) Kuznetsov, S. V.; Ren, C. C.; Woodson, S. A.; Ansari, A. *Nucleic Acids Res.***2008**, 36, 1098.

(328) Jung, J.; Van Orden, A. *J. Am. Chem. Soc.***2006**, 128, 1240.

(329) Moody, E. M.; Feerrar, J. C.; Bevilacqua, P. C. *Biochemistry***2004**, 43, 7992.

(330) Moody, E. M.; Bevilacqua, P. C. *J. Am. Chem. Soc.***2003**, 125, 16285.

(331) Bevilacqua, P. C.; Blose, J. M. *Annu. Rev. Phys. Chem.* **2008**, 59, 79.

(332) Thirumalai, D.; Hyeon, C. In *Non-Protein Coding RNAs*; Springer: **2009**, p 27.

(333) Sarkar, K.; Nguyen, D. A.; Gruebele, M. *RNA.* **2010**, 16, 2427.

(334) Chen, S. J.; Dill, K. A.*Proc. Natl. Acad. Sci.USA***2000**, 97, 646.

(335) Ditzler, M. A.; Rueda, D.; Mo, J.; Håkansson, K.; Walter, N. G. *Nucleic Acids Res.***2008**, 36, 7088.